

ANR, Appel à Projets Générique (AAPG 2019)

QCSP Project (ANR-19-CE25-0013-02)

Deliverable D2.5b Study of CCSK-OFDM

Editor:	Louis-Adrien DUFRENE (Orange Labs)
Deliverable nature:	Internal (scope: Consortium and ANR)
Due date:	September 31, 2023
Delivery date:	September 29, 2023
Version:	1.0
Total number of pages:	98 pages
Keywords:	CCSK modulation, OFDM modulation

Abstract

This deliverable studies the combination of the CCSK and OFDM modulations. Several combinations models are constructed and communications schemes are derived. Detection, synchronisation, channel estimation, equalization and demodulation algorithms are proposed and their performances are assessed and compared to the SotA. The deliverable concludes on the feasibility and usefulness of the CCSK-OFDM modulation.

DISCLAIMER

This document contains confidential information intended for the project consortium, the ANR, and the project reviewers. Its use is restricted to the purpose for which it is provided. Any disclosure, copying, or distribution of this document, or taking any action based on it is strictly prohibited.

List of Authors

Partner	Author
Orange Labs	Louis-Adrien DUFRENE (louisadrien.dufrene@orange.com)
Orange Labs	Quentin LAMPIN (quentin.lampin@orange.com)
Orange Labs	Guillaume LARUE (guillaume.larue@orange.com)

Contents

Acronyms	8
Executive Summary	8
1 Definition and Properties of Zadoff-Chu Sequences	9
1.1 Definition	9
1.2 General Properties	9
1.3 Even Length Zadoff-Chu Sequences Properties	10
1.3.1 Symmetry	11
1.3.2 Correlation with the reverse sequence	11
1.3.3 Cross-Correlation Between Different Sequences	12
2 Mathematical Toolbox	14
2.1 Greatest Common Divisor and Modular Inverse	14
2.2 Periodic Sequences	14
2.3 Linear Congruential Generator	14
2.4 Normal Distribution	15
2.4.1 Definition	15
2.4.2 White Gaussian Noise Process	15
2.4.3 Cumulative Distribution Function	15
2.5 Rayleigh Distribution	16
2.6 Jacobi symbols	16
3 DFT and IDFT of ZC Sequences	17
3.1 Closed-Form Solutions	17
3.2 Value of $F(x_u)[0]$ for 2^M length Zadoff-Chu sequences	18
3.3 Shuffle of the ZC sequence	18
3.4 Correlation Property	19
4 CCSK-OFDM: AWGN Channel	20
4.1 Reminders on OFDM	20
4.2 Reminders on CCSK	21
4.3 Single CCSK Symbol per OFDM Symbol	23
4.3.1 Transmitter and Receiver A	23
4.3.2 Transmitter and Receiver B	25
4.3.3 Transmitter and Receiver C	26
4.3.4 Performance Study	27
4.3.5 PAPR	28
4.4 Multiple CCSK Symbols per OFDM Symbol	29
4.4.1 Iterative Mapping	29
4.4.2 Scheme A	32
4.4.3 Schemes B and C	33
4.4.4 Performance Study	33
4.4.5 PAPR of Iterative Mapping	34

5 Fading Channel	37
5.1 Cyclic Prefix and Circular Convolution	37
5.2 Inclusion of the CP in Schemes A, B and C	39
5.2.1 Scheme CP-A	40
5.2.2 Scheme CP-B	40
5.2.3 Scheme CP-C	41
5.3 Channel Estimation	42
5.3.1 Pilots Positions	42
5.3.2 Least-Square Estimation	44
5.3.3 LMMSE Estimations	44
5.3.4 Interpolation Algorithms	46
5.4 Zero-Forcing Equalizer	47
5.5 Diversity Combining	47
5.6 Flatfading Performance	48
5.6.1 System Model	48
5.6.2 Constant Channel	48
5.6.3 Block Fading	53
5.7 Frequency Selective Fading Performance	56
5.7.1 System Model	56
5.7.2 Effect of the Frequency Diversity	59
5.7.3 Fading Channel Conclusion	64
6 Relative Shift Demodulation	65
6.1 CIR Estimation	65
6.2 Channel Estimation in Frequency	66
6.3 MRC Equalization with the Channel Estimate	67
6.3.1 Equalization of the Same OFDM Symbol	67
6.4 Equalization of Adjacent OFDM Symbols	68
6.5 DFTLink and GLAD Algorithms	68
6.5.1 DFT-Link: Relative Shift Probabilities Matrix	68
6.5.2 Symmetric Property	69
6.5.3 Iterative Demodulation	70
6.6 Results	75
6.6.1 Comparison with Standard Solutions	76
6.6.2 Benefits of the Iterative Approach	76
6.6.3 Channel Diversity	76
6.6.4 Scaling the OFDM Frame Size	80
6.6.5 Scaling the CCSK Sequence Length	81
6.7 Conclusion on the DFTLink and GLAD Algorithms	82
7 Time and Frequency Synchronization	84
7.1 Impact of Synchronization Error in Time	84
7.2 Impact of Synchronization Error in Frequency	86
7.3 Including Iterative Mapping	87
7.4 Detection and Synchronization System	88
7.4.1 System Model	88
7.4.2 Shifted Demodulation with a CRC	90
7.4.3 CP-Based Algorithm	91
7.5 Conclusion on Time and Frequency Synchronizations	92
8 General Conclusion	94

Appendix	95
A.1 Mathematical tools and demonstrations	95
A.1.1 Convolution Property of Fourier Transform	95
A.1.2 Fourier Transform of Gate Function	95
A.1.3 Multi-Carrier Modulation and OFDM	96
Bibliography	97

Acronyms

AWGN	Additive White Gaussian Noise
BLER	Block Error Rate
BPSK	Binary Phase-Shift Keying
CAZAC	Constant Amplitude Zero Autocorrelation
CCSK	Cyclic Code-Shift Keying
CDF	Cumulative Distribution Function
CIR	Channel Impulse Response
CP	Cyclc Prefix
CRC	Cyclic Redundancy Check
DC	Direct Component
DFT	Discrete Fourier Transform
FFT	Fast Fourier Transform
FSK	Frequency-Shift Keying
ISI	Inter-Symbols Interference
IDFT	Inverse DFT
IFFT	Inverse Fast Fourier Transform
GCD	Greatest Common Divisor
LRA	Low-Rank Approximation
LS	Least-Square
LLR	Log-Likelihood Ratio
LMMSE	Linear Minimum Mean Square Estimator
MCM	Multi-Carrier Modulation
MRC	Maximum Ratio Combining
MSE	Mean Square Error
NB-CCSK	Non-Binary CCSK
OFDM	Orthogonal Frequency-Division Multiplexing
PAPR	Peak to Average Power Ratio
PSAM	Pilot-Symbol Assisted Modulation
RF	Radio Frequency
RMS	Root Mean Square

SBLER Shifted Block Error Rate

SER Symbol Error Rate

SNR Signal to Noise Ratio

SVD Singular Value Decomposition

ZC Zadoff-Chu

ZF Zero-Forcing

Executive Summary

Work Package 2 (WP2) of the QCSP project is concerned with the proposition and evaluation of algorithms to achieve an efficient detection and synchronization of the CCSK-modulated Frame using the soft output provided to the decoder and exploiting the particular structure of the frame. The CCSK modulation is also studied in a 3GPP framework to evaluate the potential of such a modulation if included in a traditional 3GPP system.

The goal of **Task 2.5** is to find the relevant LTE-M use cases and evaluate them. The CCSK modulation properties could be useful for some 3GPP communications scenarios. The task should define them and assess the usage of the CCSK in such context. The combination of the CCSK with the usual 3GPP modulation OFDM is studied. The tasks of detection, time and frequency synchronizations, channel estimation and equalization, and the final demodulation are investigated.

This deliverable is organized as follows:

Section 1 introduces the Zadoff-Chu sequences that are used as the root CCSK sequence. These sequences are already used in 4G and 5G systems and expose several interesting properties.

Section 2 lists the mathematical tools that are employed in this report.

Section 3 provides some details on (inverse) discrete Fourier transforms of the Zadoff-Chu sequences. Moreover, some interesting properties are described.

Section 4 describes the combination of OFDM and CCSK modulations. After some reminders on OFDM and CCSK, the chapter proposes some combining schemes for single or multiple CCSK symbols per OFDM symbol, associated with a demodulation method. The performances are assessed, and some insights on complexity and feasibility aspects are provided.

Section 5 investigates the case of flat and frequency selective fading channel. The CP-OFDM modulation is described, along with state of the art channel estimation, interpolation and equalization algorithms. The combination with CCSK and CP-OFDM is studied and the performance of the system is compared in different channel condition. An emphasis on channel time and frequency diversity is proposed.

Section 6 describes two novel algorithms for channel estimation and equalization, and demodulation. Based on properties of the CCSK OFDM frame, the DFTLink and GLAD algorithms provide interesting results and pave the way to further interesting studies.

Section 7 focuses on the impact of time and frequency synchronization errors on the CCSK OFDM frame.

1 Definition and Properties of Zadoff-Chu Sequences

1.1 Definition

The general form of a Zadoff-Chu (ZC) sequence is defined as:

Definition 1

$$x_u[n] = \exp\left(-j\frac{\pi un(n + c_N + 2q)}{N}\right), \quad (1.1)$$

with $N \in \mathbb{N}^*$; $n \in \mathbb{N}$ and $0 \leq n < N$; $u \in \mathbb{N}^*$, $u < N$ and $\gcd(u, N) = 1$ (see section 2.1); $c_N \equiv N \pmod{2}$; $q \in \mathbb{Z}$.

The variable u is the index of the ZC sequence and N is the length of the sequence. Usually, $q = 0$ so that the definition simplifies to:

$$x_u[n] = \begin{cases} \exp\left(-j\frac{\pi un(n+1)}{N}\right), & \text{for } N \text{ odd,} \\ \exp\left(-j\frac{\pi un^2}{N}\right), & \text{for } N \text{ even.} \end{cases} \quad (1.2)$$

A remark on the congruence notation $x \equiv r \pmod{N}$. This equation implies that x and r have the same remainder when divided by N . In this document, we will usually make r equal to the remainder, so that $x \pmod{N} = r$ and equivalently note $x \equiv r \pmod{N}$.

1.2 General Properties

The ZC sequences were formally defined in the paper of Chu [1]. They have several interesting properties; some of them are described hereafter. The following properties apply for even and odd sequence length¹.

1. While they are originally defined as finite sequences ($0 \leq n \leq N - 1$), they can be extended as N -periodic, infinite sequences:

$$x_u[n] = x_u[n + kN], \quad \forall k \in \mathbb{Z} \quad (1.3)$$

With this property, the ZC sequence can be extended to $n \geq N$ (or even $n < 0$).

Consequently, the index n is usually defined modulo N allowing a more flexible definition of the sequence indices, and we obtain the equality:

$$x_u[n] = x_u[n \pmod{N}], \quad \forall n \in \mathbb{Z}. \quad (1.4)$$

2. They are Constant Amplitude Zero Autocorrelation (CAZAC) sequences, so they have a constant amplitude and a periodic zero auto-correlation. The auto-correlation R of the sequence $y = x_u$ is defined as:

$$R[p] = \sum_{n=0}^{N-1} y[n]x_u^*[n + p]$$

$$R[p] = \sum_{n=0}^{N-1} x_u[n]x_u^*[n + p] \quad (1.5)$$

$$(1.6)$$

¹Even though some research papers state that the ZC sequence length N has to be a prime number to have some properties, this is mostly not true and the sequence still benefits most of its properties, even in the case of N even.

The zero auto-correlation property is described by the following result:

$$R[p] = \begin{cases} 0, & \text{if } p \not\equiv 0 \pmod{N}, \\ N, & \text{if } p \equiv 0 \pmod{N}. \end{cases} \quad (1.7)$$

Note that this is the left-shifted auto-correlation version. The right-shifted auto-correlation is defined as:

$$R[p] = \sum_{n=0}^{N-1} x_u[n] x_u^*[n-p] \quad (1.8)$$

Since $-p \not\equiv 0 \pmod{N}$ is equivalent to $p \not\equiv 0 \pmod{N}$ and since $-p \equiv 0 \pmod{N}$ is equivalent to $p \equiv 0 \pmod{N}$, the right-shifted auto-correlation also verifies:

$$R[p] = \begin{cases} 0, & \text{if } p \not\equiv 0 \pmod{N}, \\ N, & \text{if } p \equiv 0 \pmod{N}. \end{cases} \quad (1.9)$$

If the sequence is right-shifted by l , denoted as $x_{u,l}[n] = x_u[n-l]$, the right-shifted auto-correlation is computed as:

$$R[p] = \sum_{n=0}^{N-1} x_{u,l}[n] x_{u,l}^*[n-p] \quad (1.10)$$

As expected, it has its maximum in $p = l$. The left-shifted auto-correlation will have its maximum $p = N - l$. A symmetric behavior applies for the left-shifted sequence and the right/left-shifted auto-correlation.

3. We can easily demonstrate the following property:

$$x_u[a+b] = x_u[a]x_u[b] \exp\left(-j\frac{2\pi u ab}{N}\right) \quad (1.11)$$

4. Closed-form solutions of the normalized Discrete Fourier Transform (DFT) and Inverse DFT (IDFT) of a right p -shifted ZC sequence can be derived:

$$\begin{aligned} \text{DFT}(x_{u,p})[k] &= F(x_{u,p})[k] = \frac{1}{\sqrt{N}} \sum_{n=0}^{N-1} x_u[n-p] \exp\left(-j2\pi \frac{nk}{N}\right) \\ F(x_{u,p})[k] &= x_u^*[u^{-1}k - p] x_u[-p] F(x_u)[0] \end{aligned} \quad (1.12)$$

$$\begin{aligned} \text{IDFT}(x_{u,p})[k] &= F^{-1}(x_{u,p})[k] = \frac{1}{\sqrt{N}} \sum_{n=0}^{N-1} x_u[n-p] \exp\left(j2\pi \frac{nk}{N}\right) \\ F^{-1}(x_{u,p})[k] &= x_u^*[-u^{-1}k - p] x_u[-p] F^{-1}(x_u)[0] \end{aligned} \quad (1.13)$$

With u^{-1} the modular multiplicative inverse of u with respect to N (see section 2.1). More information on these closed-forms are provided in section 3.

1.3 Even Length Zadoff-Chu Sequences Properties

Most of the literature on ZC sequences focus on prime length ones. This is mainly due to the fact that, when N is a prime number, there are $N - 1$ possible values for the sequence index u . Hence, prime N maximizes the number of different sequences, which is useful in the case of multi-users communications schemes, where each user would be allocated a different ZC sequence.

The current study focus on even value of N , as the sequences will be used for the modulation of binary words. More precisely, N will be expressed as 2^M , with $M \in \mathbb{N}^*$ the length of the modulated binary words. Details on the interaction between the ZC sequence, the Cyclic Code-Shift Keying (CCSK) modulation and the Orthogonal Frequency-Division Multiplexing (OFDM) modulation can be found in section 4.

1.3.1 Symmetry

In [2], the authors demonstrate a central symmetry property for odd values of N:

$$x_u[N - 1 - n] = x_u[n] \quad (1.14)$$

A similar property can be derived for even values of N:

$$\begin{aligned} x_u[N - n] &= \exp\left(-j\frac{\pi u(N - n)^2}{N}\right) \\ &= x_u[n] \exp(-j\pi u(N - 2n)) \\ &= x_u[n] \exp\left(-j2\pi u\left(\frac{N}{2} - n\right)\right) \end{aligned} \quad (1.15)$$

Since N is even, we obtain the equality:

$$x_u[N - n] = x_u[n] = x_u[-n] \quad (1.16)$$

1.3.2 Correlation with the reverse sequence

We are now interested in a right-shifted ZC sequence $x_{u,p}$, with shift value p , and its reverse sequence $y_{u,p}$. The reverse sequence takes the index of the original sequence from the end to the beginning, so from $N - 1$ to 0. We have:

$$x_{u,p}[n] = x_u[n - p] \quad (1.17)$$

and,

$$y_{u,p}[n] = x_{u,p}[N - 1 - n] = x_u[N - (n + p + 1)] \quad (1.18)$$

Using the symmetric property of ZC sequence, we demonstrate for N even:

$$y_{u,p}[n] = x_u[n + p + 1] \quad (1.19)$$

Hence, the reverse sequence $y_{u,p}$ is equal to the root sequence x_u left-shifted by $p + 1$.

From this equality, we look at the cross-correlation between $y_{u,p}$ and x_u :

$$\begin{aligned} R[s] &= \sum_{n=0}^{N-1} y_{u,p}[n] x_u^*[n - s] \\ &= \sum_{n=0}^{N-1} x_u[n + p + 1] x_u^*[n - s] \\ &= \sum_{m=p+1}^{N+p} x_u[m] x_u^*[m - p - 1 - s] \quad \text{setting } m = n + p + 1, \\ &= \sum_{m=0}^{N-1} x_u[m] x_u^*[m - (p + 1 + s)] \quad \text{from N-periodicity, see 2.2} \end{aligned} \quad (1.20)$$

By definition of the ZC auto-correlation, we have the following equality:

$$R[s] = \begin{cases} 0, & \text{if } p + s + 1 \not\equiv 0 \pmod{N}, \\ N, & \text{if } p + s + 1 \equiv 0 \pmod{N}. \end{cases} \quad (1.21)$$

The case $R[s] = N$ is solved for the right-shift $s = N - 1 - p$, considering $0 \leq p \leq N - 1$.

The cross-correlation between $x_{u,p}$ and $y_{u,p}$ can be also of interest:

$$\begin{aligned}
R[s] &= \sum_{n=0}^{N-1} x_{u,p}[n] y_{u,p}^*[n-s] \\
&= \sum_{n=0}^{N-1} x_u[n-p] x_u^*[n-s+p+1] \\
&= \sum_{m=-p}^{N-1-p} x_u[m] x_u^*[m-s+2p+1] \quad \text{setting } m = n-p, \\
&= \sum_{m=0}^{N-1} x_u[m] x_u^*[m-(s-2p-1)]
\end{aligned} \tag{1.22}$$

This leads to the equality:

$$R[s] = \begin{cases} 0, & \text{if } s-2p-1 \not\equiv 0 \pmod{N}, \\ N, & \text{if } s-2p-1 \equiv 0 \pmod{N}. \end{cases} \tag{1.23}$$

The condition leading to a correlation, $s-2p-1 \equiv 0 \pmod{N}$, means that $s-2p-1$ is even. It yields that the maximum of correlation can only be obtained for odd s values, with $s \equiv 2p+1 \pmod{N}$.

1.3.3 Cross-Correlation Between Different Sequences

In [3], the authors study the magnitude of the cross-correlation between different ZC sequences², i.e. with different indexes u .

Lets define two ZC sequences of same length N , with indexes u and v , such that, $u \neq v$, $0 < u, v < N$, $\gcd(N, u) = 1$ and $\gcd(N, v) = 1$. We also define the values $g_{u,v} = \gcd(N, u-v)$, $r_{u,v} = \frac{N}{g_{u,v}}$ and $s_{u,v} = \frac{u-v}{g_{u,v}}$. The left-shifted cross-correlation between x_u and x_v is defined as:

$$R[p] = \sum_{n=0}^{N-1} x_u[n] x_v^*[n+p] \tag{1.24}$$

Writing p as $p = i_p g_{u,v} + d_p$, where $i_p = \left\lfloor \frac{p}{g_{u,v}} \right\rfloor$ and $d_p = p - i_p g_{u,v}$, [3] provides the following result:

$$|R[p]| = \begin{cases} \sqrt{Ng_{u,v}} \delta_K(d_p), & \text{if } N \text{ and } r_{u,v} s_{u,v} \text{ are even, or } N \text{ is odd,} \\ \sqrt{Ng_{u,v}} \delta_K(d_p - \frac{g_{u,v}}{2}), & \text{if } N \text{ is even and } r_{u,v} s_{u,v} \text{ is odd} \end{cases} \tag{1.25}$$

with $\delta_K(\cdot)$ the Kronecker delta function, defined as:

$$\delta_K(k) = \begin{cases} 1, & \text{if } k = 0, \\ 0, & \text{otherwise.} \end{cases} \tag{1.26}$$

We consider our case of study, where $N = 2^M$, $M \in \mathbb{N}^*$. Since N is even, we need to check the status of the product $r_{u,v} s_{u,v}$. u and v being odd, it means that $u-v$ is even. Hence $g_{u,v}$ will have the form $g_{u,v} = 2^m$, with $1 \leq m \leq M-1$.

$$r_{u,v} = \frac{N}{g_{u,v}} = \frac{2^M}{2^m} \tag{1.27}$$

So $r_{u,v}$ is even.

$$s_{u,v} = \frac{u-v}{g_{u,v}} = \frac{2^m \alpha}{2^m} = \alpha \tag{1.28}$$

²Actually, the sequences studied are Chu sequences, whose definition is closed to the one we use in the current study. The results provided by the paper apply here.

By definition of the gcd, α has to be odd, with a minimum value of 1. Consequently, the product $r_{u,v}s_{u,v}$ is even, and we fall in the first case where:

$$|R[p]| = \sqrt{Ng_{u,v}}\delta_K(d_p) \quad (1.29)$$

$d_p = 0$ when p is a multiple of $g_{u,v}$. Since $g_{u,v} = 2^m$, all the odd values of p lead to $|R[p]| = 0$. The even values of p , multiple of $g_{u,v}$, will result in $|R[p]| = \sqrt{N2^m}$, and the others to $|R[p]| = 0$.

To get the right-shifted cross-correlation, we use the relation $R_{right}[p] = R_{left}[N-p]$. Consequently, if p is odd, then $N-p$ is also odd. If p is even and can be written as a multiple of 2^m , so can $N-p$. Thus, the magnitude of the right-shifted cross-correlation is equal to the magnitude of the left-shifted one.

2 Mathematical Toolbox

This section presents several mathematical tools useful for the following work.

2.1 Greatest Common Divisor and Modular Inverse

Considering $a, b \in \mathbb{Z}$, not both null, the Greatest Common Divisor (GCD) $r \in \mathbb{Z}$ of a and b is noted as $\gcd(a, b) = r$. We say that a and b are relatively prime if $\gcd(a, b) = 1$.

Theorem 1 (Bézout) *Considering $a, b \in \mathbb{Z}$, not both null, and r their GCD, $\gcd(a, b) = r$, then $\exists(u, v) \in \mathbb{Z}$, such that:*

$$au + bv = r$$

Moreover, a and b are relatively prime, if and only if, $\exists(u, v) \in \mathbb{Z}$, such that:

$$au + bv = 1$$

Definition 2 (Modular Multiplicative Inverse) *The modular multiplicative inverse of u with respect to N , noted u^{-1} , is defined by:*

$$uu^{-1} \equiv 1 \pmod{N}$$

Thus, $\exists v \in \mathbb{Z}$ such as,

$$uu^{-1} = vN + 1$$

Consequently, the modular inverse u^{-1} exists if and only if, u and N are relatively prime. For the same reason, u^{-1} and N are also relatively prime. Following the previous statements, an interesting equality can be directly derived. Considering $(u, N) \in (\mathbb{N}^*)^2$ and u and N relatively prime, then:

$$\exp\left(j \frac{2\pi}{N}\right) = \exp\left(j \frac{2\pi}{N}uu^{-1}\right) \quad (2.1)$$

There are an infinite number of u^{-1} values, because of the modulo N operation. Usually, the value of u^{-1} is considered modulo N and unique, so that $1 \leq u^{-1} < N$ (u^{-1} cannot be equal to 0).

2.2 Periodic Sequences

Definition 3 *A sequence $x[n]$ is N -periodic if:*

$$x[n] = x[n + N], \quad \forall n \in \mathbb{Z}$$

By recurrence, it can be shown that any sum of N consecutive elements of an N -periodic sequence $x[n]$ are equal:

$$\sum_{n=p}^{N-1+p} x[n] = \sum_{n=0}^{N-1} x[n] \quad (2.2)$$

2.3 Linear Congruential Generator

Linear congruential generators consider periodic sequences of integers defined by the relationship:

$$X_{n+1} = (aX_n + c) \pmod{m}, \quad (2.3)$$

with $m \in \mathbb{N}^*$, $a \in \mathbb{N}^*$ and $0 < a < m$, $c \in \mathbb{N}$ and $0 \leq c < m$ and $0 < X_0 < m$. X_0 is known as the seed of the sequence. With appropriate choice of a, c and m , one can obtain a sequence with known length.

Theorem 2 (Hull-Dobell [4]) *The sequence X_n has a full length m (is m -periodic), if and only if:*

1. m and c are relatively prime,
2. $a - 1$ is divisible by all prime factors of m ,
3. $a - 1$ is divisible by 4 if m is divisible by 4.

2.4 Normal Distribution

2.4.1 Definition

A random variable X follows a normal distribution of expectation μ and standard deviation σ if its probability density function $f(x)$ for $x \in \mathbb{R}$ is expressed as:

$$f(x) = \frac{1}{\sigma\sqrt{2\pi}} \exp\left(-\frac{(x-\mu)^2}{2\sigma^2}\right) \quad (2.4)$$

In this case, we adopt the following notation: $X \sim \mathcal{N}(\mu, \sigma^2)$, with σ^2 the variance of the distribution.

Normal distributions have the following properties:

1. If $x \sim \mathcal{N}(\mu, \sigma^2)$, then considering $(a, b) \in \mathbb{R}^2$, $ax + b \sim \mathcal{N}(a\mu + b, a^2\sigma^2)$.
2. If $x \sim \mathcal{N}(\mu_1, \sigma_1^2)$ and $y \sim \mathcal{N}(\mu_2, \sigma_2^2)$, and if x and y are independent, then $x + y \sim \mathcal{N}(\mu_1 + \mu_2, \sigma_1^2 + \sigma_2^2)$.

2.4.2 White Gaussian Noise Process

Considering a stationary complex white Gaussian noise process $X(t)$, the sequence of time samples $x[t]$ of $X(t)$ are independent random variables, each following a complex normal distribution, so that $x[t] \sim \mathcal{CN}(0, \sigma^2) \forall t$. Hence, $x[t]$ is expressed as $x[t] = y[t] + jz[t]$, with $y[t] \sim \mathcal{N}(0, \frac{\sigma^2}{2}) \forall t$, $z[t] \sim \mathcal{N}(0, \frac{\sigma^2}{2}) \forall t$, and the random variables from the sequence y and from the sequence z are all mutually independent. Consequently, the distribution of $x[t]$ is a circularly-symmetric central complex normal distribution, which means that for any $\phi \in \mathbb{R}$, the random variable $e^{j\phi}x \sim \mathcal{CN}(0, \sigma^2)$.

From [5], both DFT and IDFT of the sequence x , normalized by $\frac{1}{\sqrt{N}}$ with N the size of the DFT/IDFT, are a sequence of independent random variables, complex normally distributed, so that $DFT(x)[k] \sim \mathcal{CN}(0, \sigma^2)$ and $IDFT(x)[k] \sim \mathcal{CN}(0, \sigma^2) \forall k$. Moreover, all real and imaginary parts of the sequence (I)DFT(x) are mutually independent, defining new white random variables.

2.4.3 Cumulative Distribution Function

The error function, noted erf, is defined on \mathbb{C} as:

$$\text{erf}(x) = \frac{2}{\sqrt{\pi}} \int_0^x \exp(-t^2) dt. \quad (2.5)$$

The complementary error function, noted erfc, is defined as:

$$\begin{aligned} \text{erfc}(x) &= 1 - \text{erf}(x) \\ &= \frac{2}{\sqrt{\pi}} \int_x^{+\infty} \exp(-t^2) dt. \end{aligned} \quad (2.6)$$

The Cumulative Distribution Function (CDF) of the standard normal distribution $\mathcal{N}(0, 1)$ is equal to:

$$\begin{aligned}\Phi(x) &= \frac{1}{\sqrt{2\pi}} \int_{-\infty}^x \exp\left(-\frac{t^2}{2}\right) dt \\ &= \frac{1}{2} \left[1 + \operatorname{erf}\left(\frac{x}{\sqrt{2}}\right) \right].\end{aligned}\quad (2.7)$$

Equivalently, we have:

$$1 - \Phi(x) = \frac{1}{2} \operatorname{erfc}\left(\frac{x}{\sqrt{2}}\right). \quad (2.8)$$

2.5 Rayleigh Distribution

A random variable X follows a Rayleigh distribution of scale σ if its probability density function $f(x)$ for $x \in \mathbb{R}^+$ is expressed as:

$$f(x) = \frac{x}{\sigma^2} \exp\left(-\frac{x^2}{2\sigma^2}\right) \quad (2.9)$$

We note the distribution $\mathcal{R}(\sigma)$. The Rayleigh distribution of parameter σ has the following properties:

- Considering two independent Gaussian random variables $U \sim \mathcal{N}(0, \sigma^2)$ and $V \sim \mathcal{N}(0, \sigma^2)$, the random variable $X = \sqrt{U^2 + V^2}$ follows a Rayleigh distribution of scale σ : $X \sim \mathcal{R}(\sigma)$.

- The CDF is equal to:

$$\Phi(x) = 1 - \exp\left(-\frac{x^2}{2\sigma^2}\right) \quad (2.10)$$

- The expectation is equal to:

$$\mathbb{E}[X] = \sigma \sqrt{\frac{\pi}{2}} \quad (2.11)$$

- The variance is equal to:

$$\operatorname{Var}(X) = \left(1 - \frac{\pi}{2}\right) \sigma^2 \quad (2.12)$$

2.6 Jacobi symbols

The Jacobi symbol $\left(\frac{a}{n}\right)$ is defined, for $a \in \mathbb{Z}$ and $n \in \mathbb{N}^*$, n odd, as the product of the following Legendre symbols:

$$\left(\frac{a}{n}\right) = \left(\frac{a}{p_1}\right)^{e_1} \left(\frac{a}{p_2}\right)^{e_2} \cdots \left(\frac{a}{p_k}\right)^{e_k} \quad (2.13)$$

where the prime factorization of $n = p_1^{e_1} p_2^{e_2} \cdots p_k^{e_k}$.

A Legendre symbol $\left(\frac{a}{p}\right)$ takes its values in the set $\{0, 1, -1\}$ and is defined as:

$$\left(\frac{a}{p}\right) = \begin{cases} 0, & \text{if } a \equiv 0 \pmod{p}, \\ 1, & \text{if } a \equiv x^2 \pmod{p}, \text{ with } x \in \mathbb{N}^*, \\ -1, & \text{if } a \equiv y \pmod{p}, y \text{ not a square.} \end{cases} \quad (2.14)$$

3 DFT and IDFT of ZC Sequences

This section presents the special interaction between the DFT and IDFT operations and the ZC sequences. Since these operations will be at the center of the CCSK-OFDM communication scheme, we develop here some interesting results.

3.1 Closed-Form Solutions

The closed-form expression of the DFT presented in Eq.1.12 is derived in [6]. Based on the demonstration provided for the DFT we can directly find the IDFT closed-form of Eq.1.13.

DFT Proof: In [6], the author provides the following demonstration. We consider the normalized DFT of the following ZC sequence:

$$F(x_{u,p})[k] = \frac{1}{\sqrt{N}} \sum_{n=0}^{N-1} x_u[n-p] \exp\left(-j2\pi \frac{nk}{N}\right). \quad (3.1)$$

The sequence is right-shifted by p symbols, with $0 \leq p < N$. Again, the index of the ZC sequence should be read modulo N , as we consider the extended N -periodic sequence. We use a new index $l = n - p$ and the variable $d = u^{-1}k$, with u^{-1} the modular multiplicative inverse of u with respect to N (see section 2.1). u^{-1} exists since u and N are relatively prime. We obtain:

$$\begin{aligned} F(x_{u,p})[k] &= \frac{1}{\sqrt{N}} \sum_{l=-p}^{N-1-p} x_u[l] \exp\left(-j2\pi \frac{l+p}{N} ud\right) \\ F(x_{u,p})[k] &= \frac{1}{\sqrt{N}} \sum_{l=0}^{N-1} x_u[l] \exp\left(-j2\pi \frac{l+p}{N} ud\right), \end{aligned} \quad (3.2)$$

since the sequence under the sum is N -periodic. By noticing that $x_u[l+d] = x_u[l]x_u[d] \exp\left(-j2\pi \frac{uld}{N}\right)$, we obtain:

$$\begin{aligned} F(x_{u,p})[k] &= \frac{1}{\sqrt{N}} x_u^*[d] \exp\left(-j2\pi \frac{upd}{N}\right) \sum_{l=0}^{N-1} x_u[l+d] \\ &= x_u^*[d] \exp\left(-j2\pi \frac{upd}{N}\right) F(x_u)[0]. \end{aligned} \quad (3.3)$$

Using the relationship,

$$x_u^*[d] \exp\left(-j2\pi \frac{upd}{N}\right) = x_u^*[d-p]x_u[-p]$$

we directly get:

$$F(x_{u,p})[k] = x_u^*[u^{-1}k - p]x_u[-p]F(x_u)[0]. \quad (3.4)$$

To obtain the IDFT closed-form, we follow the same steps, setting $d = -u^{-1}k$:

$$F^{-1}(x_{u,p})[k] = x_u^*[-u^{-1}k - p]x_u[-p]F(x_u)[0], \quad (3.5)$$

since,

$$F(x_u)[0] = F^{-1}(x_u)[0] = \frac{1}{\sqrt{N}} \sum_{n=0}^{N-1} x_u[n].$$

Moreover, the DFT and the IDFT are linked by the relationship:

$$\mathcal{F}(x_{u,p})[N - k] = \mathcal{F}^{-1}(x_{u,p})[k] \quad (3.6)$$

In case of 2^M length ZC, using symmetry property, we have:

$$\begin{aligned} \mathcal{F}(x_{u,p})[k] &= x_u^*[u^{-1}k - p]x_u[p]\mathcal{F}(x_u)[0]. \\ \mathcal{F}^{-1}(x_{u,p})[k] &= x_u^*[u^{-1}k + p]x_u[p]\mathcal{F}(x_u)[0] \end{aligned} \quad (3.7)$$

3.2 Value of $\mathcal{F}(x_u)[0]$ for 2^M length Zadoff-Chu sequences

We consider a ZC sequence of length $N = 2^M$ with $M \in \mathbb{N}^*$. From [6] and [7], the value of the first term of the normalized DFT or IDFT of a 2^M length ZC is:

$$\mathcal{F}(x_u)[0] = \left(\frac{2N}{u}\right) \exp\left(j\frac{\pi}{4}(-1)^{\frac{u+1}{2}}\right), \quad (3.8)$$

with $\left(\frac{2N}{u}\right)$ a Jacobi symbol (see section 2.6), taking its value in the set $\{0, -1, 1\}$. In our case, $\left(\frac{2N}{u}\right) = \pm 1$. Hence, one can express $\mathcal{F}(x_u)[0]$ as:

$$\mathcal{F}(x_u)[0] = \pm \exp\left(\pm j\frac{\pi}{4}\right) \quad (3.9)$$

3.3 Shuffle of the ZC sequence

By normalizing by $\frac{x_u^*[-p]}{\mathcal{F}(x_u)[0]}$, the DFT of x_u is a sampled version of x_u^* :

$$\mathcal{F}(x_{u,p})[k] = x_u^*[u^{-1}k - p]. \quad (3.10)$$

We note $y[k]$ the sequence of sampling index $(u^{-1}k - p) \bmod (N)$, for $0 \leq k \leq N - 1$, with $y[0] = -p \bmod (N)$. The distributivity of modulo operation states:

$$(a + b) \bmod (N) = [(a \bmod (N)) + (b \bmod (N))] \bmod (N) \quad (3.11)$$

This leads to the sequence relationship:

$$y[k + 1] = (y[k] + u^{-1}) \bmod (N) \quad (3.12)$$

Since u^{-1} is relatively prime with N , we can apply the Hull-Dobell Theorem [4] (see section 2.3). It means that the sequence $y[k]$ is N -periodic. By definition, it also means that there is no value repeated within N consecutive values of $y[k]$ (since $y[k + 1]$ is entirely defined by $y[k]$). Hence the N index values defined from $y[0]$ to $y[N - 1]$ are a sampling of N unique values from 0 to $N - 1$. Thus the N -periodic sequence $x_u^*[u^{-1}k - p]$ is actually a shuffling and N -periodic sampling of the ZC sequence x_u^* .

In the case of the IDFT, the index sequence relationship is:

$$y[k + 1] = (y[k] + (-u^{-1}) \bmod (N)) \bmod (N) \quad (3.13)$$

Since we have $1 \leq u^{-1} < N$, then $(-u^{-1}) \bmod (N) = N - u^{-1}$. We can easily demonstrate that $N - u^{-1}$ is also prime with N and we can apply the Hull-Dobell Theorem. Thus the N -periodic sequence $x_u^*[-u^{-1}k - p]$ is also a shuffling and N -periodic sampling of the ZC sequence x_u^* .

3.4 Correlation Property

The right-shifted correlation function of $F(x_{u,p})$ with $F(x_u)$ is defined as:

$$R[s] = \sum_{k=0}^{N-1} F(x_{u,p})[k] F^*(x_u)[k-s] \quad (3.14)$$

Developing this expression:

$$\begin{aligned} R[s] &= \sum_{k=0}^{N-1} x_u^*[u^{-1}k - p] x_u[-p] F(x_u)[0] x_u[u^{-1}(k-s)] x_u^*[0] F^*(x_u)[0] \\ &= x_u[-p] \sum_{k=0}^{N-1} \exp\left(j \frac{\pi u(u^{-1}k - p)^2}{N}\right) \exp\left(-j \frac{\pi u(u^{-1}(k-s))^2}{N}\right) \\ &= x_u[-p] \sum_{k=0}^{N-1} \exp\left(j \frac{\pi u(u^{-1}u^{-1}k^2 - 2u^{-1}kp + p^2 - u^{-1}u^{-1}k^2 + u^{-1}u^{-1}2ks - u^{-1}u^{-1}s^2)}{N}\right) \\ &= x_u[u^{-1}s] \sum_{k=0}^{N-1} \exp\left(j \frac{2\pi k u u^{-1}(u^{-1}s - p)}{N}\right) \\ &= x_u[u^{-1}s] \sum_{k=0}^{N-1} \exp\left(j \frac{2\pi k(u^{-1}s - p)}{N}\right) \end{aligned} \quad (3.15)$$

Recognizing a sum of root of unity, we can conclude:

$$R[s] = \begin{cases} 0, & \text{if } u^{-1}s \not\equiv p \pmod{N}, \\ Nx_u[p], & \text{if } u^{-1}s \equiv p \pmod{N}. \end{cases} \quad (3.16)$$

The correlation function admits a maximum value of $Nx_u[p]$ obtained at the index s checking $u^{-1}s \equiv p \pmod{N}$. As explained in section 3.3, the series $y[s] = u^{-1}s \pmod{N}$ will browse exactly once all the integers within 0 and $N - 1$ for $s \in [0; N - 1]$. We can conclude $\exists! s \in [0; N - 1]$ so that $u^{-1}s \equiv p \pmod{N}$. Thus, the correlation function R is a perfect zero correlation function.

By extension, the IDFT of $x_{u,p}$ has also a zero auto-correlation function, with a maximum value of $Nx_u[p]$ obtained at the unique index s checking $u^{-1}s \equiv N - p \pmod{N}$:

$$R[s] = \begin{cases} 0, & \text{if } u^{-1}s \not\equiv N - p \pmod{N}, \\ Nx_u[p], & \text{if } u^{-1}s \equiv N - p \pmod{N}. \end{cases} \quad (3.17)$$

4 CCSK-OFDM: AWGN Channel

This section introduces the combination of the two modulations OFDM and CCSK. Several communication schemes are presented and the performance are assessed in an Additive White Gaussian Noise (AWGN) channel.

4.1 Reminders on OFDM

The OFDM [8] is a form of Multi-Carrier Modulation (MCM) that maps N information symbols on N sub-carriers in frequency. Hence, instead of transmitting the data on a single carrier of bandwidth B, the same bandwidth is split in N sub-carriers each of bandwidth $\frac{B}{N}$.

The Figure 4.1 describes a typical OFDM transmitter. Among the MCM, the particularity of OFDM is to use the IDFT and DFT operations, at the transmitter and receiver respectively, to map data symbols of the different sub-carriers to a physical signal and vice versa. Usually, these operations are realized by their faster algorithmic version, the Inverse Fast Fourier Transform (IFFT) and the Fast Fourier Transform (FFT).

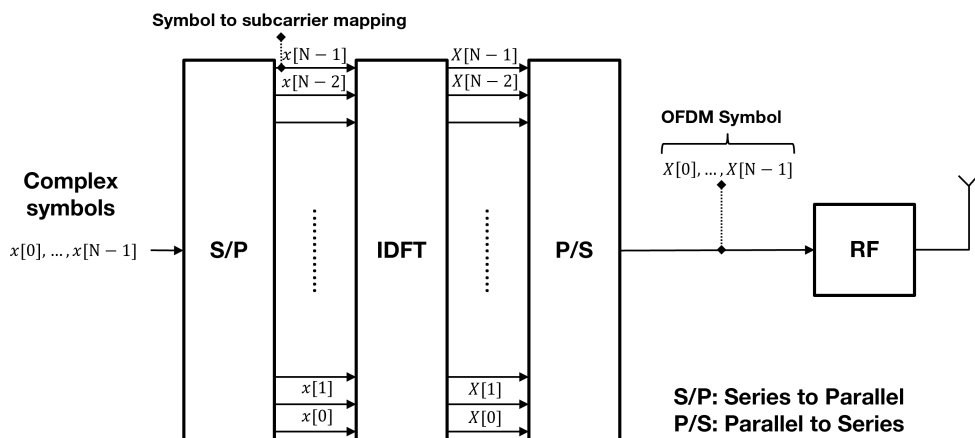


Figure 4.1: OFDM transmitter scheme.

The sequence of symbols to transmit are noted as $x[n]$ for $n \in [0; N - 1]$. The symbols can belong to any modulation constellation, as Binary Phase-Shift Keying (BPSK) for instance. The sequence $x[n]$ is then mapped from series to parallel by the “S/P” block. The mapping of each symbol in the parallel form will correspond to the associated sub-carrier in frequency.

This association is realized by the IDFT operation. One can see the IDFT as the transformation from frequency to temporal domain. The resulting normalized IDFT symbols are described as:

$$X[k] = \frac{1}{\sqrt{N}} \sum_{n=0}^{N-1} x[n] \exp \left(j2\pi \frac{kn}{N} \right) \quad \text{for } 0 \leq k \leq N - 1 \quad (4.1)$$

The IDFT symbols vector is then mapped from parallel to series by the “P/S” block. The sequence of symbols $X[k]$ is then transmitted as a continuous time signal by the Radio Frequency (RF) block. The vector of IDFT symbols constitutes one OFDM symbol. The OFDM symbol carries N data symbols, each transmitted at a rate $\frac{B}{N}$.

The OFDM receiver is described by the Figure 4.2. In baseband, the synchronized received signal $Y(t)$ is sampled at a rate $\frac{1}{B}$. Without any imperfection, the sequence of N received samples is defined as:

$$Y[k] = X[k] = \text{IDFT}(x)[k] = F^{-1}(x)[k] \quad (4.2)$$

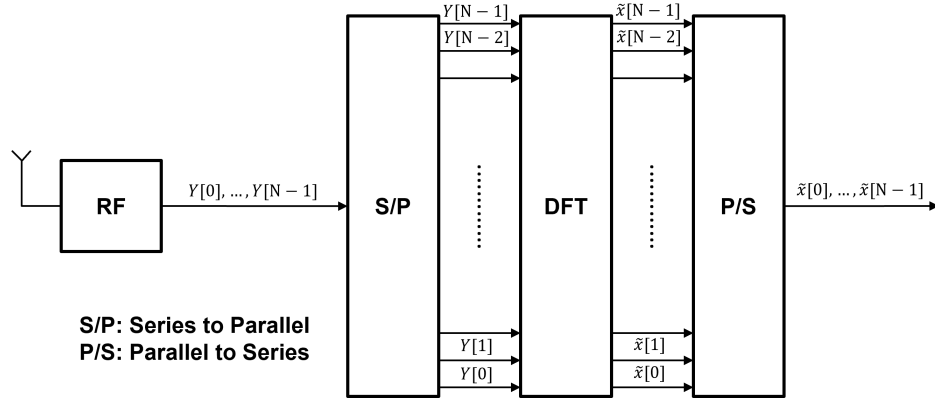


Figure 4.2: OFDM receiver scheme.

In the same manner, we note $DFT(x)[k] = F(x)[k]$. The receiver recovers the transmitted sequence $x[n]$ by applying the normalized DFT operation to the received vector of samples:

$$\begin{aligned} \tilde{x}[n] &= F(F^{-1}(x))[n] \\ &= \frac{1}{\sqrt{N}} \sum_{k=0}^{N-1} X[k] \exp\left(-j2\pi \frac{nk}{N}\right) \\ &= x[n], \quad \text{for } 0 \leq n \leq N-1 \end{aligned} \quad (4.3)$$

4.2 Reminders on CCSK

The CCSK modulation is a form of direct sequence spread-spectrum technique, where a symbol s of the set of integers $\mathbb{S}_N = \{0, 1, \dots, N-1\}$ is associated to the circular shift of a sequence of N chips in \mathbb{C}^N [9][10]. In a more traditional context, the size N is a power of 2, so that $N = 2^M$ and a symbol s can be represented as a binary word of M bits.

Considering the "root" sequence p_0 of N chips, the symbol s is mapped to the sequence p_s , defined as the sequence p_0 circularly right-shifted by s positions, so that:

$$p_s[i] = p_0[i - s \bmod (N)], \quad 0 \leq i < N \quad (4.4)$$

Consequently, a sequence of modulated symbols is a succession of circularly shifted version of p_0 . Each sequence p_s is called a CCSK symbol.

To demodulate a received CCSK symbol y , one can compute the right-shifted cross-correlation between y and the root sequence p_0 . If the sequence p_0 is well-chosen, the maximum of the cross-correlation will indicate the modulated symbol s . Hence, the auto-correlation function of the root sequence p_0 should have a spike at index 0 and low values when the sequences are not synchronized. As presented in [10], the right-shifted cross-correlation can be efficiently computed by employing DFT and IDFT operations:

$$R[k] = F^{-1}(F(y) \odot F^*(p_0))[k] = \frac{1}{\sqrt{N}} \sum_{i=0}^{N-1} y[i] p_0^*[i - k \bmod (N)] \quad (4.5)$$

with \odot the Hadamard product operator (term by term multiplication). The factor $\frac{1}{\sqrt{N}}$ appears because the DFT and IDFT operations are normalized. Consequently, the cross-correlation scores are

divided by $\frac{1}{\sqrt{N}}$, with a maximum value of \sqrt{N} . The estimated symbol \tilde{s} can be expressed as:

$$\tilde{s} = \operatorname{argmax}_{k \in \mathbb{S}_N} (R[k]) \quad (4.6)$$

Since R can take complex values, the real or absolute value of the cross-correlation is usually taken instead.

In the context of the QCSP project, the CCSK modulation is usually associated with a non-binary code, to constitute the Non-Binary CCSK (NB-CCSK) communication scheme. As explained in Deliverable 1.1, but also in [11][12], if the CCSK sequence is based on a pseudo-noise sequence with elements in $\{-1; +1\}$, the Log-Likelihood Ratio (LLR) can be efficiently computed by the cross-correlation.

We consider the transmitted CCSK symbol x corresponding to the data symbol u , affected by an AWGN. The received sequence of samples y is expressed as:

$$y[n] = x[n] + z[n], \quad \text{for } n \in [0, N - 1] \quad (4.7)$$

where z is the sequence of mutually independent random sample of noise, with $z[n] \sim \mathcal{N}(0, \sigma^2)$ for $0 \leq n < N$. It should be noted that x , z and y are all real valued. The non-binary LLR is a vector γ , where the k^{th} component is defined as:

$$\gamma[k] = \log \left(\frac{\Pr(u = 0 | y)}{\Pr(u = k | y)} \right), \quad (4.8)$$

with $\Pr(u = k | y)$ is the probability that the transmitted symbol is equal to k ($k \neq 0$), with the previous knowledge of y . Deliverable 1.1 shows that:

$$\gamma[k] = \frac{1}{\sigma^2} (y \cdot p_0 - y \cdot p_k), \quad (4.9)$$

with $y \cdot p_k = R[k] = \sum_{i=0}^{N-1} y[i] p_0^*[i - k \bmod (N)]$. The constant factor $\frac{1}{\sigma^2}$ can be removed since it will not influence the performance. Consequently, γ can be efficiently computed by a difference between $R[0]$ and the $R[k]$. For this relation to hold, the only requirement on the real sequence p_0 is that $\sum_{i=0}^{N-1} p_0[i]^2 = \sum_{i=0}^{N-1} p_k[i]^2$.

We consider now the case of a complex sequence x affected by a complex white Gaussian noise z , where each sample $z[k] \sim \mathcal{CN}(0, \sigma^2)$ (see section 2.4). The k^{th} LLR is defined as:

$$\begin{aligned} \gamma[k] &= \log \left(\frac{\Pr(u = 0 | y)}{\Pr(u = k | y)} \right) \\ &= \log \left(\frac{\Pr(x = p_0 | y)}{\Pr(x = p_k | y)} \right) \\ &= \sum_{i=0}^{N-1} \log \left(\frac{\Pr(x[i] = p_0[i] | y[i])}{\Pr(x[i] = p_k[i] | y[i])} \right) \end{aligned} \quad (4.10)$$

with the last equation obtained considering an independent distribution of errors. If we consider that the transmitted sequences are equiprobable, and applying the Bayes formula, we get:

$$\begin{aligned} \gamma[k] &= \sum_{i=0}^{N-1} \log \left(\frac{\Pr(y[i] | x[i] = p_0[i])}{\Pr(y[i] | x[i] = p_k[i])} \right) \\ &= \sum_{i=0}^{N-1} \log \left(\frac{\Pr(\Re(y[i]) | \Re(x[i]) = \Re(p_0[i]))}{\Pr(\Re(y[i]) | \Re(x[i]) = \Re(p_k[i]))} \right. \\ &\quad \left. \frac{\Pr(\Im(y[i]) | \Im(x[i]) = \Im(p_0[i]))}{\Pr(\Im(y[i]) | \Im(x[i]) = \Im(p_k[i]))} \right) \end{aligned} \quad (4.11)$$

with $\Re(\cdot)$ and $\Im(\cdot)$ the real and imaginary part respectively. We have supposed that the real and imaginary parts of the noise are independent with $\Re(z[k]) \sim \mathcal{N}(0, \frac{\sigma^2}{2})$ and $\Im(z[k]) \sim \mathcal{N}(0, \frac{\sigma^2}{2})$. Each probability has the form:

$$\Pr(\Re(y[i]) \mid \Re(x[i]) = \Re(p_0[i])) = \frac{2}{\sigma\sqrt{2\pi}} \exp\left(-2\frac{(\Re(y[i]) - \Re(p_0[i]))^2}{\sigma^2}\right) \quad (4.12)$$

Hence we have,

$$\begin{aligned} \gamma[k] &= \frac{2}{\sigma^2} \sum_{i=0}^{N-1} [-(\Re(y[i]) - \Re(p_0[i]))^2 - (\Im(y[i]) - \Im(p_0[i]))^2 \\ &\quad + (\Re(y[i]) - \Re(p_k[i]))^2 + (\Im(y[i]) - \Im(p_k[i]))^2] \\ &= \frac{2}{\sigma^2} \sum_{i=0}^{N-1} [2(\Re(y[i])\Re(p_0[i]) + \Im(y[i])\Im(p_0[i])) \\ &\quad - (\Re(y[i])\Re(p_k[i]) + \Im(y[i])\Im(p_k[i]))) \\ &\quad - \Re(p_0[i])^2 + \Re(p_k[i])^2 - \Im(p_0[i])^2 + \Im(p_k[i])^2] \end{aligned} \quad (4.13)$$

Noticing that,

$$\begin{aligned} y[i]x^*[i] &= (\Re(y[i])\Re(x[i]) + \Im(y[i])\Im(x[i])) + \\ &\quad j(\Re(x[i])\Im(y[i]) - \Re(y[i])\Im(x[i])) \end{aligned} \quad (4.14)$$

We can simplify Eq.4.13 into,

$$\gamma[k] = \frac{4}{\sigma^2}(\Re(y \cdot p_0) - \Re(y \cdot p_k)) + \frac{2}{\sigma^2} \sum_{i=0}^{N-1} |p_k[i]|^2 - |p_0[i]|^2 \quad (4.15)$$

Since we have $\sum_{i=0}^{N-1} |p_k[i]|^2 - \sum_{i=0}^{N-1} |p_0[i]|^2 = 0$, then:

$$\gamma[k] = \frac{4}{\sigma^2}(\Re(y \cdot p_0) - \Re(y \cdot p_k)) \quad (4.16)$$

Hence, in the case of complex sequence, the LLR can be also efficiently computed based on the difference of $\Re(R[0])$ and the $\Re(R[k])$.

4.3 Single CCSK Symbol per OFDM Symbol

This section will introduce three communication schemes mixing CCSK and OFDM modulations. The schemes are named scheme A, B and C for simplicity.

4.3.1 Transmitter and Receiver A

The first communication scheme A is inspired from the one provided by the state of the art on the combination of CCSK and OFDM in [13] and [12].

We consider a transmission scheme, mixing the CCSK and OFDM modulation, described by Figure 4.3 and named Transmitter A. The data symbols s belong to the set of integers $\mathbb{S}_N = \{0, 1, \dots, N-1\}$, with $N = 2^M$ and $M \in \mathbb{N}^*$. Each symbol can be represented as a unique M-long binary word. The data symbols are first modulated by the CCSK, based on a ZC sequence $x_u[n]$ of length N. One can note that [13] uses a Chu sequence for the CCSK modulation and [12] a pseudo-noise sequence of $\{-1; +1\}$ values. Since N is even, the ZC sequence has the following definition:

$$x_u[n] = \exp\left(-j\pi \frac{un^2}{N}\right) \quad (4.17)$$

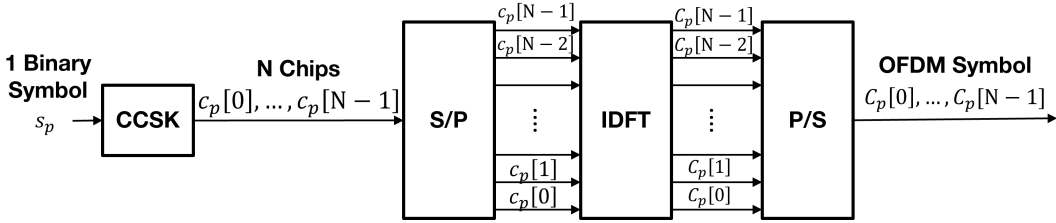


Figure 4.3: CCSK-OFDM Transmitter A, single CCSK symbol modulated.

with $0 < u < N$ and $\gcd(u, N) = 1$. Because $N = 2^M$, we can deduce that u can be any odd number between 1 and $N-1$. There are $\frac{N}{2}$ possible values for u .

We consider a standard CCSK mapping, where the symbol s_p of numerical value p is modulated as a right shift of the ZC sequence of p chips, $0 \leq p < N - 1$. The resulting modulated sequence of N chips c_p is:

$$c_p[n] = x_u[n - p], \quad \text{for } 0 \leq n < N \quad (4.18)$$

We then map a single CCSK symbol on the corresponding OFDM sub-carriers. The chip index n is mapped to the sub-carrier n , leading to the normalized IDFT signal:

$$F^{-1}(c_p)[k] = C_p[k] = \frac{1}{\sqrt{N}} \sum_{n=0}^{N-1} x_u[n - p] \exp\left(j2\pi \frac{kn}{N}\right) \quad \text{for } 0 \leq k \leq N - 1 \quad (4.19)$$

The N complex symbols C_p constitutes the transmitted OFDM symbol. We first consider the communication scheme described by the Figure 4.4, where the transmitted signal is only affected by an AWGN.



Figure 4.4: CCSK-OFDM communication scheme over AWGN channel.

Hence the received sequence of samples y is defined as:

$$Y[k] = C_p[k] + W[k] \quad (4.20)$$

where the random process W is a stationary white Gaussian noise, and each sample $W[k] \sim \mathcal{CN}(0, \sigma^2)$ and are independent for $0 \leq k < N - 1$. The receiver, named Receiver A, is described in Figure 4.5. We assume that the signal is received in perfect time and frequency synchronization conditions. The received signal is first processed by a DFT as in a standard OFDM receiver. The resulting samples \tilde{c}_p can then be processed by a standard CCSK demodulator, using the equation $R[k] = F^{-1}(F(\tilde{c}_p) \odot F^*(c_0))[k]$. In the correlator block, the DFT of \tilde{c}_p is term by term multiplied with the conjugate of the DFT of the root ZC sequence $c_0 = x_u$. The IDFT of the result provides the cross-correlation of c_0 and \tilde{c}_p . Taking the real part of the cross-correlation, the index of the maximum should then provide the most likely binary symbol \tilde{s}_p .

In this communication scheme (Transmitter and Receiver A), the modulation and demodulation steps of CCSK and OFDM are performed independently and successively. Thus, the system keeps the flexibility advantage of the OFDM, and the transmitted N -length sequence could be placed anywhere within a wider spectrum, padding zeros on the unused sub-carriers of the IDFT. At the receiver, the second DFT operation starts the CCSK demodulation and should be a N -points DFT to enable the efficient cross-correlation computation.

For the moment, we assume that the transmitted sequence occupies the whole system spectrum. Hence the system uses N -points IDFT and DFT, and there is no zero-padding in the IDFT at the

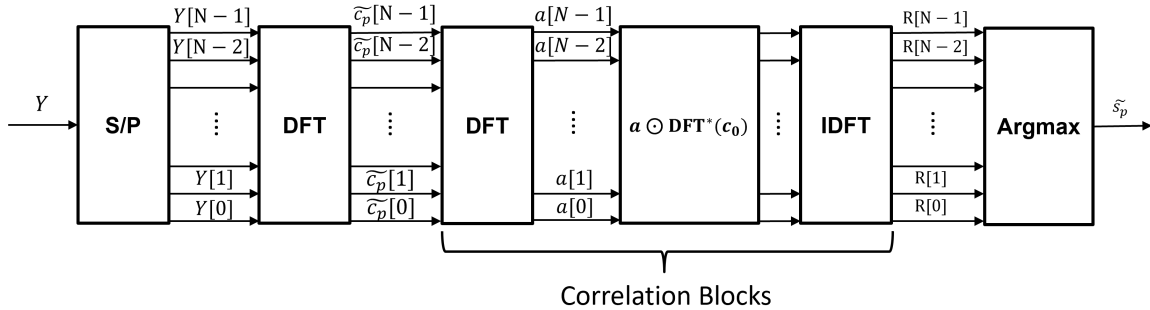


Figure 4.5: CCSK-OFDM Receiver A.

transmitter. We are interested in the noise distribution after the correlation process. After the OFDM-DFT, the output samples \tilde{c}_p have the form:

$$\tilde{c}_p[k] = c_p[k] + w[k], \quad (4.21)$$

where $c_p[k] = x_u[k - p]$ and, from section 2.4, $w[k] \sim \mathcal{CN}(0, \sigma^2)$. Then, the receiver processes the DFT of samples \tilde{c}_p , do an Hadamard product with the complex conjugate of the DFT of c_0 and finally computes the IDFT, leading to:

$$R[k] = F^{-1}(F(c_p) \odot F^*(c_0))[k] + F^{-1}(F(w) \odot F^*(c_0))[k] \quad (4.22)$$

The first term of the sum is the cross-correlation part, noted $A[k]$. The second term, noted $B[k]$, is the noise term. From section 2.4, we know that $F(w)[k] = w'[k] \sim \mathcal{CN}(0, \sigma^2)$. As developed in [6] and in section 3, one can express the $F^*(c_0)[k]$ as $\pm e^{j\phi[k]}$ with $\phi[k]$ a phase term depending on u , u^{-1} , N and p . From its circularly-symmetric property, $w''[k] = \pm w'[k]e^{j\phi[k]} \sim \mathcal{CN}(0, \sigma^2)$. Consequently, we have $B[k] = F^{-1}(w'')[k] \sim \mathcal{CN}(0, \sigma^2)$. Hence, the noise affecting the cross-correlation term has the same distribution as the original one. Also, it is clear that the resulting $B[k]$ values are independent identically distributed complex Gaussian random variables.

The value of the cross-correlation term $A[k]$ will depend on the size N of the ZC sequence and the actual shift value p . Moreover, because of the normalization used for the DFT and IDFT, the values will be multiplied by $\frac{1}{\sqrt{N}}$. Since the term $A[k]$ is real-valued (0 or \sqrt{N}), it is more efficient to take the real part of $R[k]$ instead of the absolute complex value, to decrease the noise term: $\Re(R[k]) = A[k] + \Re(B[k])$, with $\Re(B[k]) \sim \mathcal{N}(0, \frac{\sigma^2}{2})$.

4.3.2 Transmitter and Receiver B

In the scheme B, we move forward the correlation operation to realize the OFDM-DFT and CCSK-DFT in a single process. The Transmitter B is the same as the Transmitter A described in Figure 4.3. The Receiver B is described in Figure 4.6. The received signal Y is directly correlated with the conjugate of the IDFT of the root ZC sequence c_0 . Then, the DFT is processed, resulting in the sequence of samples R defined as:

$$R[k] = F(F^{-1}(c_p) \odot F^{-1}(c_0)^*)[k] + F(W \odot F^{-1}(c_0)^*)[k], \quad (4.23)$$

with $W \sim \mathcal{CN}(0, \sigma^2)$. The equation is similar to Eq.4.22, leading to similar performance results as scheme A for an AWGN channel.

Contrary to the communication scheme A, the scheme B cannot allow the mapping of several CCSK symbols next to one another in frequency. The received signal Y should only contain one single CCSK symbol, occupying the whole system bandwidth. Yet, if the RF block is able to filter and extract groups of frequencies, each containing one transmitted CCSK symbol, then it should be possible to process each CCSK symbol individually.

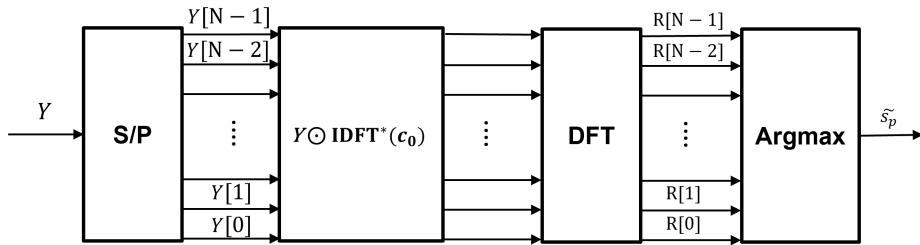


Figure 4.6: CCSK-OFDM Receiver B.

Hence, the scheme B does not really use the flexibility of OFDM and one can say that this scheme moved the first CCSK-IDFT of a standard CCSK receiver (without OFDM) to the transmitter. Consequently, and in these perfect reception conditions, the receiver is less complex than the Receiver A and than a standard CCSK receiver.

4.3.3 Transmitter and Receiver C

The communication scheme C keeps bringing the correlation operation forward in the processing chain, and actually placed it in the transmitter, as depicted in Figure 4.7. After the OFDM-IDFT, the samples are term by term multiplied by the IDFT of the root ZC sequence c_0 . The resulting signal is transmitted. The receiver described in Figure 4.8 has then simply to process the common OFDM- and CCSK-DFT to achieve the cross-correlation operation. The values of R are expressed as:

$$R[k] = F(F^{-1}(c_p) \odot F^{-1}(c_0)^*)[k] + F(W)[k], \quad (4.24)$$

with $W \sim \mathcal{CN}(0, \sigma^2)$. The scheme C also has the same performances as the scheme A in an AWGN channel.

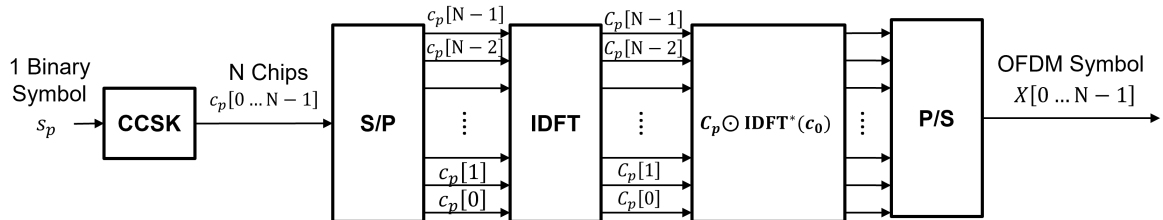


Figure 4.7: CCSK-OFDM Transmitter C.

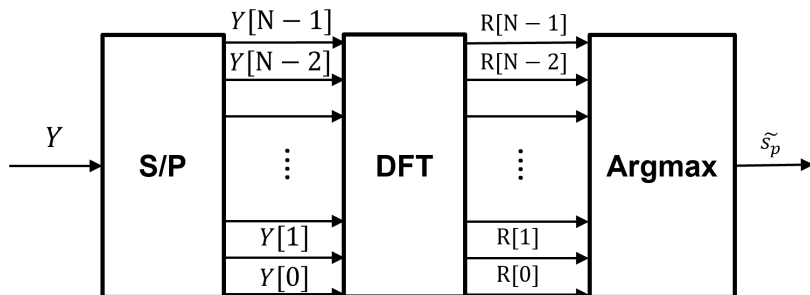


Figure 4.8: CCSK-OFDM Receiver C.

The scheme C does not allow the mapping of several CCSK symbols next to one another in frequency. The transmitted CCSK symbol should occupy the whole system bandwidth. Consequently and as for the scheme B, the system does not really use the OFDM advantages and simply push the complexity of the CCSK modulation towards the transmitter. In these perfect synchronization conditions and AWGN channel, the receiver is here extensively simple.

After the DFT operation at the receiver, only one sub-carrier should have a spike of energy and the position of this spike indicates the modulated binary symbol. This means that the modulation is equivalent to a M-Frequency-Shift Keying (FSK) combined with OFDM. At the transmitter, one could simply map the spike of energy directly on the right sub-carrier, providing the same results without the complexity of the Hadamard product.

4.3.4 Performance Study

The analytical performance of the previous schemes can be derived from [9]. Considering $R[k]$, two outputs are possible. The first output is the index corresponding to the correct shift p :

$$R_p = R[p] = \sqrt{N} + z[p], \quad (4.25)$$

where $z[p] \sim \mathcal{N}(0, \frac{\sigma^2}{2})$. The second output corresponds to the $N-1$ incorrect indexes:

$$R_k = R[k \neq p] = z[k]. \quad (4.26)$$

A CCSK symbol error occurs when there is at least one index $k \neq p$ so that $R[k] > R_p$. The probability of correct demodulation P_c is then equal to:

$$P_c = \int_{-\infty}^{+\infty} \Pr(R_p > R_k, \forall k \neq p | R_p) p(R_p) dR_p \quad (4.27)$$

and the probability of symbol error $P_e = 1 - P_c$. The distribution of R_p and R_k are derived from the noise distribution, such as,

$$p(R_p) = \frac{1}{\sigma\sqrt{\pi}} \exp\left(-\frac{(R_p - \sqrt{N})^2}{\sigma^2}\right) \quad (4.28)$$

$$p(R_k) = \frac{1}{\sigma\sqrt{\pi}} \exp\left(-\frac{R_k^2}{\sigma^2}\right) \quad (4.29)$$

Since all R_k are statistically independent, the joint probability in Eq.4.27 can be expressed as the product of $N - 1$ marginal probabilities. One marginal can be expressed as:

$$\begin{aligned} P_m &= \frac{1}{\sigma\sqrt{\pi}} \int_{-\infty}^{R_p} \exp\left(-\frac{R_k^2}{\sigma^2}\right) dR_k \\ &= \frac{1}{\sqrt{2\pi}} \int_{-\infty}^{\frac{R_p\sqrt{2}}{\sigma}} \exp\left(-\frac{u^2}{2}\right) du \\ &= 1 - \frac{1}{2} \operatorname{erfc}\left(\frac{R_p}{\sigma}\right) \end{aligned} \quad (4.30)$$

For the last equality, see section 2.4. Consequently the probability of symbol error P_e is expressed as:

$$\begin{aligned} P_e &= 1 - \frac{1}{\sigma\sqrt{\pi}} \int_{-\infty}^{+\infty} \left(1 - \frac{1}{2} \operatorname{erfc}\left(\frac{R_p}{\sigma}\right)\right)^{N-1} \exp\left(-\frac{(R_p - \sqrt{N})^2}{\sigma^2}\right) dR_p \\ &= \frac{1}{\sigma\sqrt{\pi}} \int_{-\infty}^{+\infty} \left[1 - \left(1 - \frac{1}{2} \operatorname{erfc}\left(\frac{R_p}{\sigma}\right)\right)^{N-1}\right] \exp\left(-\frac{(R_p - \sqrt{N})^2}{\sigma^2}\right) dR_p \\ &= \frac{1}{\sqrt{2\pi}} \int_{-\infty}^{+\infty} \left[1 - \left(1 - \frac{1}{2} \operatorname{erfc}\left(\frac{u}{\sqrt{2}}\right)\right)^{N-1}\right] \exp\left(-\left(\frac{u}{\sqrt{2}} - \sqrt{\frac{N}{\sigma^2}}\right)^2\right) du \\ &= \frac{1}{\sqrt{2\pi}} \int_{-\infty}^{+\infty} \left[1 - \left(1 - \frac{1}{2} \operatorname{erfc}\left(\frac{u}{\sqrt{2}}\right)\right)^{N-1}\right] \exp\left(-\left(\frac{u}{\sqrt{2}} - \sqrt{\frac{E_s}{N_0}}\right)^2\right) du \end{aligned} \quad (4.31)$$

with $E_s = N$ the mean energy per transmitted symbol, and $N_0 = \sigma^2$ the power of the complex noise.

We simulate the performance of the communication system A (equivalent to system B and C as explained in previous sections). Based on the previous analytical expression, we plot the Symbol Error Rate (SER) versus $\frac{E_b}{N_0}$ curves, with E_b is the mean energy per bit and $E_b = \frac{E_s}{M}$. The Figure 4.9 presents the results of a CCSK modulation using a ZC sequence of size 64. The analytical curve has been numerically evaluated.

The simulation matches the analytical results when the real part of the cross-correlation score is taken. When the absolute value is taken instead, there is a performance loss due to the amplitude of noise being greater than its real part. Hence, in case of an AWGN channel and in perfect synchronization conditions, it is advantageous to take the real part of the cross-correlation.

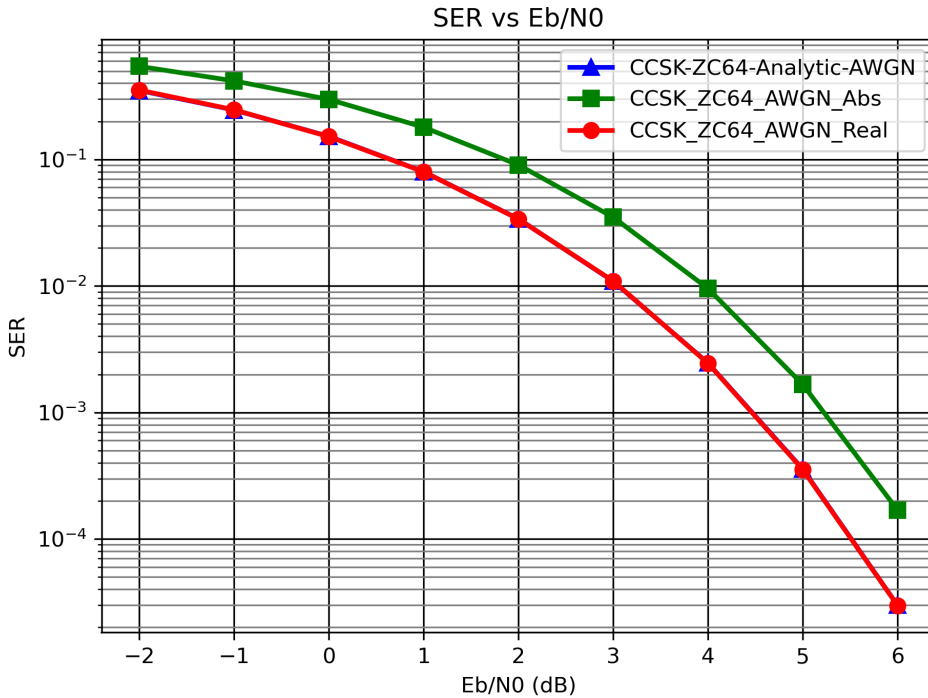


Figure 4.9: SER vs E_b/N_0 in an AWGN channel.

4.3.5 PAPR

The Peak to Average Power Ratio (PAPR) of the transmitted signal is usually a major constraint in OFDM system. The PAPR of a discrete time signal s in decibel is defined as:

$$\text{PAPR}_{\text{dB}}(s) = 10 \log_{10} \left(\frac{|s_{\text{peak}}|^2}{s_{\text{RMS}}^2} \right) \quad (4.32)$$

with $|s_{\text{peak}}|^2$ the highest energy within the signal samples and s_{RMS} the root mean square of the signal samples. The PAPR of a standard OFDM signal is usually high, depending on the symbols modulated and the size of the IDFT, leading to complex and costly power amplifier implementations, with lower energy efficiency. We propose to analyse the PAPR of the proposed CCSK-OFDM schemes.

First, we consider the transmitted signal of the scheme A or B, defined as:

$$C_p[k] = \frac{1}{\sqrt{N}} \sum_{n=0}^{N-1} x_u[n-p] \exp \left(j2\pi \frac{kn}{N} \right), \quad (4.33)$$

As described in section 3, the transmitted signal C_p can be expressed as:

$$C_p[k] = x_u^*[-u^{-1}k - p]x_u[-p]C_p[0], \quad (4.34)$$

with $C_p[0]$ defined in section 3.2 as,

$$\begin{aligned} C_p[0] &= \left(\frac{2N}{u}\right) \exp\left(j\frac{\pi}{4}(-1)^{\frac{u+1}{2}}\right), \\ &= \pm \exp\left(\pm j\frac{\pi}{4}\right). \end{aligned} \quad (4.35)$$

Consequently, the amplitude of $C_p[k]$ is constant and equal to 1. Hence, in our system, the DFT and IDFT of a ZC sequence has a constant unitary amplitude. This also applies to the transmitted signal of the scheme C, defined as:

$$x[k] = (\mathbf{F}^{-1}(c_p) \odot \mathbf{F}^{-1}(c_0)^*)[k] \quad (4.36)$$

A direct consequence of the constant amplitude, is that the $\text{PAPR}_{\text{dB}} = 0\text{dB}$ for the communication scheme A, B and C, allowing an efficient power amplifier implementation.

4.4 Multiple CCSK Symbols per OFDM Symbol

In the previous section, three transmitters and receivers combining the CCSK and OFDM modulations were presented, while only a single CCSK symbol was mapped on the OFDM sub-carriers. It could be interesting to map several CCSK symbols within a single OFDM symbol, increasing the data rate of the system.

A block mapping can be used, positioning each CCSK symbol on different sub-carriers blocks. These blocks could be positioned next to one another in frequency or dispatched over the whole available bandwidth. While this block mapping is compatible with the transceiver A, it is not with the transceivers B and C. Indeed each sub-carriers block (each CCSK symbol) needs an individual correlation/demodulation chain, which is not (easily) possible with the scheme B and C, that mix OFDM and CCSK demodulations.

4.4.1 Iterative Mapping

To enable the multiple CCSK symbols transmission for schemes B and C, a new mapping is proposed. In this new mapping, named "Iterative Mapping", the CCSK symbols are iteratively mapped on successive sub-carriers, as described on Figure 4.10. The mapping scheme first maps the first chip of each CCSK symbol, then the second chip, and so on.

We consider q N-length CCSK symbols c_{p_i} , with $i \in [0; q - 1]$ and $p_i \in [0; N - 1]$ the CCSK right shift value modulating the information. The system uses a total of $K = qN$ sub-carriers. One should note that all the CCSK symbols use the same root sequence c_0 . The corresponding transmitted IDFT samples are defined as:

$$C[k] = \frac{1}{\sqrt{K}} \sum_{n=0}^{K-1} c[n] \exp\left(j2\pi \frac{nk}{K}\right) \quad (4.37)$$

with c the resulting sequence of CCSK chips mapped on the sub-carriers, so that $c[n] = c_{p_i}[l]$ for $n = lq + i$ and $l \in [0, N - 1]$.

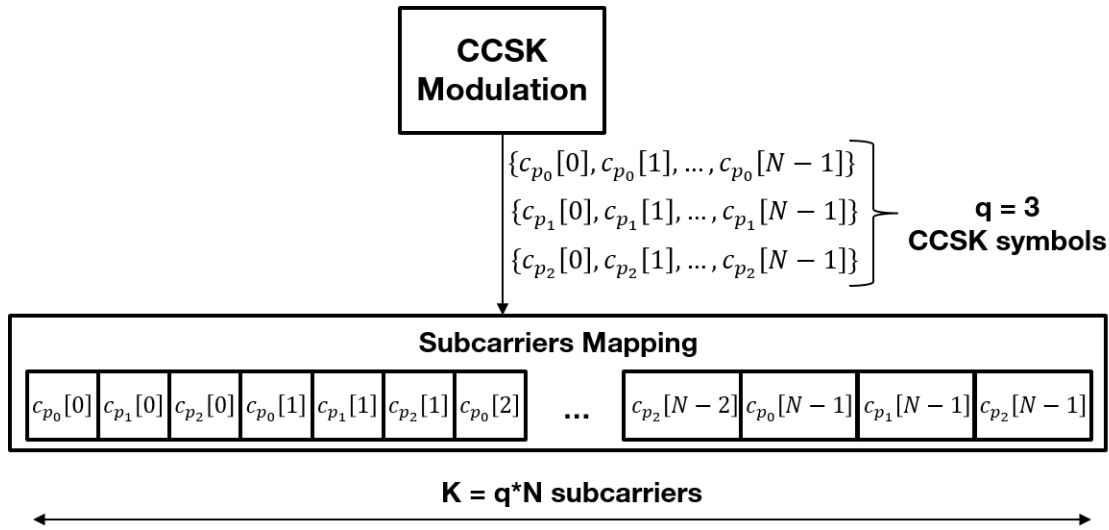


Figure 4.10: Iterative mapping example with 3 CCSK symbols.

$$\begin{aligned}
 C[k] &= \frac{1}{\sqrt{K}} \sum_{n=0}^{K-1} c[n] \exp \left(j2\pi \frac{nk}{K} \right) \\
 &= \frac{1}{\sqrt{K}} \sum_{i=0}^{q-1} \sum_{l=0}^{N-1} c[lq+i] \exp \left(j2\pi \frac{(lq+i)k}{qN} \right) \\
 &= \frac{1}{\sqrt{K}} \sum_{i=0}^{q-1} \sum_{l=0}^{N-1} c_{p_i}[l] \exp \left(j2\pi \frac{lk}{N} \right) \exp \left(j2\pi \frac{ik}{K} \right) \\
 &= \frac{\sqrt{N}}{\sqrt{K}} \sum_{i=0}^{q-1} \exp \left(j2\pi \frac{ik}{K} \right) F^{-1}(c_{p_i})[k]
 \end{aligned} \tag{4.38}$$

Using the closed-form of the IDFT of the ZC sequence (see Eq. 1.13), we have:

$$C[k] = \frac{F(c_0)[0]}{\sqrt{q}} \sum_{i=0}^{q-1} x_u^*[-u^{-1}k - p_i] x_u[-p_i] \exp \left(j2\pi \frac{ik}{K} \right) \tag{4.39}$$

with the first term of the normalized N-length IDFT: $F^{-1}(c_0)[0] = F(c_0)[0] = \pm \exp(\pm j\frac{\pi}{4})$ (see Eq. 3.9). At the receiver, the correlation operation in frequency is done with the following sequence of length K:

$$b[n] = \begin{cases} c_0[l] & , \text{if } n \equiv 0 \pmod{q} = lq \\ 0 & , \text{otherwise} \end{cases} \tag{4.40}$$

An example of the sequence b for three CCSK symbols is provided in Figure 4.11.

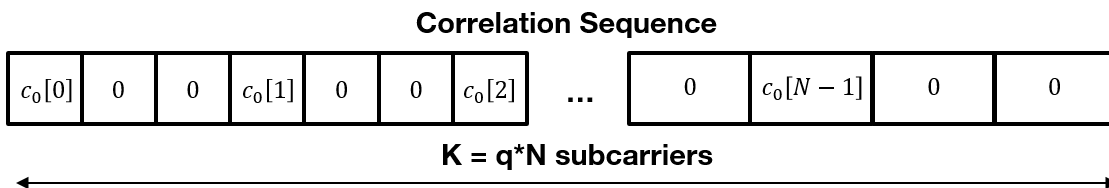


Figure 4.11: Iterative correlation sequence considering 3 CCSK symbols.

The right-shifted cross-correlation of the sequences c and b , noted R , is expressed as:

$$\begin{aligned}
R[k] &= \sum_{n=0}^{K-1} c[n] b^*((n-k) \bmod K) \\
&= \sum_{i=0}^{q-1} \sum_{l=0}^{N-1} c[lq+i+k] b^*[lq+i] \quad \text{with } n-k \equiv lq+i \bmod K \\
&= \sum_{l=0}^{N-1} c[lq+k] b^*[lq] \quad \text{because of the definition of } b \\
&= \sum_{l=0}^{N-1} c[(l+z)q+d] b^*[lq] \quad \text{with } k = zq + d \\
&= \sum_{l=0}^{N-1} c_{pd}[(l+z) \bmod N] c_0^*[l] \\
&= \sum_{l=0}^{N-1} c_{pd}[l] c_0^*[(l-z) \bmod N]
\end{aligned} \tag{4.41}$$

The last equation is exactly the cross-correlation of the sequence c_{pd} with c_0 estimated in z , $R_{pd}[z] = \sum_{l=0}^{N-1} c_{pd}[l] c_0^*[(l-z) \bmod N]$. Hence, the cross-correlation between the sequences c and b can be expressed with the cross-correlation of the original CCSK symbols. The mapping of the result follows the iterative mapping. An example for three CCSK symbols is depicted in Figure 4.12.

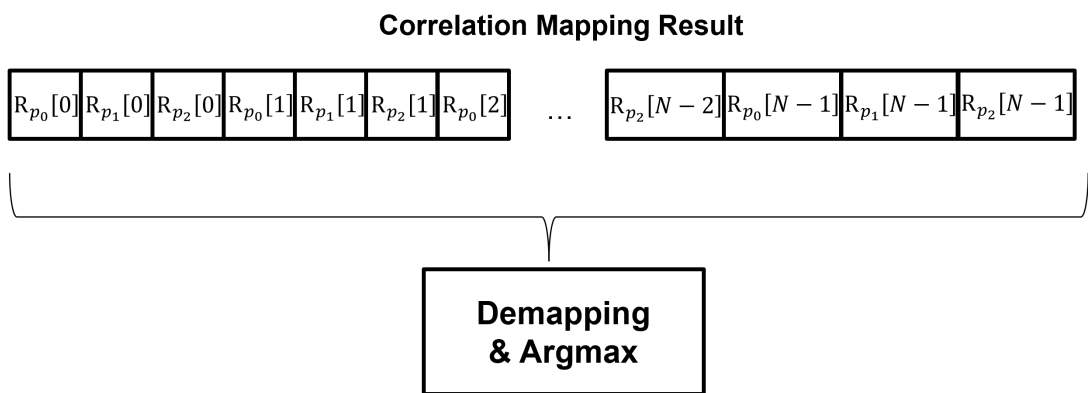


Figure 4.12: Correlation with iterative mapping.

Consequently, the iterative mapping provides an efficient way to realize the demodulation of the q CCSK symbols, as it is done in a single correlation operation instead of q . The output vector of the correlation must then be reordered to separate the part corresponding to the correlation of each CCSK symbol. The maximum argument of each part can then be taken, concluding the demodulation of the symbols.

In our approach, the cross-correlation is computed with normalized DFT and IDFT operation.

Considering the IDFT of the root sequence b :

$$\begin{aligned}
 B[k] &= \frac{1}{\sqrt{K}} \sum_{n=0}^{K-1} b[n] \exp\left(j2\pi \frac{nk}{K}\right) \\
 &= \frac{1}{\sqrt{K}} \sum_{l=0}^{N-1} b[lq] \exp\left(j2\pi \frac{lqk}{K}\right) \\
 &= \frac{1}{\sqrt{K}} \sum_{l=0}^{N-1} c_0[l] \exp\left(j2\pi \frac{lk}{N}\right) \\
 &= \frac{F(c_0)[0]}{\sqrt{q}} x_u^*[-u^{-1}k]
 \end{aligned} \tag{4.42}$$

Hence, the energy of a sample is $|B[k]|^2 = \frac{1}{q}$. To normalize the IDFT, we need to multiply each sample by \sqrt{q} , so that:

$$B[k] = F(c_0)[0] x_u^*[-u^{-1}k] \tag{4.43}$$

In this case, the cross-correlation is equal to:

$$\begin{aligned}
 R[k] &= F(F^{-1}(c) \odot F^{-1}(b)^*)[k] \\
 &= \frac{1}{\sqrt{K}} \sum_{n=0}^{K-1} C[n] B^*[n] \exp\left(-j2\pi \frac{nk}{K}\right) \\
 &= \frac{1}{\sqrt{qK}} \sum_{n=0}^{K-1} x_u[-u^{-1}n] \sum_{i=0}^{q-1} x_u^*[-u^{-1}n - p_i] x_u[-p_i] \exp\left(j2\pi \frac{in}{K}\right) \exp\left(-j2\pi \frac{nk}{K}\right) \\
 &= \frac{1}{\sqrt{qK}} \sum_{i=0}^{q-1} \sum_{n=0}^{K-1} \exp\left(j2\pi \frac{n(p_i q + i - k)}{K}\right)
 \end{aligned} \tag{4.44}$$

The cross-correlation is not null when $k = p_i q + i$, with a correlation score of \sqrt{N} . As expected, we find the same result as in Eq.4.41, with the cross-correlation arrangement presented in Figure 4.12.

4.4.2 Scheme A

As stated before, the scheme A successively processes the CCSK modulation and the OFDM modulation. Consequently, any sub-carriers mapping can be used, including the iterative mapping.

The Figures 4.13 and 4.14 respectively describe the transmitter and receiver A including the iterative mapping. Again, the scheme A can consider empty sub-carriers at the transmitter and receiver, and modulates other data in the sub-carriers not used by the CCSK symbols.

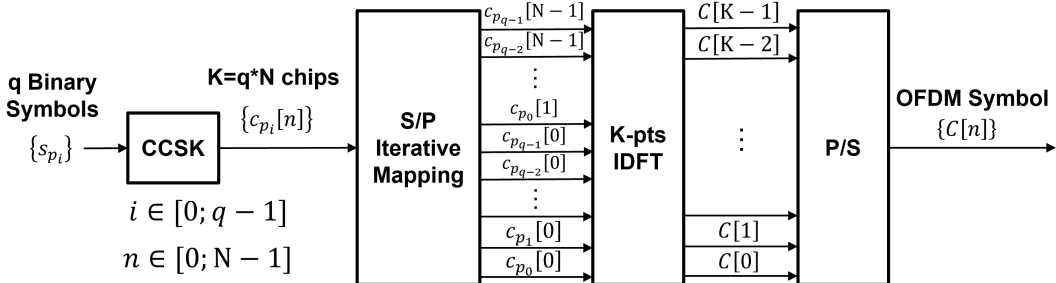


Figure 4.13: Transmitter A with iterative mapping.

At the receiver, the CCSK symbols are processed with a single operation of correlation over the K sub-carriers. As stated before, we scale the conjugate of the DFT of the root sequence by a factor of \sqrt{q} to retrieve a maximum cross-correlation of \sqrt{N} . Moreover, this normalization preserve the complex noise distribution of $\mathcal{CN}(0, \sigma^2)$ after the Hadamard product.

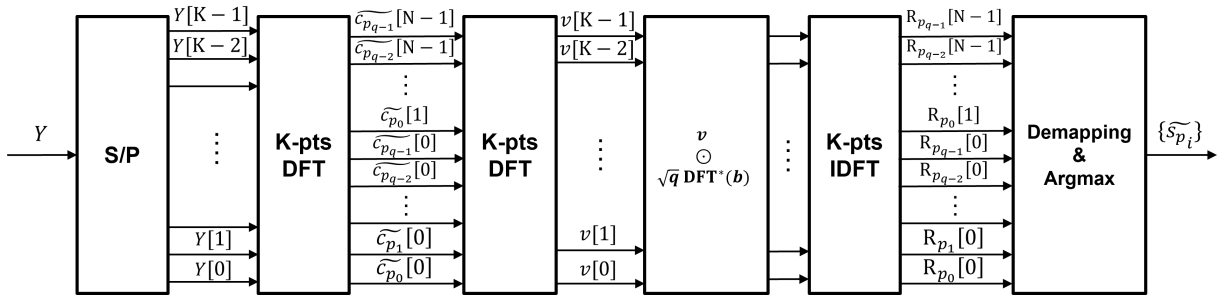


Figure 4.14: Receiver A with iterative mapping.

The complexity of the DFT and IDFT operations can be reduced to $\mathcal{O}(K \log(K))$ with FFT and IFFT implementations. Thus, it could be more interesting, in terms of number of operations, to actually split the q received CCSK symbols, and process them individually in separated CCSK demodulation chain instead of a single one. Each demodulation chain would run shorter DFT and IDFT operations leading to a decrease in complexity. Yet, this remark may not be true, depending on the actual implementation and the number of different DFT and IDFT sizes to consider, as well as the system capacity to execute these operations in parallel.

4.4.3 Schemes B and C

Contrary to scheme A, the schemes B and C cannot use any kind of mapping for multiple CCSK symbols transmission. Since the Hadamard product is done on the received (scheme B) or transmitted (scheme C) OFDM symbol, the system cannot isolate the CCSK symbols mapped on the sub-carriers. This property also constrains the system to use all the sub-carriers, but provides significant complexity reduction.

The iterative mapping enables the multiple CCSK symbols transmission for the schemes B and C. The Figure 4.15 describes the receiver B with the iterative mapping. As a reminder, the transmitter B is equivalent to the transmitter A. The Figures 4.16 and 4.17 respectively depict the transmitter and receiver C implementing the iterative mapping.

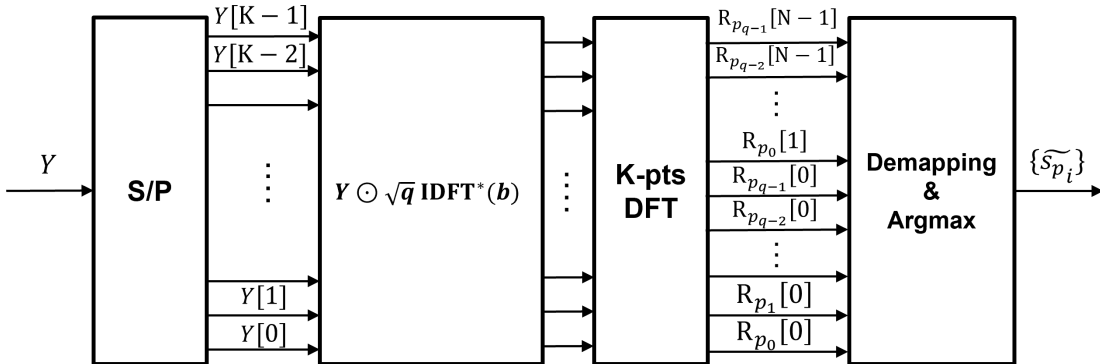


Figure 4.15: Receiver B with iterative mapping.

4.4.4 Performance Study

To complete the study on the multiple CCSK symbols transmission, the SER of the system under an AWGN channel is studied. The performance curves are presented in the Figure 4.18. The label *OFDM CCSK ZC64 qX* corresponds to the performance of a CCSK modulation using a ZC sequence of size 64 with an iterative mapping of size $q = X$. When $X = 1$, the scheme is equivalent to a single CCSK symbol transmission.

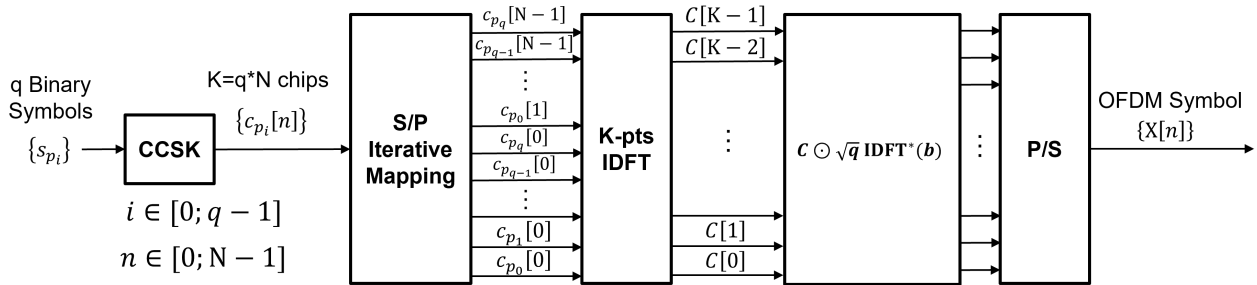


Figure 4.16: Transmitter C with iterative mapping.

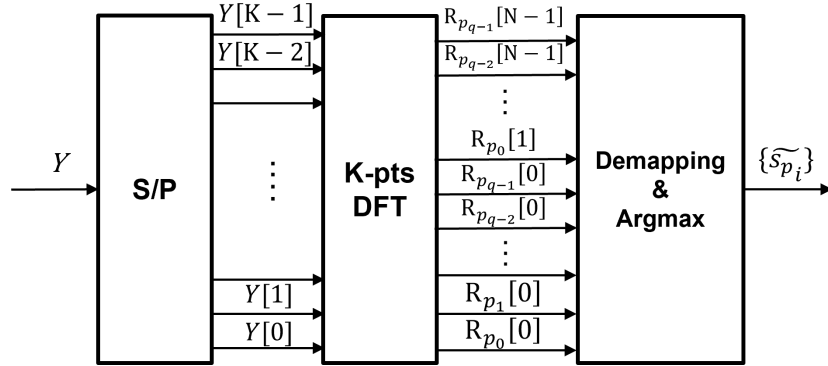


Figure 4.17: Receiver C with iterative mapping.

As for the single CCSK symbol transmission, the performances of scheme A, B or C are equivalent (only one scheme is plotted). Since the energy spent per transmitted bit E_b does not depend on q , the value of N_0 is the same for a level of $\frac{E_b}{N_0}$ and is independent of q . A direct consequence is that the power of the noise in frequency is the same for all the sub-carriers, leading to error probability and performance independent of q .

4.4.5 PAPR of Iterative Mapping

This section studies the impact of the iterative mapping on the PAPR. The Eq. 4.39 provides the transmitted signal expression after the OFDM-IDFT operation (scheme A or B):

$$C[k] = \frac{F(x_u)[0]}{\sqrt{q}} \sum_{i=0}^{q-1} x_u^*[-u^{-1}k - p_i] x_u[-p_i] \exp\left(j2\pi \frac{ik}{K}\right) \quad (4.45)$$

The energy of the k^{th} sample is defined as:

$$|C[k]|^2 = \frac{|F(x_u)[0]|^2}{q} \sum_{i,l=0}^{q-1} x_u^*[-u^{-1}k - p_i] x_u[-u^{-1}k - p_l] x_u[-p_i] x_u^*[-p_l] \exp\left(j2\pi \frac{(i-l)k}{K}\right) \quad (4.46)$$

As detailed in Eq. 3.9 $F(x_u)[0] = \pm \exp(\pm j\frac{\pi}{4})$, leading to $|F(x_u)[0]|^2 = 1$. Hence we have:

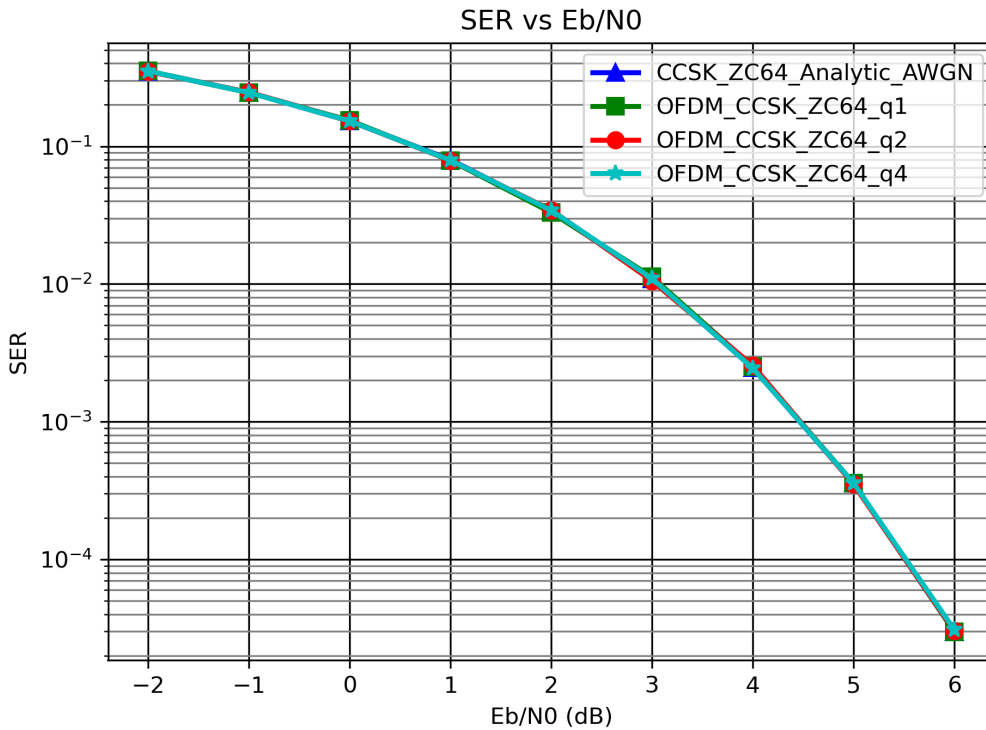


Figure 4.18: SER vs E_b/N_0 considering iterative mapping, AWGN channel.

$$\begin{aligned}
 |C[k]|^2 &= \frac{1}{q} \sum_{i,l=0}^{q-1} \exp \left(j\pi \frac{u(-u^{-1}k - p_i)^2 - u(-u^{-1}k - p_l)^2}{N} \right) \\
 &\quad \exp \left(j\pi \frac{u(-p_l)^2 - u(-p_i)^2}{N} \right) \exp \left(j2\pi \frac{(i-l)k}{K} \right) \\
 &= \frac{1}{q} \sum_{i,l=0}^{q-1} \exp \left(j\pi \frac{2uu^{-1}k(p_i - p_l) + u(p_i^2 - p_l^2)}{N} \right) \exp \left(j\pi \frac{up_l^2 - up_i^2}{N} \right) \\
 &\quad \exp \left(j2\pi \frac{(i-l)k}{K} \right) \\
 &= \frac{1}{q} \sum_{i,l=0}^{q-1} \exp \left(j\pi \frac{2uu^{-1}k(p_i - p_l)}{N} \right) \exp \left(j2\pi \frac{(i-l)k}{K} \right)
 \end{aligned} \tag{4.47}$$

By definition, $\exists \alpha \in \mathbb{N}$ so that $uu^{-1} = \alpha N + 1$. Consequently, we obtain:

$$\begin{aligned}
|C[k]|^2 &= \frac{1}{q} \sum_{i,l=0}^{q-1} \exp \left(j\pi \frac{2k(p_i - p_l)}{N} \right) \exp \left(j2\pi \frac{(i-l)k}{K} \right) \\
&= \frac{1}{q} \sum_{i,l=0}^{q-1} \exp \left(j2\pi k \frac{q(p_i - p_l) + (i-l)}{K} \right) \\
&= 1 + \frac{1}{q} \sum_{\substack{i,l=0 \\ i \neq l}}^{q-1} \exp \left(j2\pi k \frac{q(p_i - p_l) + (i-l)}{K} \right) \\
&= 1 + \frac{2}{q} \sum_{i=1}^{q-1} \sum_{l=0}^{i-1} \cos \left(2\pi k \frac{q(p_i - p_l) + (i-l)}{K} \right)
\end{aligned} \tag{4.48}$$

The maximum sample energy is reached if all the cosine are equal to 1, which is only the case when $k = 0$. The maximum is then $\max(|C[k]|^2) = q$. The mean energy (or power) of the transmitted samples is defined as:

$$\frac{1}{K} \sum_{k=0}^{K-1} |C[k]|^2 = 1 + \frac{1}{qK} \sum_{\substack{i,l=0 \\ i \neq l}}^{q-1} \sum_{k=0}^{K-1} \exp \left(j2\pi \frac{q(p_i - p_l) + (i-l)}{K} \right)^k \tag{4.49}$$

The remaining summations are applied to K^{th} roots of unity non equal to 1, which means that the sums are null. The mean sample energy is then always equal to one. Finally, the PAPR associated with the iterative mapping in scheme A and B is always equal to:

$$\text{PAPR}_{\text{dB}} = 10 \log_{10} \left(\frac{|s_{\text{peak}}|^2}{s_{\text{RMS}}^2} \right) = 10 \log_{10}(q) \tag{4.50}$$

It is interesting to note that the PAPR is independent of the $(p_i)_{i \in [0:q-1]}$, the ZC sequence index or the sequence length N. Also, when $q = 1$, we retrieve the equality $\text{PAPR}_{\text{dB}} = 0$.

In the case of the communication scheme C, an Hadamard product is applied between the IDFT of the CCSK symbols, noted C , and the complex conjugate of the IDFT of the correlation sequence b , noted B . The Hadamard product between C and B^* (see Eq.4.43), noted X , is defined as:

$$X[k] = (C \odot B^*)[k] = \frac{|\mathcal{F}_0|^2}{\sqrt{q}} x_u[-u^{-1}k] \sum_{i=0}^{q-1} x_u^*[-u^{-1}k - p_i] x_u[-p_i] \exp \left(j2\pi \frac{ik}{K} \right) \tag{4.51}$$

The energy of the k^{th} sample is:

$$\begin{aligned}
|X[k]|^2 &= \frac{1}{q} \sum_{i,l=0}^{q-1} \exp \left(j2\pi k \frac{q(p_i - p_l) + (i-l)}{K} \right) \\
&= \frac{1}{q} \sum_{i,l=0}^{q-1} \exp \left(j2\pi k \frac{q(p_i - p_l) + (i-l)}{K} \right)
\end{aligned} \tag{4.52}$$

From previous results, we directly obtained that $\max(|X[k]|^2) = q$ and that $\frac{1}{K} \sum_{k=0}^{K-1} |X[k]|^2 = 1$. The PAPR is then the same for all the schemes A, B and C, and is equal to $10 \log_{10}(q)$ dB.

5 Fading Channel

5.1 Cyclic Prefix and Circular Convolution

The Cyclic Prefix (CP) is part of the CP-OFDM modulation, usually used in communication system as the 4G and 5G communications systems. The CP is a copy of the end of the OFDM symbol (after the IDFT), placed at the beginning of the OFDM symbol. The number of samples copied depends on the system. At the receiver, the CP is removed before processing the DFT operation. The transmitter and receiver of CP-OFDM are respectively described on Figure 5.1 and Figure 5.2.

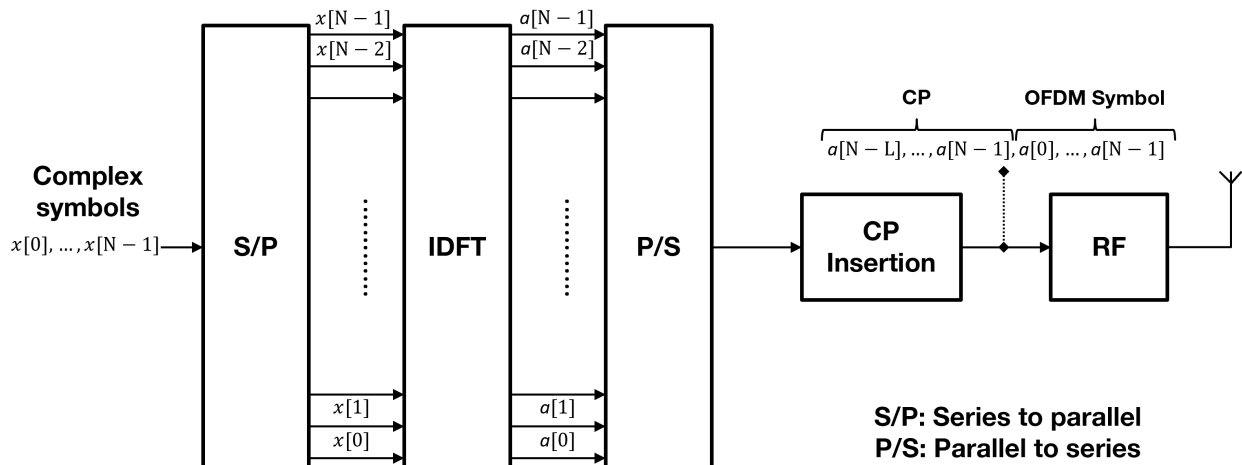


Figure 5.1: Standard CP-OFDM transmitter.

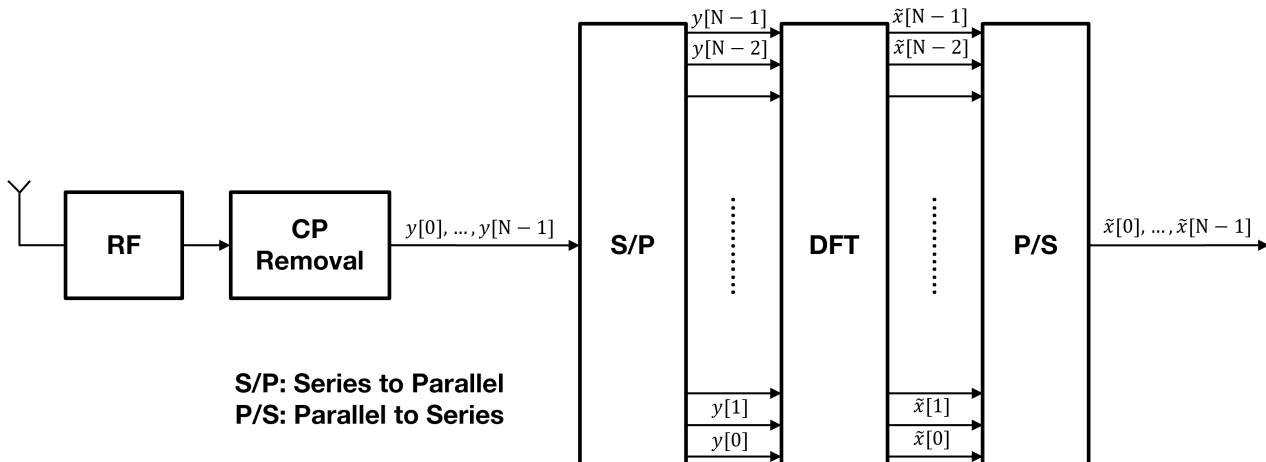


Figure 5.2: Standard CP-OFDM receiver.

We consider a multipath channel with a Channel Impulse Response (CIR) of several taps, i.e. the channel can be defined as a sequence of complex values $[h_0, h_1, \dots, h_{L-1}]$, convoluted to the transmitted signal. Usually, the taps are defined at symbol rate, so the CIR describes the temporal Inter-Symbols Interference (ISI) due to multipath propagation. In the case of OFDM, this ISI results in breaking the orthogonality of the sub-carriers.

Using the CP removes the ISI, allowing a one-tap channel equalization process in frequency. The only condition is for the CP length to be superior or equal to the CIR length. To understand the effect

of the CP, we consider a CIR of length L defined as $h = [h_0, h_1, \dots, h_{L-1}]$ and a CP also of length L. The transmitted signal a is defined as the sequence of length N + L time samples:

$$a = [a[N-L], \dots, a[N-1], a[0], \dots, a[N-1]] \quad (5.1)$$

Affected by the propagation channel h , the received signal y is defined as the convolution of the channel h with the signal a :

$$y[k] = (h * a)[k] \quad (5.2)$$

Removing the CP, the first L symbols of the OFDM symbol are affected by ISI from the CP symbols, i.e. the last L symbols of the OFDM symbol. Hence the OFDM symbol appears as locally N-periodic and the previous convolution becomes a circular convolution:

$$y[k] = (h_N \circledast a_{[L:N+L]}[k]) \quad (5.3)$$

with h_N the CIR padded with zero to length N and $a_{[L:N+L]}$ the OFDM symbol without CP. Using the convolution theorem of the (discrete) Fourier transform, the DFT operation at the receiver can be expressed as:

$$F(y)[k] = F(h_N \circledast a_{[L:N+L]}[k]) = \sqrt{N} F(h_N)[k] F(a_{[L:N+L]}[k]) \quad (5.4)$$

The term $F(a_{[L:N+L]})$ correspond to the DFT of the OFDM symbol as in the standard OFDM modulation. The first term however, correspond to the DFT of the channel on each sub-carrier. Hence, after the DFT at the receiver, each symbol mapped on a sub-carrier is affected by a one-tap channel, i.e. a complex scalar, equal to the unnormalized DFT of the channel at the corresponding sub-carrier. This lead to a simple equalization process and is one of the reasons behind the success of CP-OFDM.

Another explanation can be provided by a matrix-based description of the problem. The circular convolution can be described by a standard matrix multiplication between a circulant matrix \mathbf{H} and the vector of symbols \mathbf{a} :

$$\mathbf{y} = \mathbf{H}\mathbf{a} = \begin{pmatrix} h_0 & 0 & 0 & \dots & h_2 & h_1 \\ h_1 & h_0 & 0 & \dots & h_3 & h_2 \\ h_2 & h_1 & h_0 & \dots & h_4 & h_3 \\ \ddots & \ddots & \ddots & & & \\ \ddots & \ddots & \ddots & & & \\ 0 & 0 & 0 & \dots & h_1 & h_0 \end{pmatrix} \begin{pmatrix} a[0] \\ a[1] \\ \vdots \\ a[N-1] \end{pmatrix} \quad (5.5)$$

The vector \mathbf{a} contains the OFDM symbol without the CP. The matrix \mathbf{H} is a square matrix of size N, representing the circular convolution of the channel with \mathbf{a} . A circulant matrix is a special case of Toeplitz matrix, where each line is the right-shifted version of the one above. To simplify the following equations, we define the first line of \mathbf{H} as $[h_0, h_{N-1}, h_{N-2}, \dots, h_2, h_1]$, with $h_{N-1} = h_{N-2} = h_L = 0$. The following lines are then right-shifted versions of the first one.

$$\mathbf{H} = \begin{pmatrix} h_0 & h_{N-1} & h_{N-2} & \dots & h_2 & h_1 \\ h_1 & h_0 & h_{N-1} & \dots & h_3 & h_2 \\ h_2 & h_1 & h_0 & \dots & h_4 & h_3 \\ \ddots & \ddots & \ddots & & & \\ \ddots & \ddots & \ddots & & & \\ h_{N-1} & h_{N-2} & h_{N-3} & \dots & h_1 & h_0 \end{pmatrix} \quad (5.6)$$

It can be shown that any circulant matrix is diagonalizable on \mathbb{C} . Its eigenvectors, which form a basis of \mathbb{C}^N by definition, are the Fourier coefficients. The normalized eigenvector \mathbf{g}_k , for $k \in [0; N-1]$,

is defined as:

$$\mathbf{g}_k = \frac{1}{\sqrt{N}} \begin{pmatrix} 1 \\ \exp(j2\pi \frac{k}{N}) \\ \exp(j2\pi \frac{2k}{N}) \\ \vdots \\ \exp(j2\pi \frac{(N-1)k}{N}) \end{pmatrix} \quad (5.7)$$

The associated eigenvalue, noted λ_k , is defined as:

$$\lambda_k = h_0 + h_{N-1} \exp\left(j2\pi \frac{k}{N}\right) + h_{N-2} \exp\left(j2\pi \frac{2k}{N}\right) + \dots + h_1 \exp\left(j2\pi \frac{(N-1)k}{N}\right) \quad (5.8)$$

For the N^{th} root of unity, we have the equality $\exp(j2\pi \frac{n}{N}) = \exp(-j2\pi \frac{N-n}{N})$. This leads to:

$$\lambda_k = \sum_{n=0}^{N-1} h_n \exp\left(-j2\pi \frac{nk}{N}\right) \quad (5.9)$$

Consequently, the eigenvalue λ_k corresponds to the k^{th} sample of the N-length unnormalized DFT of the CIR (padded with zeros). This last observation is equivalent to the result of Equation 5.4.

Since \mathbf{H} is diagonalizable, we have:

$$\mathbf{H} = \mathbf{F}^H \mathbf{D} \mathbf{F} \quad (5.10)$$

where \cdot^H is the Hermitian transpose (or conjugate transpose, or adjoint matrix) operator, \mathbf{D} is the diagonal matrix where the diagonal elements are the eigenvalues of \mathbf{H} and \mathbf{F} is a unitary¹ matrix whose columns are the normalized eigenvectors of \mathbf{H} in the canonical basis of \mathbb{C}^N :

$$\mathbf{F} = \frac{1}{\sqrt{N}} \begin{pmatrix} 1 & 1 & \dots & 1 \\ 1 & \exp(-j2\pi \frac{1}{N}) & \dots & \exp(-j2\pi \frac{(N-1)}{N}) \\ 1 & \exp(-j2\pi \frac{2}{N}) & \dots & \exp(-j2\pi \frac{2(N-1)}{N}) \\ \vdots & & & \vdots \\ 1 & \exp(-j2\pi \frac{(N-1)}{N}) & \dots & \exp(-j2\pi \frac{(N-1)^2}{N}) \end{pmatrix} \quad (5.11)$$

Moreover, the matrix \mathbf{F} also describes the DFT function of length N. Hence, computing the DFT of a sequence x of length N, represented as a vector \mathbf{x} , is defined as \mathbf{Fx} . The elements of the resulting vector are the elements of the DFT. The IDFT operation is realized by a multiplication with the matrix \mathbf{F}^H .

Consequently, in the receiver, the DFT of \mathbf{y} can be represented as:

$$\begin{aligned} \mathbf{F}(\mathbf{y}) &= \mathbf{Fy} \\ &= \mathbf{FHx} \\ &= \mathbf{FF}^H \mathbf{DFx} \\ &= \mathbf{DFx} \end{aligned} \quad (5.12)$$

\mathbf{Fx} corresponds to the DFT of \mathbf{x} , and each element is multiplied by the eigenvalues of \mathbf{H} on the diagonal of \mathbf{D} .

5.2 Inclusion of the CP in Schemes A, B and C

The following sections present the modification of schemes A, B and C to include a CP. The CP is always added just before the Radio Frequency (RF) block in the transmitter and removed just after the RF block in the receiver. In this section, q CCSK symbols per OFDM symbol are considered with an iterative mapping.

¹ $\mathbf{F}\mathbf{F}^H = \mathbf{I}$, with \mathbf{I} the identity matrix.

5.2.1 Scheme CP-A

The scheme CP-A realizes the CCSK modulation followed by the OFDM modulation without any specific interaction between them. The CCSK symbol are simply mapped on the OFDM sub-carriers as standard modulated symbols. Consequently, the usage of the CP is straightforward as showed in Figure 5.3. After the DFT, the symbols of the CCSK are equalized. As described in Section 5.1, this equalization has a single tap, leading to a simple process. The equalized CCSK symbol is then demodulated. This standard receiver enables an efficient coherent demodulation of the CCSK symbol.

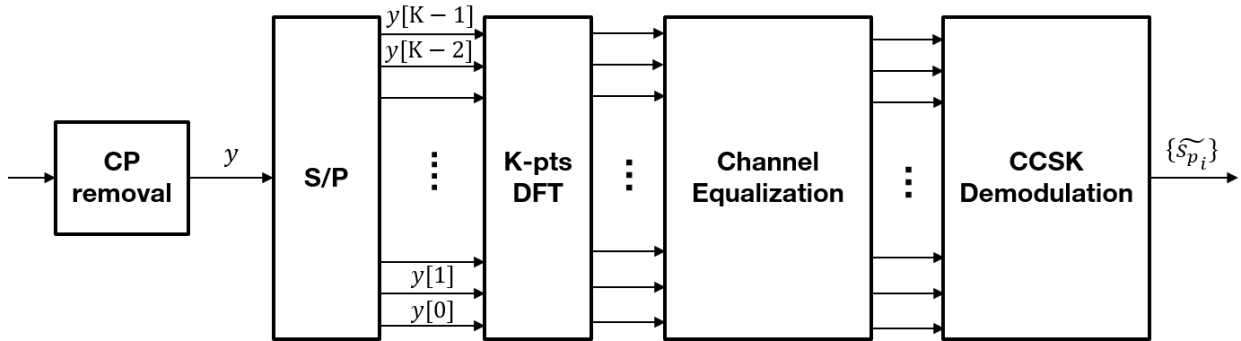


Figure 5.3: Receiver of scheme CP-A.

5.2.2 Scheme CP-B

The scheme CP-B applies an Hadamard product between the received OFDM symbol without the CP and the conjugate of the IDFT of the root sequence, scaled by \sqrt{q} . The Figure 5.4 describes this receiver.

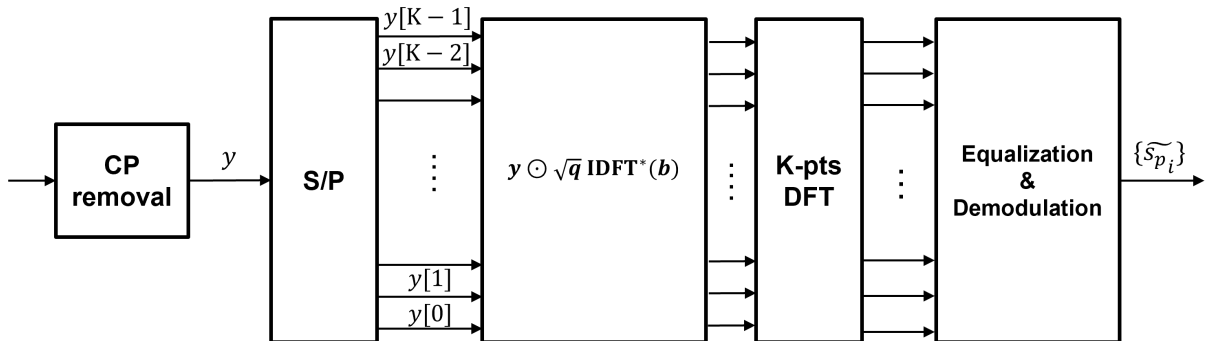


Figure 5.4: Receiver of scheme CP-B.

To understand the impact of the Hadamard product, we consider the matrix representation of y , without noise, as:

$$\mathbf{y} = \mathbf{H}\mathbf{x} = \mathbf{F}^H \mathbf{D}\mathbf{F}\mathbf{x} \quad (5.13)$$

where \mathbf{y} is the vector of received samples, \mathbf{H} is the circular channel matrix and \mathbf{x} is the vector of transmitted symbols. The matrices representing the DFT and IDFT operations are respectively noted \mathbf{F} and \mathbf{F}^H , with \cdot^H is the Hermitian transpose (or conjugate transpose, or adjoint matrix) operator. The DFT matrix is expressed as in Equation 5.11. The matrix \mathbf{D} is diagonal, with the eigenvalues of \mathbf{H} on its diagonal. The vector of the root ZC sequence is noted \mathbf{c}_0 and the oversampled version is defined as:

$$b[n] = \begin{cases} c_0[l] & , \text{if } n \equiv 0 \pmod{q} = lq \\ 0 & , \text{otherwise} \end{cases} \quad (5.14)$$

with the associated vector \mathbf{b} . The transmitted samples are expressed as $\mathbf{x} = \mathbf{F}^H \mathbf{c}$, with the sequence c defined as $c[lq + i] = c_{p_i}[l]$, $l \in [0; N - 1]$ and $i \in [0; q - 1]$. Finally, noting the vector or matrix complex conjugate operator as $\bar{\cdot}$, we obtain after the DFT in reception:

$$\begin{aligned}\mathbf{F}(\mathbf{y} \odot \sqrt{q} \bar{\mathbf{F}^H \mathbf{b}}) &= \sqrt{q} \mathbf{F}(\mathbf{F}^H \mathbf{D} \mathbf{F} \mathbf{x} \odot \bar{\mathbf{F}^H \mathbf{b}}) \\ &= \sqrt{q} \mathbf{F}(\mathbf{F}^H \mathbf{D} \mathbf{F} \mathbf{F}^H \mathbf{c} \odot \bar{\mathbf{F}^H \mathbf{b}}) \\ &= \sqrt{q} \mathbf{F}(\mathbf{F}^H \mathbf{D} \mathbf{c} \odot \bar{\mathbf{F}^H \mathbf{b}})\end{aligned}\quad (5.15)$$

On the last equation, we recognize the formula of the right-shifted cross-correlation (see Eq.4.45) scaled by $\frac{1}{\sqrt{N}}$ between the sequences $\mathbf{D} \mathbf{c}$ and \mathbf{c}_0 . Noting as λ_k for $k \in [0; K - 1]$ the eigenvalues of \mathbf{H} corresponding to the unnormalized DFT of the CIR, the symbol on the i^{th} sub-carrier is:

$$\theta[i] = \frac{1}{\sqrt{N}} \sum_{k=0}^{K-1} \lambda_k c[k] b^*[k - i] \quad (5.16)$$

Without noise, the $\theta[i]$ represents the cross-correlation between the transmitted sequence affected by the propagation channel in frequency and the root sequence. This expression is similar as the Eq.4.41, but the summation is weighted by the λ_k . Consequently, the result is not easy to compute as it depends on the correlation of the channel across the sub-carriers.

5.2.3 Scheme CP-C

The scheme CP-C applies the Hadamard product at the transmitter, before the CP block is added. Ignoring the noise in the receiver, the CP is removed and the DFT of the samples \mathbf{y} is expressed as:

$$\begin{aligned}\mathbf{Fy} &= \sqrt{q} \mathbf{F} \mathbf{F}^H \mathbf{D} \mathbf{F} (\mathbf{F}^H \mathbf{c} \odot \bar{\mathbf{F}^H \mathbf{b}}) \\ &= \sqrt{q} \mathbf{D} \mathbf{F} (\mathbf{F}^H \mathbf{c} \odot \bar{\mathbf{F}^H \mathbf{b}})\end{aligned}\quad (5.17)$$

Consequently, the symbol on the i^{th} sub-carrier is:

$$\theta[i] = \frac{\lambda_i}{\sqrt{N}} \sum_{k=0}^{K-1} c[k] b^*[k - i] \quad (5.18)$$

Hence, the symbol $\theta[i]$ is equal to the cross-correlation of the transmitted sequence and root sequence which is equivalent to the usual case of Eq.4.41. The correlation value is weighted by the complex channel coefficient on this sub-carrier. This means that the standard OFDM one-tap equalization process can be used, as proposed on the Figure 5.5.

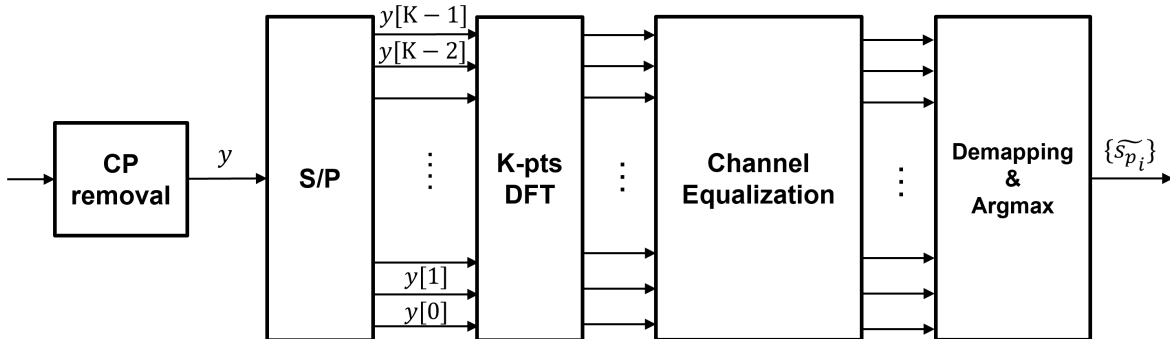


Figure 5.5: Receiver of scheme CP-C.

Noting the maximum correlation index set I_s , we have:

$$\theta[i] = \begin{cases} \lambda_i \sqrt{N} & , \text{if } i \in I_s \\ 0 & , \text{otherwise} \end{cases} \quad (5.19)$$

Thus, without noise, the correlation absolute value depends solely on the channel coefficient. In case of deep fading at the wrong sub-carrier, the correct shift value could be hidden by the noise.

5.3 Channel Estimation

5.3.1 Pilots Positions

Channel estimation in CP-OFDM has been largely studied in the literature [14] [15]. The objective of the channel estimation step is to get an estimation of the one tap channel complex value on each data sub-carrier. In this regard, communications systems usually place pilots symbols on specific sub-carriers, to be able to get an accurate channel estimation for these sub-carriers, and then interpolate the channel to the rest of the sub-carriers. This technique is called Pilot-Symbol Assisted Modulation (PSAM). One common way to position the pilots is described in Figure 5.6. In this case, the pilots occupy entire OFDM symbols (in frequency). This pilots positioning is known as block pilots. After the channel estimation at the pilot sub-carriers, the receiver can interpolate the channel in time to obtain a channel estimation for the rest of the sub-carriers and then be able to equalize the channel. In case of several OFDM symbols dedicated to pilots, this supposes to first receive the whole frame (all the OFDM symbols) and then process the interpolation. Block type arrangement are well suited for slowly varying channel (slow fading) and highly frequency selective channel [16].

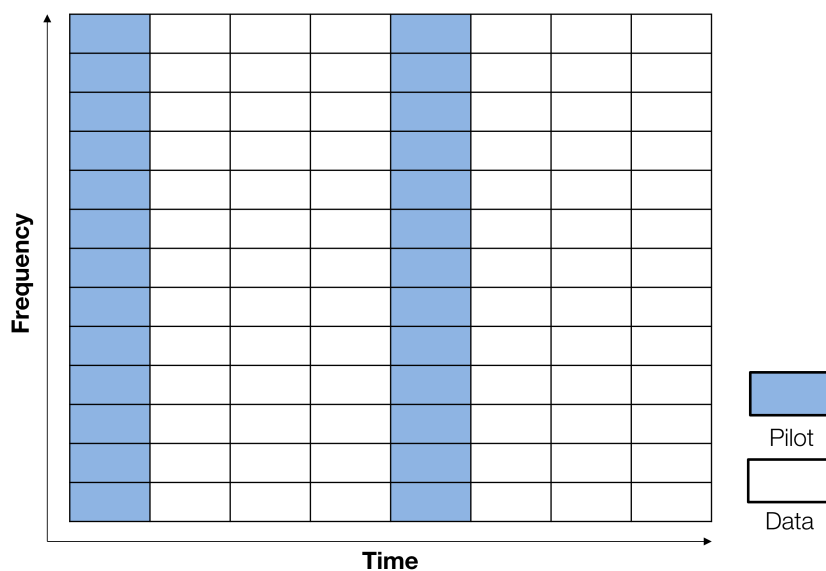


Figure 5.6: Block-type pilots arrangement.

Another pilots positioning is proposed in Figure 5.7. The pilots are spread in time, always on the same sub-carriers. In this case, the receiver interpolates the channel in frequency to get the channel values on the data sub-carriers. This arrangement, the comb-type, is adapted to fast fading but is more sensitive to frequency selectivity [16].

A sparse version of the pilots positioning is presented in Figure 5.8. The interpolation will then be processed in frequency and time, as either a 2D process or on one dimension and then another. The quality of the interpolation depends on the algorithm used, but also on the channel auto-correlation function in frequency and time.

From now on, we assume that the channel is a wide-sens stationary process, with uncorrelated paths. The channel coherence bandwidth dictates the correlation between channel values on different sub-carriers. If the channel coherence bandwidth is far larger than the system bandwidth, one can assume the channel as constant on all the sub-carriers of an OFDM symbol. In this case, the CIR is a one-tap channel: there is no ISI (in time) and the channel is not frequency selective. Such a fading is said flat. If the channel has a multi-tap CIR, the channel coherence bandwidth is then shorter than the system bandwidth, and the channel is not constant in frequency. The channel coherence

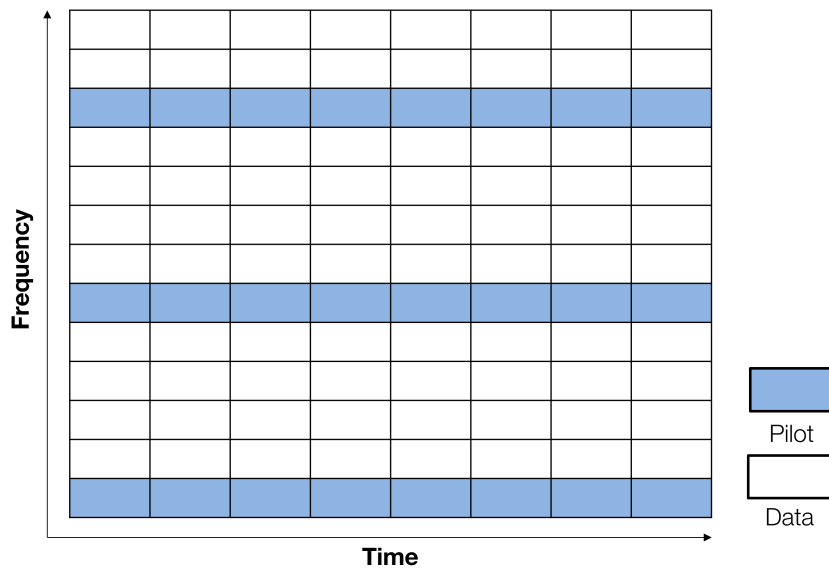


Figure 5.7: Comb-type pilots arrangement.

bandwidth is inversely proportional to the root mean square delay spread:

$$B \approx \frac{1}{\tau_{\text{rms}}} \quad (5.20)$$

where τ_{rms} is the root mean square delay spread of the channel, which represents the dispersion of the channel power in time. Hence, the higher the channel power spreading, the shorter the coherence bandwidth.

The channel time correlation on each sub-carrier depends on the maximum Doppler shift. The larger the Doppler shift, the quicker the channel evolves in time, resulting in a shorter channel coherence time. If the maximum Doppler shift is null, the channel on each sub-carrier is then constant in time. The (one-sided) maximum Doppler shift f_{\max} and a definition of the channel coherence time T are:

$$\begin{aligned} f_{\max} &= \frac{v}{c} f_c \\ T &\approx \frac{1}{f_{\max}} \end{aligned} \quad (5.21)$$

where v is the relative movement speed of the transmitter from the receiver in m/s, c is the light speed and f_c is the carrier frequency.

Consequently, there is a minimal channel sampling rate in time and frequency to be able to capture its evolutions. The sampling theorem tells us that the pilots positions have to respect the following rules [17] [18] [19]:

- Noting τ_{\max} the maximum path delay in second and Δ_f the sub-carrier spacing in Hz, the pilot spacing in frequency N_k should respect the following inequality:

$$N_k \leq \frac{1}{\tau_{\max} \Delta_f} \quad (5.22)$$

- Noting T_{Symbol} the total duration of the OFDM symbol and CP in second, the pilot spacing in time N_n should respect the following inequality:

$$N_n \leq \frac{1}{2 f_{\max} T_{\text{Symbol}}} \quad (5.23)$$

An oversampling of four seems to be a good balance between performance and transmission efficiency [18].

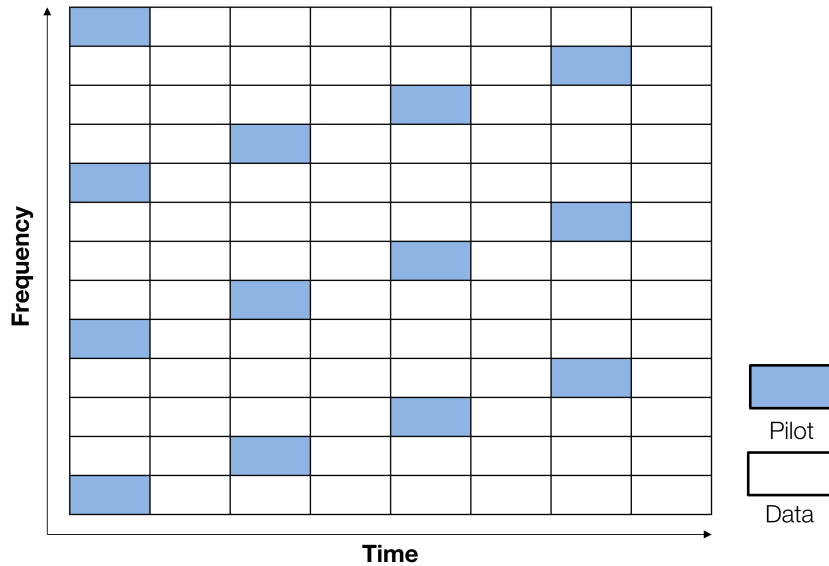


Figure 5.8: Sparse pilots positioning.

5.3.2 Least-Square Estimation

We assume an OFDM communication system transmitting an OFDM frame constituted of S OFDM symbols of K sub-carriers each. In the frequency domain, the received n^{th} OFDM symbol is expressed as:

$$\mathbf{y}_n = \mathbf{X}_n \mathbf{h}_n + \mathbf{w}_n \quad (5.24)$$

where $\mathbf{y}_n = [y_{0,n}, \dots, y_{K-1,n}]^T \in \mathbb{C}^{K \times 1}$ is the vector of received complex symbols on each sub-carriers, $\mathbf{w}_n = [w_{0,n}, \dots, w_{K-1,n}]^T \in \mathbb{C}^{K \times 1}$ is the vector of AWGN samples, \mathbf{X}_n is a diagonal matrix of size $K \times K$ containing the transmitted complex symbols $x_{k,n}$ on each sub-carrier and $\mathbf{h}_n = [h_{0,n}, \dots, h_{K-1,n}]^T \in \mathbb{C}^{K \times 1}$ is the vector containing the unnormalized DFT of the time channel CIR of size L padded with zeros to a size of K. We note (p, n_p) the sub-carrier and OFDM symbol indices of any pilot. The Least-Square (LS) estimate is the solution of the following equation:

$$\mathbf{h}_{n_p}^{\text{LS}} = \underset{\mathbf{h}}{\operatorname{argmin}} \|\mathbf{X}_{n_p} \mathbf{h} - \mathbf{y}_{n_p}\|^2 \quad (5.25)$$

In the single tap channel case, and for non null pilots, the solution is simply:

$$\mathbf{h}_{n_p}^{\text{LS}} = \mathbf{X}_{n_p}^{-1} \mathbf{y}_{n_p} \quad (5.26)$$

Hence, the LS estimate of the channel at pilots sub-carriers is defined as:

$$h_{p,n_p}^{\text{LS}} = \frac{y_{p,n_p}}{x_{p,n_p}} = h_{p,n_p} + \frac{w_{p,n_p}}{x_{p,n_p}} \quad (5.27)$$

If we assume that the complex pilots are on the unit circle, so that the resulting noise component has the same distribution as w_{p,n_p} , we have $h_{p,n_p}^{\text{LS}} = h_{p,n_p} + w'_{p,n_p}$. Hence, the LS estimate is directly affected by a complex Gaussian noise.

5.3.3 LMMSE Estimations

The optimal channel estimation algorithm, in the mean square sens, is the Linear Minimum Mean Square Estimator (LMMSE). Related to the 1D version of the Wiener filter [17] [20] [15] [18], and developed in [21] [22], the LMMSE estimate solves the following equation:

$$h_{k,n}^{\text{LMMSE}} = \underset{\tilde{h} \in \mathbb{C}}{\operatorname{argmin}} \mathbb{E}[|h_{k,n} - \tilde{h}|^2] \quad (5.28)$$

The following expressions assume block-type pilot positioning, so all the sub-carriers of one or several OFDM symbols are filled with pilots symbols. In frequency, the LMMSE estimate in a pilot OFDM symbol of index n_p is defined as:

$$\mathbf{h}_{n_p}^{\text{LMMSE}} = \mathbf{R}_{\mathbf{hh}}(\mathbf{R}_{\mathbf{hh}} + \sigma^2(\mathbf{X}_{n_p}\mathbf{X}_{n_p}^H)^{-1})^{-1}\mathbf{h}_{n_p}^{\text{LS}} \quad (5.29)$$

where $\mathbf{R}_{\mathbf{hh}}$ is the channel frequency auto-correlation matrix, defined as $\mathbf{R}_{\mathbf{hh}} = \mathbb{E}[\mathbf{h}\mathbf{h}^H]$, σ^2 is the noise variance, \mathbf{X}_{n_p} is the diagonal matrix containing the pilots symbols of the OFDM symbol n_p on its diagonal, and $\mathbf{h}_{n_p}^{\text{LS}}$ is the LS channel estimate of the channel in the OFDM symbol n_p . The block $\mathbf{R}_{\mathbf{hh}}(\mathbf{R}_{\mathbf{hh}} + \sigma^2(\mathbf{X}_{n_p}\mathbf{X}_{n_p}^H)^{-1})^{-1}$ acts as a noise smoothing filter on $\mathbf{h}_{n_p}^{\text{LS}}$ to improve the channel estimation. The performance of the LMMSE are close to those of a perfect channel knowledge [15]. Note that the LMMSE can also be applied in time with comb-type pilots arrangement. In this case, $\mathbf{R}_{\mathbf{hh}}$ is the time auto-correlation matrix. Finally, the noise power σ^2 is supposed known or can be approximated by the system.

The LMMSE formula implies expensive computation, due to large matrix inversions and multiplication, and computation of the channel auto-covariance matrix $\mathbf{R}_{\mathbf{hh}}$. Consequently, several simplifications of the above formula are available in the literature [15]. First of all, assuming that the pilots are of constant unitary power, so that $|x_{p,n_p}|^2 = 1$, we obtain the first common simplification of the formula as:

$$\mathbf{h}_{n_p}^{\text{LMMSE}} = \mathbf{R}_{\mathbf{hh}}(\mathbf{R}_{\mathbf{hh}} + \sigma^2 \mathbf{Id})^{-1}\mathbf{h}_{n_p}^{\text{LS}} \quad (5.30)$$

where \mathbf{Id} is the identity matrix of dimension $K \times K$. Another simplification comes from the fact that $\mathbf{R}_{\mathbf{hh}}$ is Hermitian and thus is diagonalisable in \mathbb{C} as $\mathbf{R}_{\mathbf{hh}} = \mathbf{UDU}^H$, with \mathbf{U} a unitary matrix composed by the eigenvectors and \mathbf{D} a diagonal matrix containing the real eigenvalues of $\mathbf{R}_{\mathbf{hh}}$ on its diagonal, noted λ_k for $k \in [0, K - 1]$ [22]. The LMMSE estimate can then be expressed as:

$$\mathbf{h}_{n_p}^{\text{LMMSE}} = \mathbf{UD}_\sigma \mathbf{U}^H \mathbf{h}_{n_p}^{\text{LS}} \quad (5.31)$$

where \mathbf{D}_σ is a diagonal matrix, with its diagonal elements expressed as:

$$\delta_k = \frac{\lambda_k}{\lambda_k + \sigma^2} \quad (5.32)$$

With this diagonalisation, no computation intensive matrix inversion is needed and the final complexity is greatly decrease. The last problem is that, in real life cases, the channel auto-correlation matrix is not known. A common way to circumvent this problem is the Low-Rank Approximation (LRA), which assumes a generic channel power delay profile and pre-computes the auto-correlation matrix and the eigenvalues. The power delay profile of a channel is a function of the delay providing the power of the channel in time. Two common power delay profiles are used. The first one is the exponentially decaying power delay profile, expressed as:

$$\Gamma(\tau) = C \exp\left(-\frac{\tau}{\tau_{\text{rms}}}\right) \quad (5.33)$$

with C a normalization coefficient and τ_{rms} the root mean square delay spread of the channel. For this power delay profile, the element (u, v) of the normalized auto-correlation matrix is equal to [22] [18]:

$$(\mathbf{R}_{\mathbf{hh}})_{u,v} = \frac{1 - \exp\left(-\frac{\tau_{\text{max}}}{\tau_{\text{rms}}}\right) \exp\left(-j2\pi\frac{\tau_{\text{max}}(u-v)}{K}\right)}{(1 - \exp\left(-\frac{\tau_{\text{max}}}{\tau_{\text{rms}}}\right))(1 + j2\pi\frac{\tau_{\text{rms}}(u-v)}{K})} \quad (5.34)$$

where τ_{max} and τ_{rms} are normalized by the sampling time. The normalization implies $(\mathbf{R}_{\mathbf{hh}})_{u,u} = \mathbb{E}[|h_u|^2] = 1$. Since the value of τ_{rms} and τ_{max} are not known a priori, it is possible to consider $\tau_{\text{rms}} = \tau_{\text{max}}$ and τ_{max} equal to the CP number of samples [15]. In this case, the power delay profile becomes:

$$\Gamma(\tau) = C \exp\left(-\frac{\tau}{\tau_{\text{max}}}\right) \quad (5.35)$$

and the auto-correlation matrix becomes:

$$(\mathbf{R}_{\mathbf{h}\mathbf{h}})_{u,v} = \frac{1 - \exp(-1) \exp\left(-j2\pi\frac{\tau_{\max}(u-v)}{K}\right)}{(1 - \exp(-1))(1 + j2\pi\frac{\tau_{\max}(u-v)}{K})} \quad (5.36)$$

The second commonly used power delay profile is the constant one:

$$\Gamma(\tau) = C \quad (5.37)$$

Leading to the normalized auto-correlation matrix [15][22]:

$$(\mathbf{R}_{\mathbf{h}\mathbf{h}})_{u,v} = \begin{cases} \frac{1 - \exp\left(-j2\pi\frac{\tau_{\max}(u-v)}{K}\right)}{j2\pi\frac{\tau_{\max}(u-v)}{K}}, & \text{when } u \neq v \\ 1, & \text{when } u = v \end{cases} \quad (5.38)$$

In both cases, the performances are usually between those of the exact LMMSE estimate and those of the LS estimate. The gap depends on the actual nature of the channel auto-correlation matrix [15]. Nevertheless, these two approximations offer a good compromise between performance and complexity. Other low complexity methods to obtain the channel auto-correlation and to estimate the noise variance are presented in [15].

5.3.4 Interpolation Algorithms

After channel estimation at pilot positions, the system still needs to provide an estimation at data positions. Interpolation algorithms are used to provide these channel estimations based on computed LS or (LRA-)LMMSE estimates. Looking at the OFDM frame as a 2D matrix, the optimal interpolation would be in 2D (Wiener Filter) [17] [18], but for complexity reason, it is usually done in (2x)1D. In this study, we consider an interpolation done first in frequency and then in time to map the whole OFDM frame with channel estimates. We also suppose that the pilots positions respect the sampling conditions provided in section 5.3.1. Consequently and for the purpose of clarity in the following sections, the interpolators operate only in frequency, on an arbitrary OFDM symbol where channel estimates has been computed at $N_p < K$ sub-carriers. The interpolators are presented in expected increasing performance order [23] [16] [24]. After the interpolation in frequency, the same interpolators can be used in time, reusing the same equations.

Nearest Neighbour Interpolator

The nearest neighbour interpolator simply takes the closest channel estimate in terms of sub-carrier index as the channel interpolate. This is the simplest interpolator possible, as no new computation is necessary. This interpolation algorithm can be of interest if the channel is highly correlated in frequency (or slowly evolving in time for time interpolation).

Linear Interpolator

We assume that two consecutive pilots are separated by a constant gap of M sub-carriers in frequency. The channel interpolate at sub-carrier position $kM + m$, between pilots at sub-carrier positions kM and $(k+1)M$, with $0 \leq m \leq M$, is equal to:

$$\tilde{h}_{kM+m} = h_{kM} + \frac{(h_{(k+1)M} - h_{kM})m}{M} \quad (5.39)$$

where h_{kM} and $h_{(k+1)M}$ are respectively the channel estimates at pilots kM and $(k+1)M$. For estimation at the edge, where there is no $h_{(k+1)M}$, we use the condition $h_{(k+1)M} = h_{kM}$.

Second-Order Polynomial Interpolator

With same assumptions and with the edge condition $h_{(k+1)M} = h_{kM} = h_{(k-1)M}$, the second-order polynomial interpolator is expressed as:

$$\tilde{h}_{kM+m} = \frac{\alpha(\alpha-1)}{2}h_{(k-1)M} - (\alpha^2 - 1)h_{kM} + \frac{\alpha(\alpha+1)}{2}h_{(k+1)M} \quad (5.40)$$

where $\alpha = \frac{m}{M}$.

Spline Cubic Interpolator

The concept behind the spline cubic interpolation is to construct a piece-wise function as third degree polynomials, that interpolates through all data points, is continuous over the whole interpolation interval, and the first and second derivative are also continuous (see [25] for a description of the algorithm). In this study, we have implemented a spline cubic interpolator that verify the “natural” condition, making the second derivative at endpoints equals to zero.

LMMSE Interpolator

The optimal interpolator in the sens of Mean Square Error (MSE) is the LMMSE [22]. To use the LMMSE algorithm as an interpolator, we modify the Eq.5.30 as (the dimension of the matrices has been noted as a subscript for clarity):

$$\mathbf{h}_{K \times 1}^{\text{LMMSE}} = \mathbf{R}_{\mathbf{h}\mathbf{h} K \times N_p} (\mathbf{R}_{\mathbf{h}\mathbf{h} N_p \times N_p} + \sigma^2 \mathbf{Id}_{N_p \times N_p})^{-1} \mathbf{h}_{N_p \times 1}^{\text{LS}} \quad (5.41)$$

where $\mathbf{h}_{N_p \times 1}^{\text{LS}}$ is the LS channel estimate at the pilots sub-carriers, considering N_p sub-carriers; $\mathbf{R}_{\mathbf{h}\mathbf{h} N_p \times N_p}$ is the auto-correlation matrix $\mathbf{R}_{\mathbf{h}\mathbf{h}}$ where only the rows and columns corresponding to the pilots sub-carriers positions has been extracted; $\mathbf{R}_{\mathbf{h}\mathbf{h} K \times N_p}$ is the auto-correlation matrix $\mathbf{R}_{\mathbf{h}\mathbf{h}}$ where only the columns corresponding to the pilots sub-carriers positions has been taken. The LMMSE interpolation can be used with the LRA approximations, but the Singular Value Decomposition (SVD) simplification of Eq.5.31 is not possible since the matrix are not square anymore.

Instead of interpolating, one can compute the LMMSE estimates at the N_p positions by replacing the auto-correlation matrix $\mathbf{R}_{\mathbf{h}\mathbf{h}}$ by $\mathbf{R}_{\mathbf{h}\mathbf{h} N_p \times N_p}$ in Eq.5.30. The LMMSE estimates is more accurate than their LS counterpart and can be used as inputs of other interpolation algorithms.

5.4 Zero-Forcing Equalizer

The Zero-Forcing (ZF) equalizer [26] is commonly used in CP-OFDM systems where each sub-carrier is affected by flatfading. In this case, the ZF equalizer is equivalent to the match filtering and the minimum mean square equalizer. To retrieve an estimate of the data x_k transmitted on sub-carrier k , the ZF equalizes the received data y_k with the estimated channel \tilde{h}_k :

$$\tilde{x}_k = \frac{y_k}{\tilde{h}_k} = x_k \frac{h_k}{\tilde{h}_k} + \frac{w_k}{\tilde{h}_k} \quad (5.42)$$

where w_k is the noise sample. Consequently, the ZF equalizer suffers from deep fading in frequency: when the channel magnitude at the sub-carrier is close to null, the noise sample is amplified and the information is lost. Hence, channel diversity is important to ensure that all the data sub-carriers are not affected by a deep fading at the same time.

5.5 Diversity Combining

As said above, the ZF equalizer is commonly used to retrieve the data symbol on each sub-carrier. Yet, in the case of the CCSK modulation, a cross-correlation along the sub-carriers has to be computed

to retrieve the modulated information. This means that the equalization should take into account the correlation operation. The ZF equalization would mitigate the correlation score, as deeply faded sub-carrier would increase the noise samples. Since the cross-correlation is equivalent to a weighted sum, the problem becomes a diversity combining one [27] [28]. With the right weights, the correlation can be improved by using the channel diversity across the sub-carriers.

In the following, we consider the Maximum Ratio Combining (MRC) for the diversity combining. The MRC multiplies each sub-carrier by the complex conjugate of the channel and normalizes the result. It acts as an equalizer, in addition to maximizing the resulting Signal to Noise Ratio (SNR) after the correlation. The traditional MRC equation is:

$$r = \frac{\sum_{k=0}^{K-1} h_k^* y_k}{\sum_{n=0}^{K-1} |h_n|^2} \quad (5.43)$$

5.6 Flatfading Performance

5.6.1 System Model

In the following, the system is designed with the following assumptions and described in Figure 5.9:

- The transmitter and receiver are based on CP-OFDM and CCSK schemes A, B or C. The CP length is fixed to 10 symbols, which is always longer than the channel length.
- The dimension of the OFDM symbol is equal to the size of the ZC sequence, and noted $N = 64$. Consequently, each OFDM symbol carries a single ZC sequence, corresponding to a single CCSK symbol, representing binary word of 6 bits.
- We do not use the iterative mapping to simplify the system, the explanations and the equations. Also the inclusion of the iterative mapping would only marginally modify the performances, as it would only change the interaction with the channel frequency diversity parameter.
- The OFDM frame is composed of 20 successive OFDM symbols.
- The first and the last OFDM symbols are used as block pilot symbols. Hence the channel is estimated on each sub-carrier in the first and last OFDM symbols, and then interpolated with the linear interpolator in time over the data symbols. We use the root ZC sequence for the pilots symbols.
- We use the MRC scheme as an equalizer to improve the cross-correlation operation and the performance of the systems.
- The received signal is in base-band, perfectly synchronized at symbol rate.

In this section, the propagation channel considered is a single tap channel. We use the usual Clarke's 2D isotropic model [29][30] to generate the channel coefficients. Consequently, the channel impulse response is described as a single complex coefficient h_t , whose amplitude follows a normalized Rayleigh distribution $\mathcal{R}(\frac{1}{\sqrt{2}})$, so that $h_t = h_r + jh_i$ and $h_r \sim \mathcal{N}(0, \frac{1}{2})$, $h_i \sim \mathcal{N}(0, \frac{1}{2})$ and $\mathbb{E}[|h_t|^2] = 1$. Its phase is uniformly distributed on $[0; 2\pi]$.

Because of its single tap nature, the channel is constant in frequency, also known as flatfading. The channel on any sub-carrier k , h_k , is equal to h_t . Hence, the normalization in time also leads to the normalization in frequency with $\mathbb{E}[|h_k|^2] = 1$ for $0 \leq k < N$.

5.6.2 Constant Channel

Equalization schemes

We first assume that the channel is constant over the whole OFDM frame. Equivalently, the maximum Doppler shift is equal to zero. In Figure 5.10, we compare standard approaches presented in section

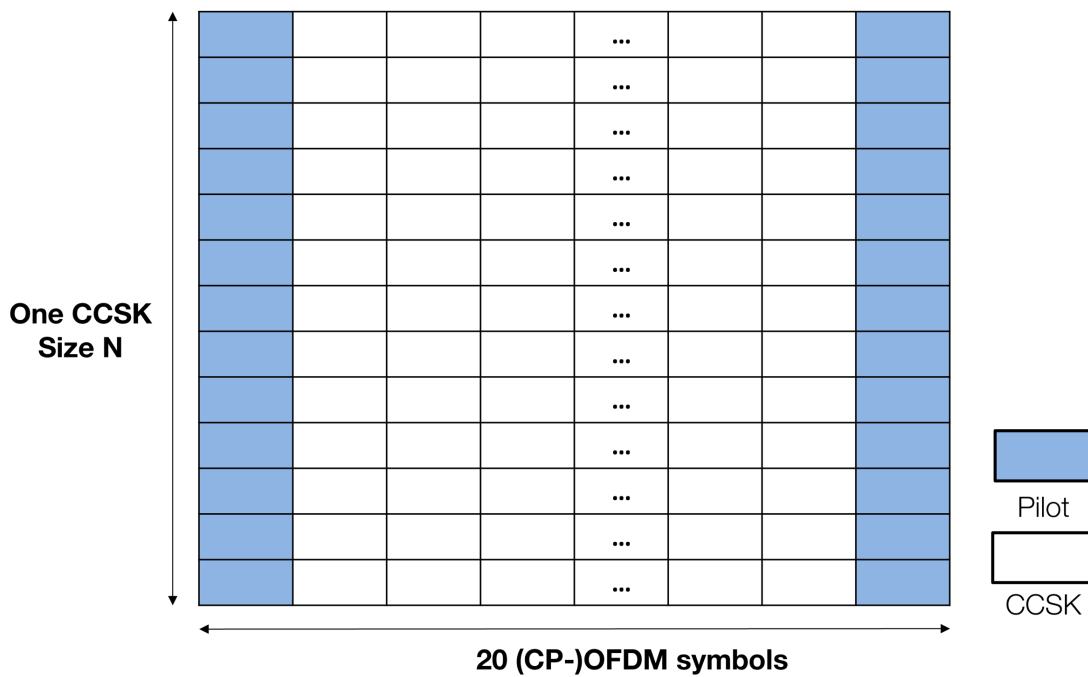


Figure 5.9: Description of the OFDM Frame.

5.3. A basic nearest neighbor time interpolator is here considered. All these schemes use the previously defined CCSK scheme A. The real part of the cross-correlation value is taken.

Five different equalizers are compared. The worst performance are obtained by the LS equalizer, as it is the more basic one. The two LMMSE approximations LRA-LMMSE-Uniform and LRA-LMMSE-ExpTmax respectively use the approximations of equations Eq.5.37 and Eq.5.35. The true noise power is used to compute the auto-correlation matrices, even if this supposition can be alleviate by using a dedicated estimator or a low enough fixed value [22]. The value of τ_{\max} is fixed and equal to the CP length. Both estimators provides similar results. The LMMSE equalizer uses the exact channel auto-correlation matrix, computed from the channel distribution and noise power. The LMMSE leads to the same results as the perfect channel estimation, named perfectCSI, in the case of a constant flatfading channel. The perfect channel estimation scheme uses the exact channel at all sub-carriers, including the data sub-carriers. No interpolation is done. This is the best performance obtainable by this system. To conclude, the uniform and exponential LMMSE approximation provides here a good trade-off between performances and complexity.

Schemes without equalization

The three CCSK schemes A, B and C are now considered without channel equalization. The data symbols are demodulated as such after the DFT at the receiver. The absolute value of the correlation is here taken instead of the real part. At first, we still consider the two block-pilot OFDM symbols, to keep the same E_b/N_0 ratio than the conventional schemes. The results are presented in Figure 5.11.

All three schemes without equalization have the same performances as the perfect channel estimation with absolute value system. To explain this equality, we take a look at the equalized symbols. As a reminder, the symbol on the i^{th} sub-carrier after the receiver DFT, for each scheme A, B and C,

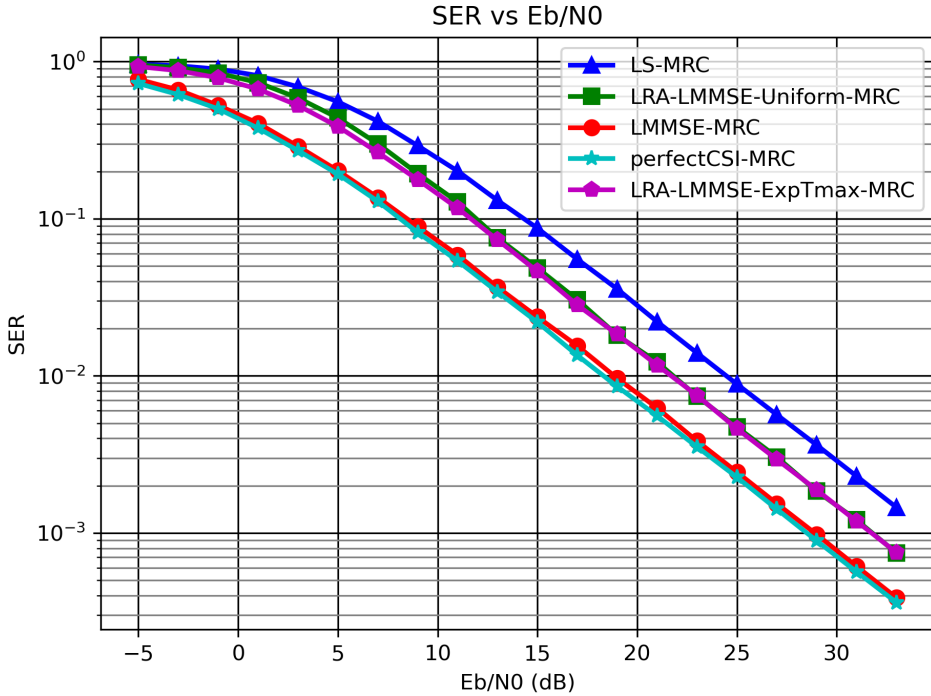


Figure 5.10: SER vs Eb/N0 with constant Rayleigh flatfading.

without equalization is respectively equal to:

$$\theta_A[i] = h[i]c[i] + w[i] \quad (5.44)$$

$$\theta_B[i] = \frac{1}{\sqrt{N}} \sum_{k=0}^{N-1} h[k]c[k]c_0^*[k-i] + w[k] \quad (5.45)$$

$$\theta_C[i] = \begin{cases} h[i]\sqrt{N} + w[i] & , \text{ if } i = p \\ w[i] & , \text{ otherwise} \end{cases} \quad (5.46)$$

To improve the clarity, we have adopted here the sequence element notation $[i]$ to designate the i^{th} element of a vector or a sequence, instead of the subscript \cdot_i notation. The samples of the noise sequence w have a complex white Gaussian noise of distribution $\mathcal{CN}(0, \sigma^2)$. The transmitted CCSK sequence of interest is shifted by a value p .

In the case of the scheme C, taking the absolute value of the sub-carriers symbols and considering that $h[i] = h \forall i$ (flatfading) lead to:

$$\theta_C[i] = \begin{cases} |h\sqrt{N} + w[p]| & , \text{ if } i = p \\ |w[i]| & , \text{ otherwise} \end{cases} \quad (5.47)$$

The system then take the argmax to find the most probable shift value.

In case of scheme B, since $h[k] = h \forall k$ it can be taken out of the sum. The usual ZC cross-correlation formula appears, leading to:

$$\theta_B[i] = \begin{cases} |h\sqrt{N} + w[p]| & , \text{ if } i = p \\ |w[i]| & , \text{ otherwise} \end{cases} \quad (5.48)$$

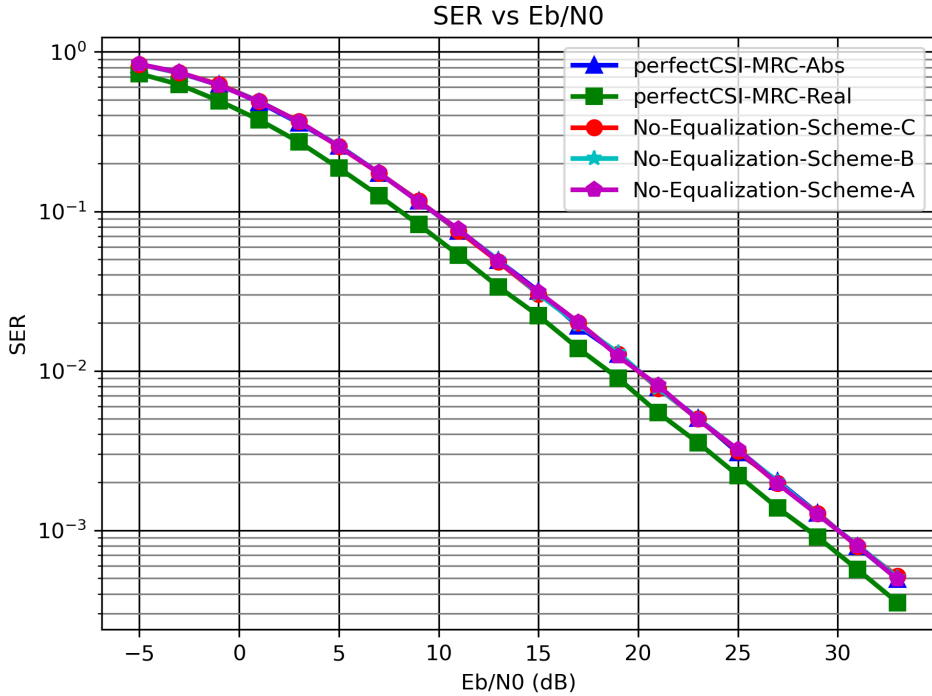


Figure 5.11: SER vs Eb/N0 with constant Rayleigh flatfading.

For the scheme A, the cross-correlation operation gives the equation:

$$\begin{aligned}
 R_A[i] &= \left| \frac{1}{\sqrt{N}} \sum_{k=0}^{N-1} h[k] c[k] c_0^*[k-i] + w[k] c_0^*[k-i] \right| \\
 R_A[i] &= \left| \frac{1}{\sqrt{N}} h \sum_{k=0}^{N-1} c[k] c_0^*[k-i] + w'[k] \right| \\
 R_A[i] &= \begin{cases} |h\sqrt{N} + w'[p]| & , \text{if } i = p \\ |w'[i]| & , \text{otherwise} \end{cases} \quad (5.49)
 \end{aligned}$$

The noise samples of the sequences w and w' have the same distribution. Consequently, all three schemes A, B and C, when not equalized in a flatfading channel, have the same performance, as illustrated in Figure 5.11. They reach the same level of performances as the perfect channel estimation with absolute value. In the latter case, the i^{th} sub-carrier coefficient after the MRC equalization is equal to:

$$\theta_{\text{perfect}}[i] = c[i] + \frac{w[i]}{h} \quad (5.50)$$

In the latter equality, we have removed a $\frac{1}{N}$ scaling factor as it has no impact on the noise and data ratio. Computing the cross-correlation for the CCSK demodulation and taking the absolute value of the result leads to the cases:

$$R_{\text{perfect}}[i] = \begin{cases} |\sqrt{N} + \frac{w'[p]}{h}| & , \text{if } i = p \\ \left| \frac{w'[i]}{h} \right| & , \text{otherwise} \end{cases} \quad (5.51)$$

Non equalized schemes and the perfect channel estimation equations are linked by a multiplication by $|h|$, explaining the performance equality when looking at the argmax value. Nevertheless, when the real part of the perfect channel estimation is taken, the performances are improved as the imaginary part of the noise is removed from the equation, without impacting the cross-correlation result. It

would not be the case for the schemes without equalization, as the complex scalar value h may rotate the correlation score \sqrt{N} into the imaginary region, nullifying the result. This aspect is studied in the next section.

For the sake of completeness, the Figure 5.12 provides the performances of the non equalized schemes with the correct Eb/N0 values. For these schemes, the two block OFDM symbols used as pilots should not be taken into account when computing the actual Eb value as they are not used by the system. As expected, the results show a small gain (around 0.46dB) compared to the equal Eb/N0 case. The gain would be greater if the frame was shorter or, equivalently, if the number of pilot OFDM symbols was higher. In the current system, as the difference does not change the ranking of the studied schemes and does not have an impact on the conclusion of the study, we keep the equal Eb/N0 assumption, unless explicitly notify.

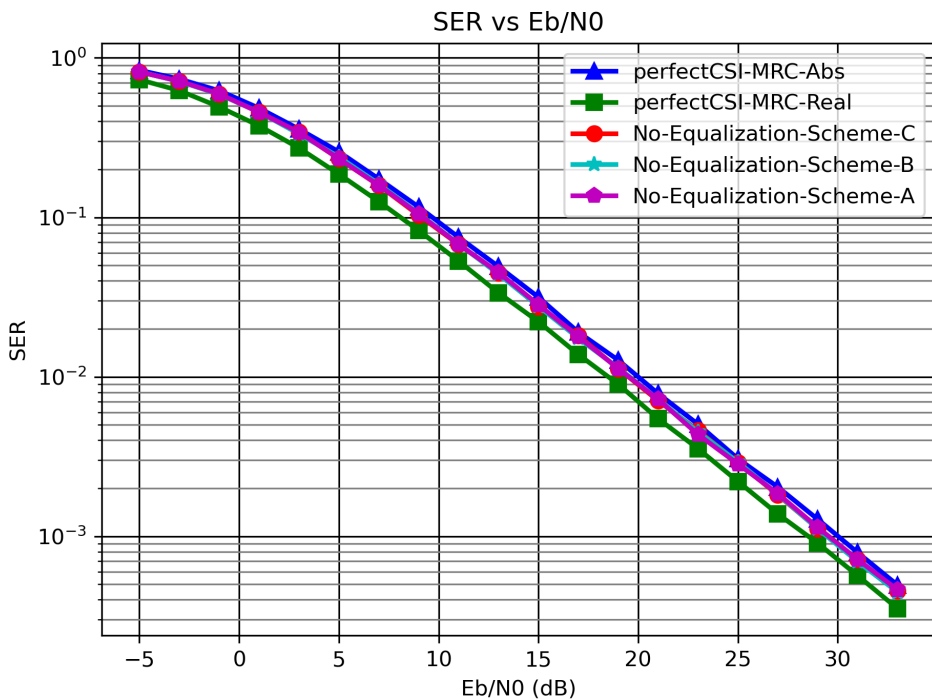


Figure 5.12: SER vs Eb/N0 with constant Rayleigh flatfading, fixed Eb/N0 values.

Absolute Value Versus Real Part

We want to compare the impact of taking the absolute value compared to the real part of the cross-correlation score. The correlation value should be a real integer when the summation is not affected by the channel and the noise. In the case of an AWGN channel, the Figure 4.9 showed the decrease in performance when the absolute value is considered as it includes the real and imaginary part of the noise. In case of a propagation channel, the resulting correlation score may be multiplied by a complex scalar if the channel is not perfectly equalized. In Figure 5.13, all the schemes equalizing the channel improve their performance when using the real part of the correlation. The remaining phase shift in the correlation score caused by the unperfectly equalized channel is less detrimental than adding the energy of the imaginary part of the noise.

The scheme A without equalization, as well as the scheme B and C, cannot use the real part operator as the random phase shift included in the channel scalar value may rotate the real correlation score into the imaginary region.

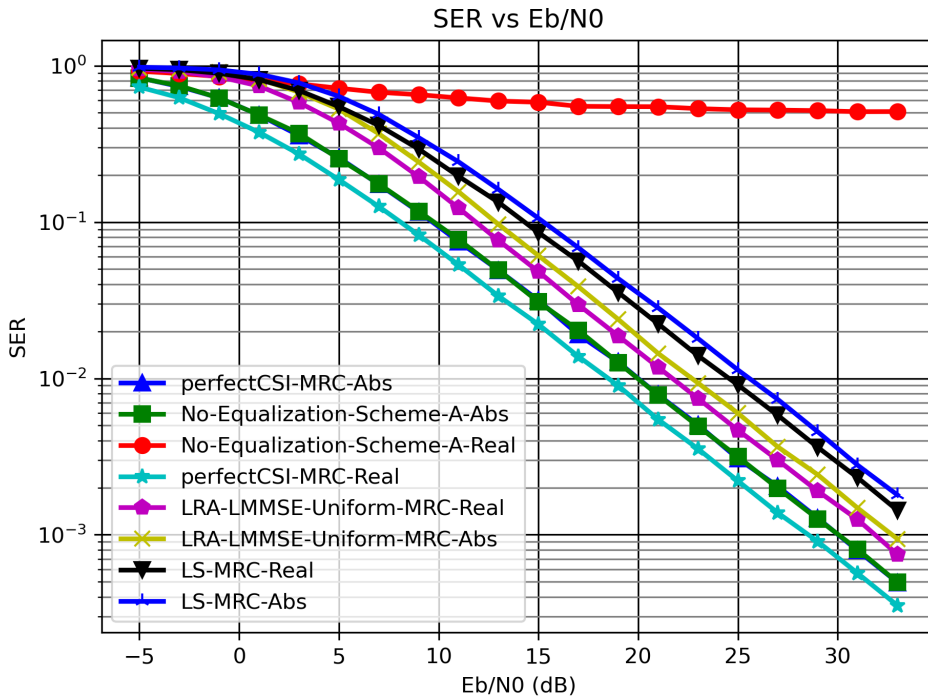


Figure 5.13: SER vs Eb/N0 with constant Rayleigh flatfading.

Maximum Ratio Combining Versus Zero Forcing

Finally, in Figure 5.14, we compare the MRC and ZF equalizers. As stated before, since the real part of the correlation score provides better performances, it is taken from now on, except for schemes without equalization. As expected, the MRC approach gives the best performances as it is expected to maximize the SNR at the right correlation index, i.e. when all the element of the cross-correlation should be equal to one. Nevertheless, we couldn't provide a theoretical analysis, proving that the MRC is the best diversity combining and equalization scheme in case of a cross-correlation computation. This would mean that the MRC maximize the difference between the value at the right correlation index and all the other correlation indices.

In addition, in Figure 5.14, both perfect channel estimation schemes have the same performances, as the MRC and ZF result in the same sub-carrier symbol value when the channel is perfectly estimated in flatfading condition.

Constant Channel Conclusion

In conclusion, when the channel is flat in frequency and constant in time, and in perfect time and frequency synchronization conditions, schemes A, B or C without channel equalization clearly provide the best performances for very low complexity.

Moreover, for conventional scheme, it is better to consider the MRC approach and the real part of the correlation.

5.6.3 Block Fading

We now consider that the flatfading channel is evolving in time. A block fading model is used and the channel is considered constant on each OFDM symbol, but evolving between them. The channel time correlation is linked to the maximum Doppler shift. The higher the Doppler shift, the lower the correlation between channels affecting adjacent OFDM symbols. In the context of terrestrial IoT communications, the propagation channel is usually considered to be slowly evolving. Indeed, the

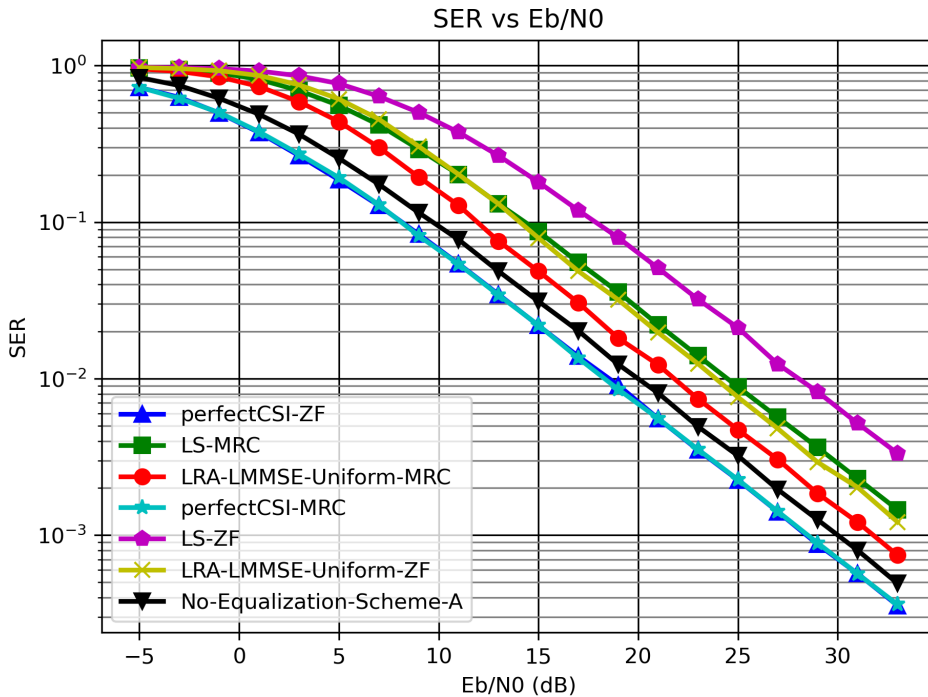


Figure 5.14: SER vs Eb/N0 with constant Rayleigh flatfading.

static or low speed nature of many IoT systems, leads to a radio environment almost static at the scale of the data frame. However, this study try to also address broader use cases and show the system limits when the channel evolves to fast.

Impact of the Time Interpolator

We consider a transmission at 900 MHz central frequency and 15 kHz sub-carrier spacing. The total bandwidth of the system is 960 kHz. To obtain the channel between the first and last OFDM symbols, where the pilots are, we test two interpolation techniques presented in section 5.3.4: the nearest neighbor and the linear interpolator. The latter was used in the previous section. The results are presented in Figures 5.15 to 5.18, with a maximum Doppler shift of 0, 50, 100 and 200Hz. These maximum Doppler shifts are respectively equivalent to a device speed of 0 km/h, 60 km/h, 120 km/h and 240 km/h and can be interpreted as static, medium, fast and very fast channel evolution rate.

For the LS and the LRA-LMMSE-Uniform approximation, the benefit of the linear interpolator over the nearest-neighbor is clear. The linear interpolator describes a progressive evolution of the channel between the start and the end of the OFDM frame. On the contrary, the nearest-neighbor assigns the first channel estimation to the first half of the frame, and the second channel estimation to the second half of the frame. Hence it cannot describe the natural evolution of the channel along the time. This becomes obvious in the 200 Hz Doppler shift case, where both curves reach a performance floor, because the equalizers use an outdated channel estimation, uncorrelated with the real channel. The linear interpolator is more resilient, but it also starts to fail at 200 Hz Doppler shift, because the two pilots OFDM symbols are too far apart for the interpolator to represent the dynamic of the channel.

The perfect channel estimation SER performance is not affected by the channel time diversity, as the channel is always perfectly known and equalized. An equivalent remark can be made for the schemes A, B or C without equalization, as the flatfading channel is never estimated.

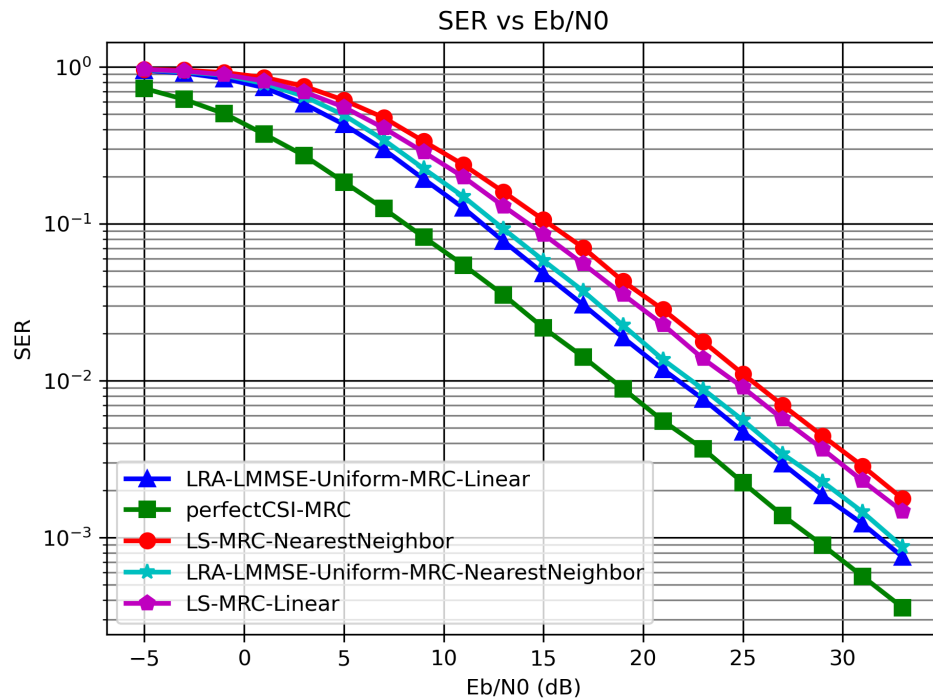


Figure 5.15: SER vs Eb/N0 with evolving Rayleigh flatfading, maximum Doppler shift of 0Hz.

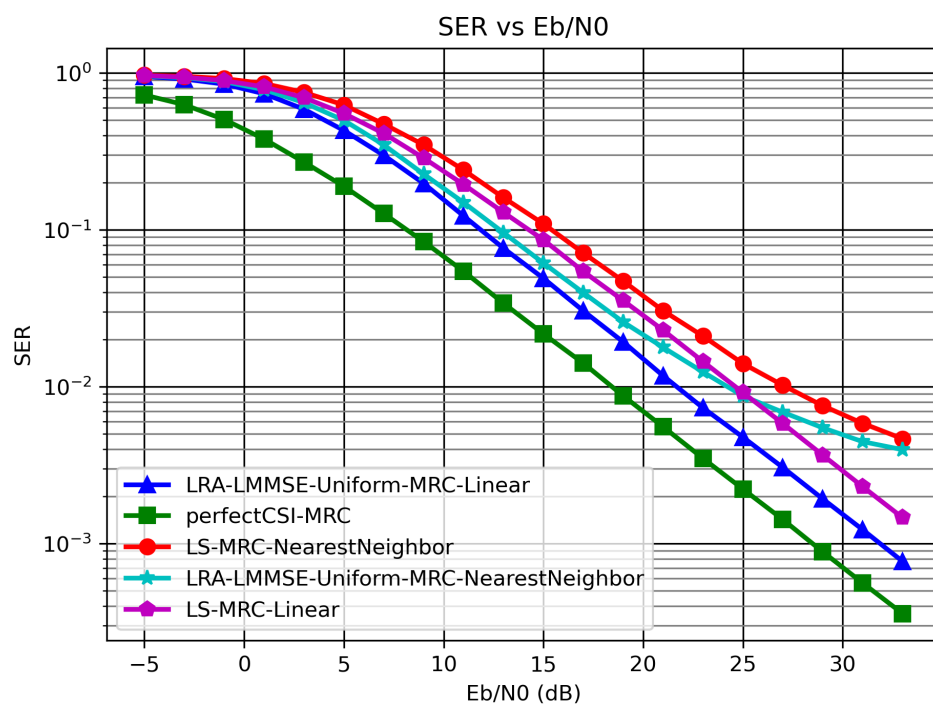


Figure 5.16: SER vs Eb/N0 with evolving Rayleigh flatfading, maximum Doppler shift of 50Hz.

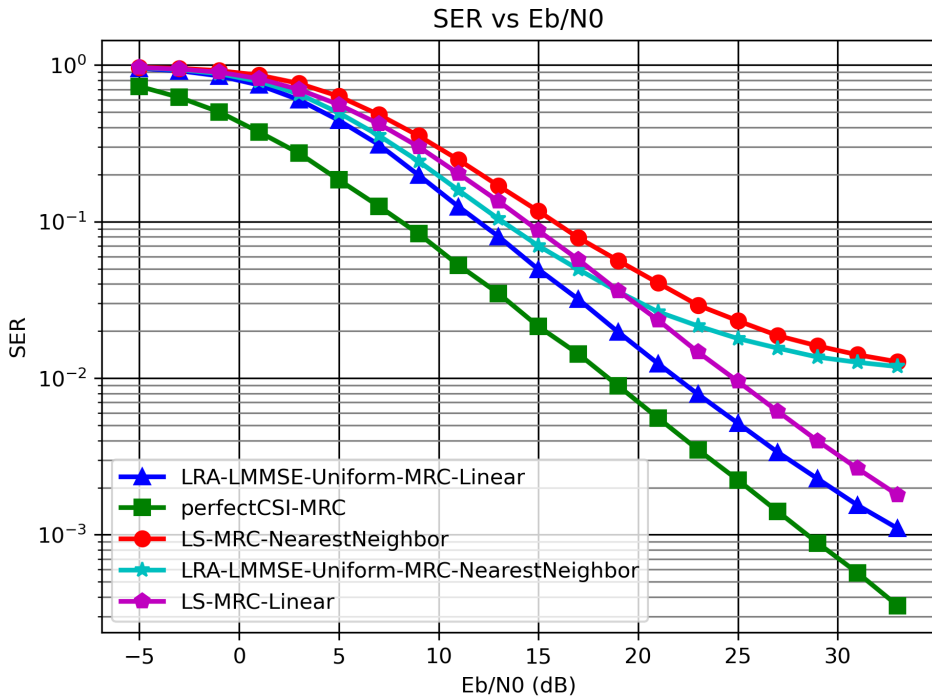


Figure 5.17: SER vs Eb/N0 with evolving Rayleigh flatfading, maximum Doppler shift of 100Hz.

Effect on Block Error Rate

While the SER performance of the perfect channel estimation is not affected by the channel time evolution rate, the Block Error Rate (BLER) performance decrease with more channel diversity. As there is no method included in the system to take advantage of the time diversity, like an error correcting code, the increasing Doppler shift results in an increased chance of experiencing a poor channel within an OFDM frame. Hence an increased BLER.

Block Fading Conclusion

In conclusion, if the channel is known to be a flatfading one, and in perfect time and frequency synchronization conditions, it is sufficient to consider any CCSK scheme without equalization. This leads to a low complexity receiver, reaching performance close to the perfect channel estimation ones. The model is valid independently of the channel evolution speed, as long as the orthogonality between the sub-carriers is guaranteed. Yet, this model is limited to flatfading channel, which may not be the case in standard IoT transmission conditions. While the channel may be slowly evolving, the propagation environment is usually indoor or urban, leading to multiple paths, even at the scale of the current system bandwidth. Moreover, frequency selective channels may provide channel frequency diversity for our system, that the current MRC can use to improve the performance.

5.7 Frequency Selective Fading Performance

5.7.1 System Model

In this section we consider a frequency selective channel instead of a flatfading one. The system is described as follow:

- The OFDM frame is still composed of 20 OFDM symbols, with the first and last one used as block pilots, and a linear interpolator is used in time. The CP length is 10 symbols long, which

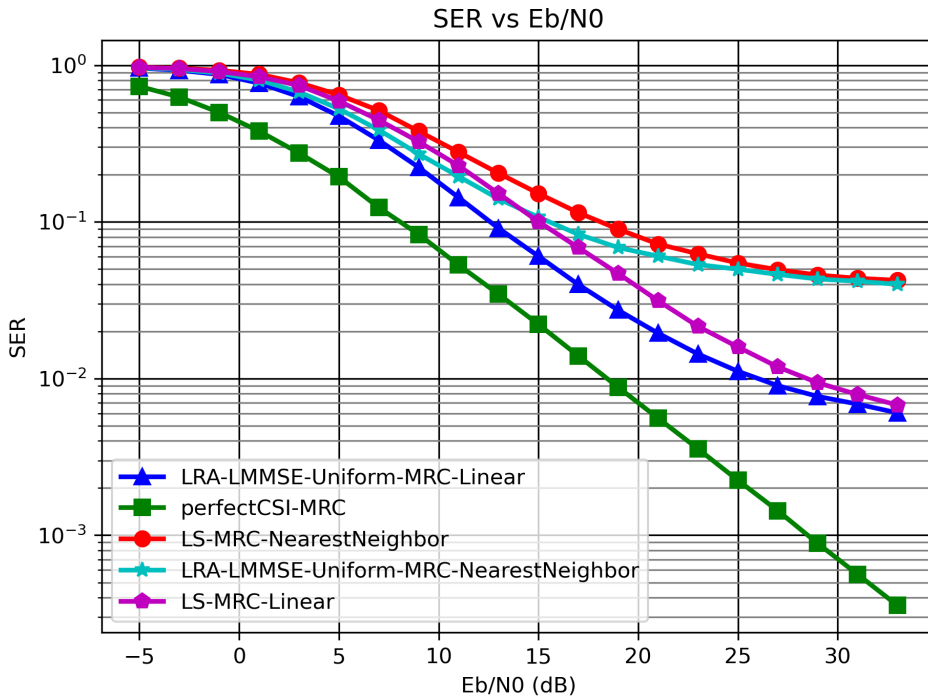


Figure 5.18: SER vs Eb/N0 with evolving Rayleigh flatfading, maximum Doppler shift of 200Hz.

is always longer than the channel.

- The CCSK sequences are ZC sequences of length 64. The system still consider that a single CCSK sequence is carried by an OFDM symbol. The MRC equalizer is also used.
- By lack of time, the iterative mapping is not studied in the following sections. Nevertheless, it can bring interesting results and system design when the channel is evolving in frequency. This case need to be developed in a different study.
- The channel coefficients are not anymore constant in frequency and vary along the sub-carriers. Hence, in time, the channel does not appear as a single path anymore, but as a multipath channel introducing ISI in time.
- Between successive OFDM symbols, the channel on the same sub-carrier is constant, i.e. the maximum Doppler shift is fixed to 0Hz.
- The system still assumes a perfect synchronization in time and frequency at symbol rate.

In time, the channel is modeled as a succession of L main paths (or taps) associated with different delays, summarized in the CIR. Again, we use the Clarke's 2D isotropic model. The complex coefficients of each path are independent and follows the same distribution: the magnitude is Rayleigh distributed and the phase is uniformly distributed. Different powers are associated to each path, but the total power is normalized so that $\sum_{t=0}^{L-1} \mathbb{E}[|h[t]|^2] = 1$.

To better simulate the impact of the multipath channel, the transmitted and received signals are oversampled by a factor of 4. At the transmitter, the CCSK symbols are still mapped around DC, but zeros are added at the edge of the spectrum. For a CCSK symbol of size N , $1.5N$ zeros are placed on each side. Applying the IDFT operator to that spectrum results in an oversampling of 4 of the actual CCSK symbol, and is equivalent to apply a cyclic sinc filter in time. The CP takes into account the oversampled symbols. To normalize the useful energy within the spectrum, we multiply the transmitted oversampled signal by 2 ($=\sqrt{4}$). At the receiver, the signal is downsampled by 4 (with

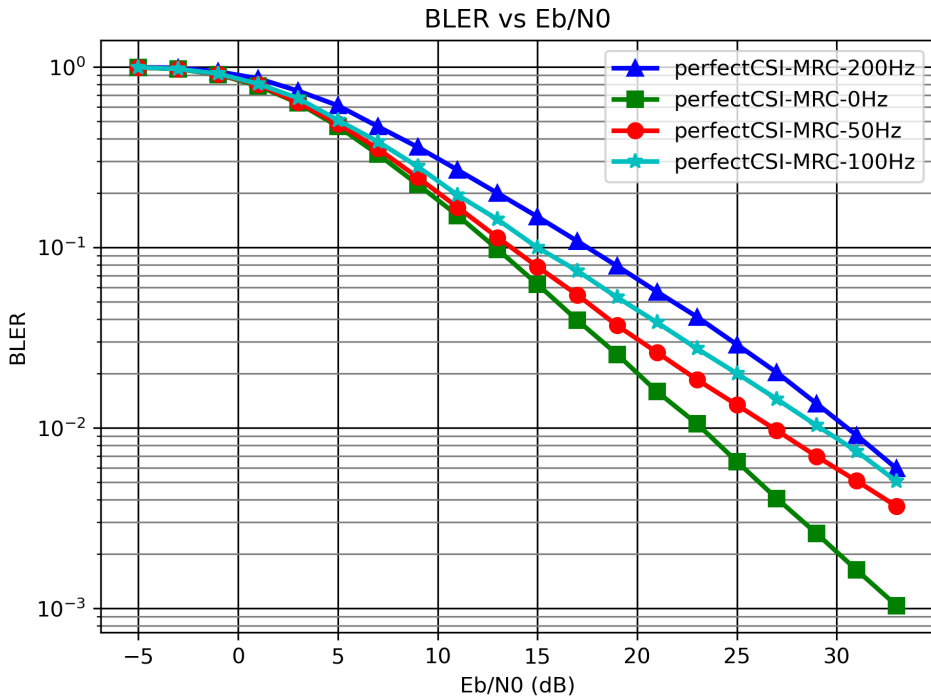


Figure 5.19: BLER vs Eb/N0 with evolving Rayleigh flatfading, maximum Doppler shift from 0Hz to 200Hz.

perfect synchronization) and, after removing the CP, the DFT operator can be directly applied to retrieve the sent CCSK symbols. Because the spectrum outside the CCSK symbol are zeros, there is no aliasing in frequency.

To characterize the selectiveness in frequency, we use the Root Mean Square (RMS) delay spread characteristic of the CIR. By manually increasing the RMS delay spread, the CIR is stretched in time, but the relative delays between the channel paths are kept². As explained in Eq.5.20, a higher RMS delay spread decreases the coherence bandwidth, implying that a longer CIR leads to more ISI (in time) and a channel becomes more selective in frequency. Since the CP is designed to always be longer than the CIR, the channel coefficients on each sub-carrier is equal to the unnormalized DFT of the actual time channel vector padded with zeros to the size of the DFT.

To obtain the channel coefficient at a sample instant we need to use an interpolation method. The interpolation is done by a sinc filter at sample rate. Each path is first filtered independently to obtain the complex coefficients at each sample time. Then, the sum of all the interpolated paths provides the final complex channel coefficients.

Two examples are provided in Figures 5.20 and 5.21, where the base channel model is the EPA model described in Table 5.7.1, and the RMS delay spread has been respectively fixed to 100ns and 400ns. The oversampled CIR at sample time is represented by the blue dots on the figures, considering an oversampling of 4. The figures highlight the link between the increase of the RMS delay spread, the increase of the ISI in time, and consequently the increase of the frequency selectivity. To decrease the system complexity, we restrict the final CIR length so it always contains at least 99% of the channel power and we normalize it to an accumulated power of 1.

²The base channel model paths delays are normalized to have a unit RMS. Then, the paths delays are scaled by the desired RMS value.

path	delays (normalized)	powers (dB, relative)
0	0.00	0.0
1	0.70	-1.0
2	1.62	-2.0
3	2.09	-3.0
4	2.55	-8.0
5	4.41	-17.2
6	9.51	-20.8

Table 5.1: EPA channel model, with paths delays normalized by the RMS delay spread and paths power in dB relative to the most powerful path.

5.7.2 Effect of the Frequency Diversity

To observe the effect of an increasing channel diversity in frequency, four RMS delay spreads are evaluated: 0ns in Figure 5.22, 100ns in Figure 5.23, 200ns in Figure 5.24 and 400ns in Figure 5.25.

Firstly, the CCSK schemes A and B without equalization suffer from the increased channel frequency diversity. Since the channel is not constant in frequency, the complex value h cannot be taken out of the sum in Eq.5.45 and Eq.5.49. Consequently, the summations include uncorrelated complex channel scalars, mitigating the correlation values when the channel diversity increases. To compute the Eb/N0, the two pilot OFDM symbols are again taken into account to facilitate the comparison with other schemes and as it does not change our analysis and conclusion.

On the contrary, the CCSK scheme C is not influenced by the frequency diversity, since the correlation value is scaled by the channel coefficient of a single sub-carrier after the OFDM DFT. Consequently, the performance are the same as in the flatfading case. It is also an inconvenient, as the scheme do not benefit from the channel frequency diversity.

The other schemes that use channel estimation and equalization benefit from the channel frequency diversity. The MRC equalization takes advantage of the varying channel quality along the sub-carriers to improve on average the SNR after the correlation.³ This leads to better performances on average since there is a higher chance to correctly demodulate the CCSK sequence. This is symbolized by the crossing point between the scheme C without equalization and the LS curves being progressively shifted to lower Eb/N0 when the channel diversity increases.

Consequently, when the channel presents enough frequency selectivity, it becomes more interesting to use channel estimation and equalization schemes. LS and LRA-LMMSE Uniform algorithms provide a good balance between performance and complexity.

³A theoretical study has to be conducted to evaluate the gain achieved by the increasing channel diversity on the average SNR and more generally on the correct demodulation probability gain. This work do not include such study.

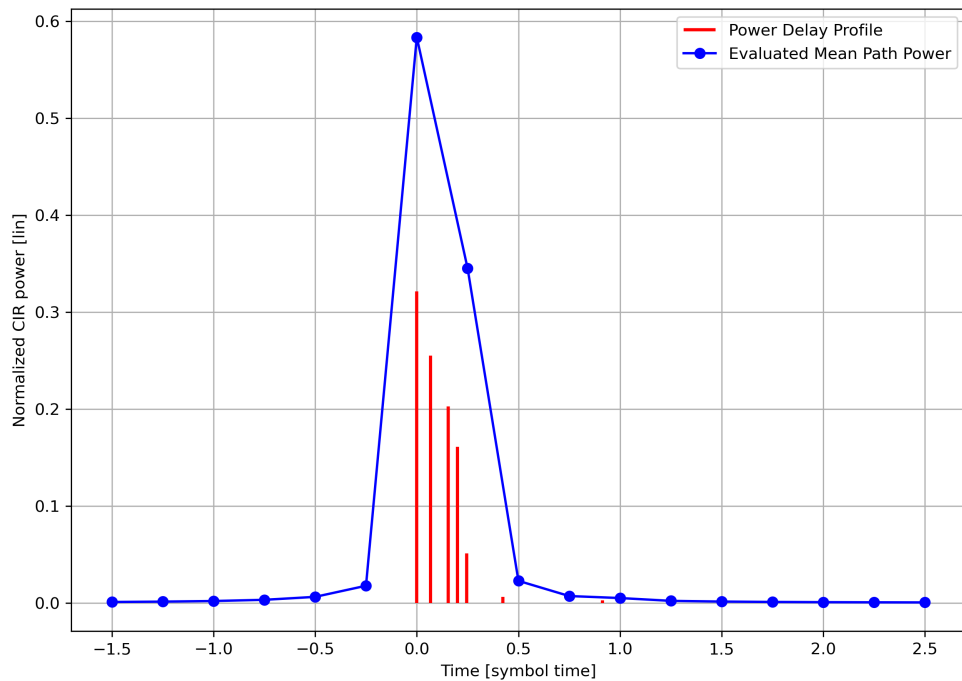


Figure 5.20: Representation of the sampled CIR power with an oversampling factor of 4. Base channel model paths with a RMS delay spread of 100ns are drawn as red lines. Blue dots represent the interpolated channel power at each sample time.

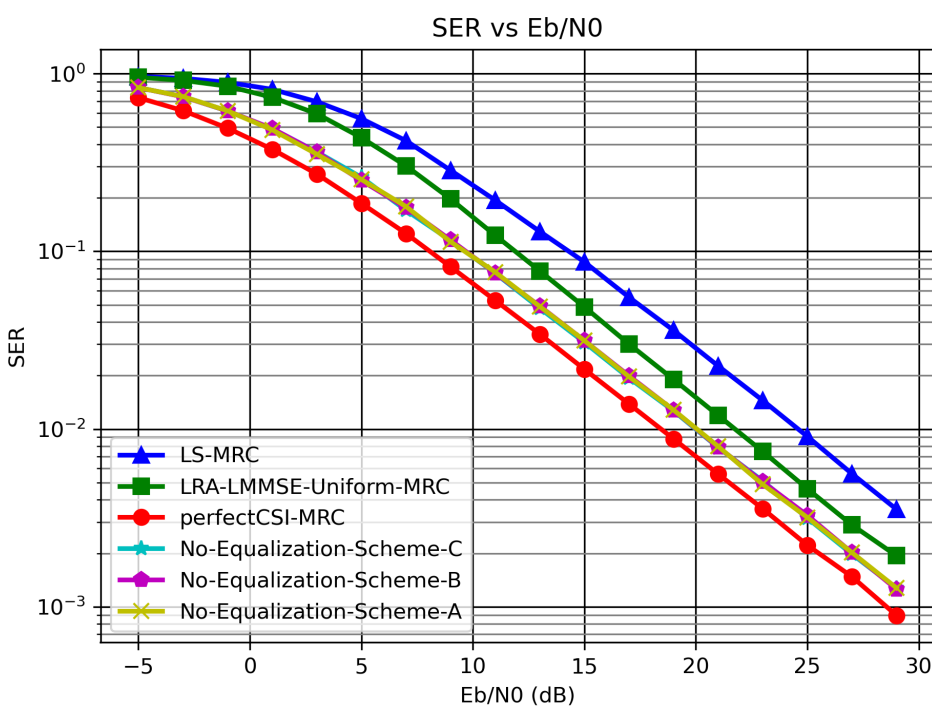


Figure 5.22: SER vs Eb/N0 with flatfading channel and constant channel in time.

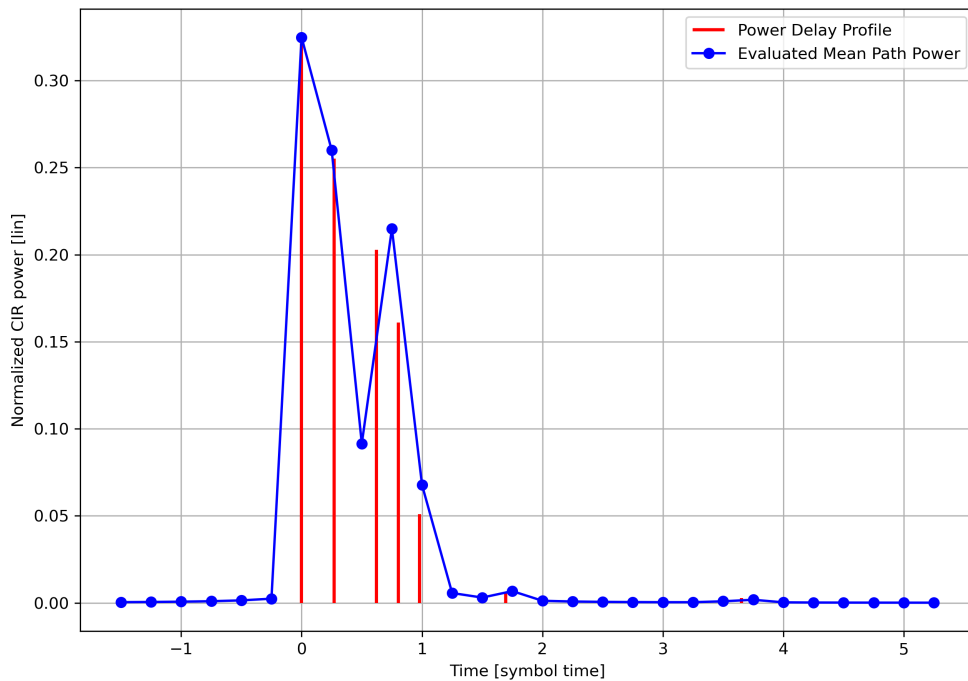


Figure 5.21: Representation of the sampled CIR power with an oversampling factor of 4. Base channel model paths with a RMS delay spread of 400ns are drawn as red lines. Blue dots represent the interpolated channel power at each sample time.

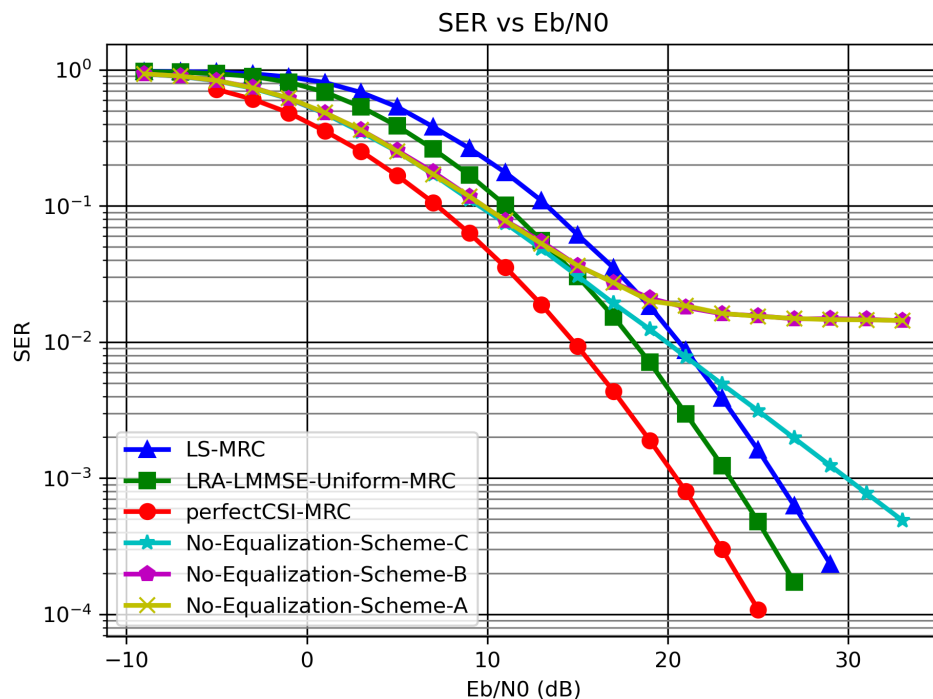


Figure 5.23: SER vs Eb/N0 with constant selective fading channel, maximum Doppler shift of 0Hz and 100ns RMS delay spread.

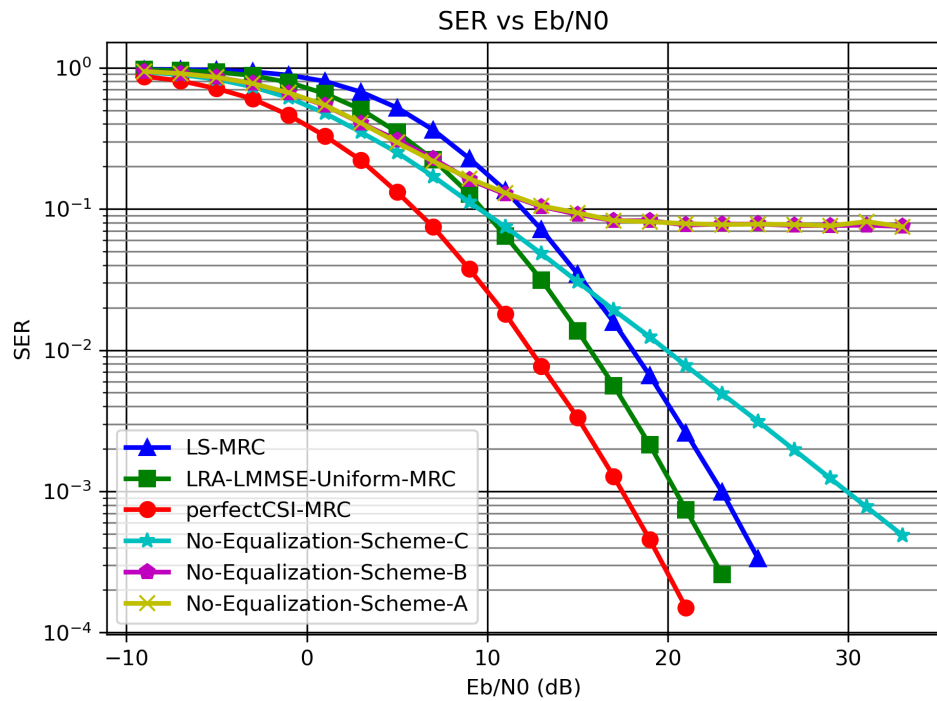


Figure 5.24: SER vs Eb/N0 with constant selective fading channel, maximum Doppler shift of 0Hz and 200ns RMS delay spread.

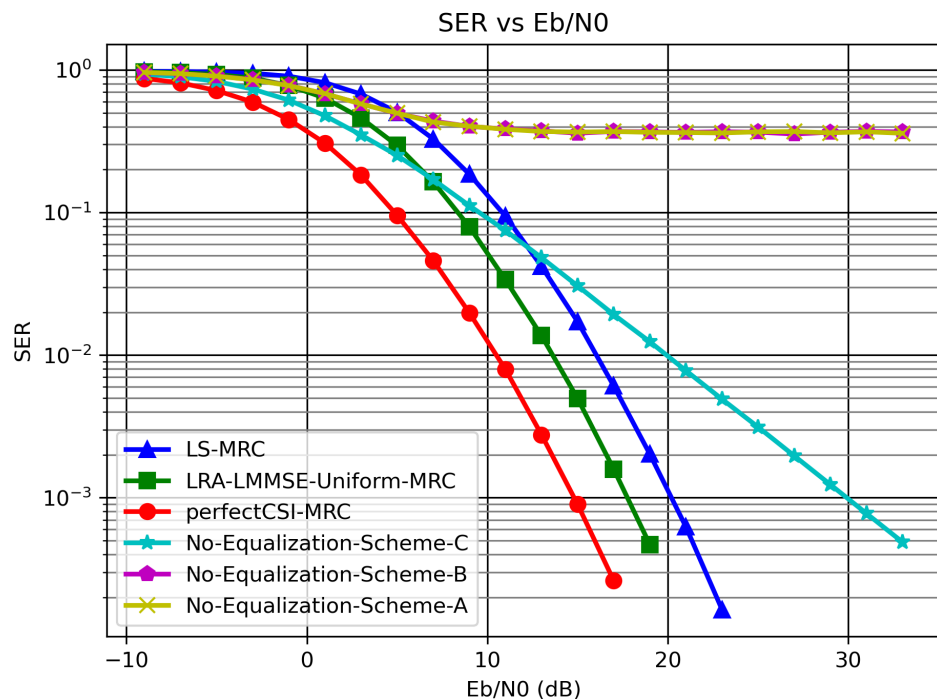


Figure 5.25: SER vs Eb/N0 with constant selective fading channel, maximum Doppler shift of 0Hz and 400ns RMS delay spread.

Absolute Value Versus Real Part

The Figure 5.26, confirms the results obtained in case of flatfading. Taking the real part of the correlation values provides better performance than the absolute part.

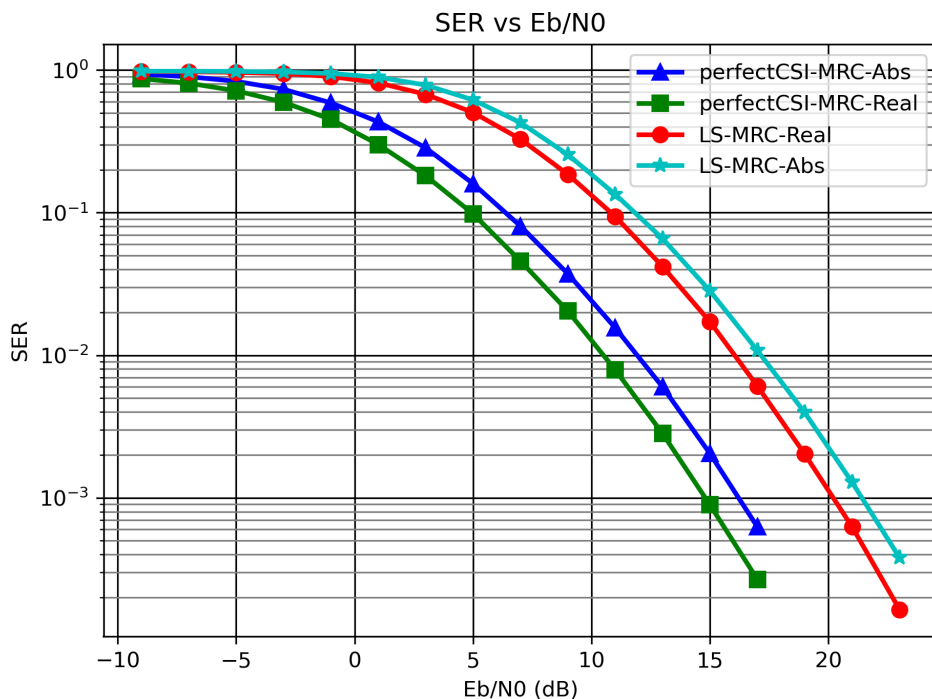


Figure 5.26: SER vs Eb/N0 with constant selective fading channel, maximum Doppler shift of 0Hz and 400ns RMS delay spread.

Maximum Ratio Combining Versus Zero Forcing

In case of flatfading, the Figure 5.14 demonstrated the advantage of the MRC above the ZF equalization scheme. The gain is even more convincing here, as the MRC benefits from the channel frequency diversity, as expected from the algorithm.

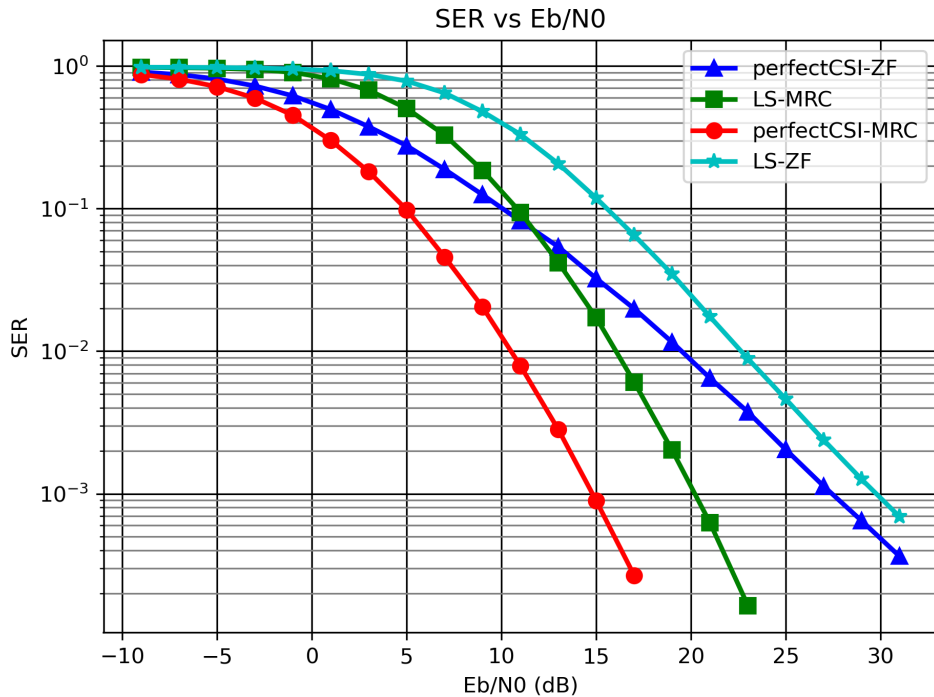


Figure 5.27: SER vs Eb/N0 with constant selective fading channel, maximum Doppler shift of 0Hz and 400ns RMS delay spread.

5.7.3 Fading Channel Conclusion

In case the flatfading channel, there is no channel diversity in frequency and the conventional schemes cannot benefit from it. In this case, it is useful to consider the receiver schemes without equalization. Nevertheless, frequency selectivity is a common channel condition, especially when using CP-OFDM as the presence of the CP removes the ISI in frequency. In this case, all the schemes using equalization mechanisms benefit from the channel diversity, in particular thanks to the MRC equalizer. LS and LRA-LMMSE Uniform channel estimators provides great performances for low and reasonable complexity.

6 Relative Shift Demodulation

We have studied the effect of the fading channel on the CCSK-CP-OFDM communications scheme. We have more specifically treated the case of state of the art channel estimation, interpolation and equalization techniques. The following sections study a new channel equalization and demodulation scheme, which uses the cross-correlation between all the received CCSK sequences as a basis to demodulate the information contained in the frame.

6.1 CIR Estimation

In the following, the equations do not consider the oversampling as the processing is done after the downsampling. The system works at symbol rate with perfect synchronization.

We consider a CIR $[h[0], h[1], \dots, h[L - 1]]$ of independent taps, whose magnitude are Rayleigh distributed, and with L lower or equal to the CP length. We pad the CIR with zeros up to a length N : $[h[0], h[1], \dots, h[N - 1]]$.

The received sequence of time symbols, after the channel convolution and AWGN, and after removing the CP, is equal to:

$$Y[n] = \sum_{l=0}^{N-1} h[l] F^{-1}(x_{u,p})[n-l] + w[n] \quad \text{for } n \in [0; N-1] \quad (6.1)$$

where $F^{-1}(x_{u,p})$ is the IDFT of the ZC sequence x_u right-shifted by p , modulating the information in the CCSK scheme. As $F^{-1}(x_{u,p})$ is an N -periodic sequence, we extend the sequence indices as if they were modulo N , omitting the modulo operator.

As stated in section 3.4, the IDFT of $x_{u,p}$ has a perfect auto-correlation function, so that when normalized:

$$R[s] = \frac{1}{\sqrt{N}} \sum_{k=0}^{N-1} F^{-1}(x_{u,p})[k] F^{-1}(x_u)^*[k-s] \quad (6.2)$$

$$R[s] = \begin{cases} 0, & \text{if } u^{-1}s \not\equiv N-p \pmod{N}, \\ \sqrt{N}x_u[p], & \text{if } u^{-1}s \equiv N-p \pmod{N}. \end{cases} \quad (6.3)$$

The value of s verifying the correlation condition is unique in $[0; N]$ for a value of p . Computing the auto-correlation of the received sequence, we have:

$$\begin{aligned} R[s] &= \frac{1}{\sqrt{N}} \sum_{n=0}^{N-1} Y[n] F^{-1}(x_u)^*[n-s] \\ R[s] &= \frac{1}{\sqrt{N}} \sum_{l=0}^{N-1} h[l] \sum_{n=0}^{N-1} F^{-1}(x_{u,p})[n-l] F^{-1}(x_u)^*[n-s] + \frac{1}{\sqrt{N}} \sum_{n=0}^{N-1} w[n] F^{-1}(x_u)^*[n-s] \end{aligned} \quad (6.4)$$

The noise term is equivalent to a complex Gaussian term of the same distribution $\mathcal{CN}(0, \sigma^2)$. We use the simplified notation $w_{eq}[s]$. In the correlation term, we recognize the usual auto-correlation expression:

$$\frac{1}{\sqrt{N}} \sum_{n=0}^{N-1} F^{-1}(x_{u,p})[n-l] F^{-1}(x_u)^*[n-s] \quad (6.5)$$

where $F^{-1}(x_{u,p})[n-l]$ is the sequence $F^{-1}(x_{u,p})[n]$ right-shifted by l positions. There is a unique value of s , noted s_0 , that implies a maximum of correlation for $l = 0$, and null correlation values with

all the shifted versions $l \neq 0$:

$$\begin{aligned} R[s_0] &= \frac{1}{\sqrt{N}} h[0] \sum_{n=0}^{N-1} F^{-1}(x_{u,p})[n] F^{-1}(x_u)^*[n - s_0] + w_{eq}[s_0] \\ R[s_0] &= h[0]\sqrt{N}x_u[p] + w_{eq}[s_0] \end{aligned} \quad (6.6)$$

At index $s_0 + l$, the correlation happens with the l^{th} term of the first sum:

$$R[s_0 + l] = h[l]\sqrt{N}x_u[p] + w_{eq}[s_0 + l] \quad (6.7)$$

Since the convolution between the channel and the signal is circular, the CIR and the correlation sequence R can be seen as N -periodic sequences. Without noise, the resulting correlation sequence R corresponds to a shifted version of the CIR $[h[0], h[1], \dots, h[N-1]]$ scaled by $\sqrt{N}x_u[p]$. This sequence is right-shifted by s_0 , so that:

$$R[s] = \sqrt{N}x_u[p]h[s - s_0] + w_{eq}[s] \quad (6.8)$$

Consequently, the result of the auto-correlation is an estimation of the CIR, scaled by \sqrt{N} , with a phase offset of $x_u[p]$ and shifted by s_0 . The noise term decreases the accuracy of the estimation and is equal to:

$$w_{eq}[s] = \frac{1}{\sqrt{N}} \sum_{n=0}^{N-1} w[n] F^{-1}(x_u)^*[n - s] \quad (6.9)$$

6.2 Channel Estimation in Frequency

We compute the normalized DFT of the estimated CIR to obtain an estimation of the channel in frequency. Similar to the true CIR, the DFT provides an estimate of the channel on each sub-carrier. The estimate of the channel on sub-carrier k is:

$$\begin{aligned} \tilde{H}[k] &= \frac{1}{\sqrt{N}} \sum_{s=0}^{N-1} R[s] \exp\left(-j2\pi\frac{ks}{N}\right) \\ \tilde{H}[k] &= x_u[p] \sum_{s=0}^{N-1} h[s - s_0] \exp\left(-j2\pi\frac{ks}{N}\right) + \frac{1}{\sqrt{N}} \sum_{s=0}^{N-1} w_{eq}[s] \exp\left(-j2\pi\frac{ks}{N}\right) \end{aligned} \quad (6.10)$$

Again, the noise term is equivalent to a complex Gaussian term of the same distribution $\mathcal{CN}(0, \sigma^2)$, and we use the notation $W_{eq}[k]$. With a change of variable $s' = s - s_0$, we have:

$$\tilde{H}[k] = x_u[p] \exp\left(-j2\pi\frac{ks_0}{N}\right) \sum_{s'=-s_0}^{N-1-s_0} h[s'] \exp\left(-j2\pi\frac{ks'}{N}\right) + W_{eq}[k] \quad (6.11)$$

Extending the sequence h as N -periodic, and remembering that the DFT of the true CIR is equal to $H[k] = \sum_{s=0}^{N-1} h[s] \exp\left(-j2\pi\frac{ks}{N}\right)$, we finally obtain:

$$\tilde{H}[k] = x_u[p] \exp\left(-j2\pi\frac{ks_0}{N}\right) H[k] + W_{eq}[k] \quad (6.12)$$

By definition of s_0 , we have $u^{-1}s_0 \equiv N - p \pmod{N}$. Thus, $s_0 \equiv -up \pmod{N}$. Using Eq.1.11, we have:

$$\begin{aligned} \tilde{H}[k] &= x_u[p] \exp\left(j2\pi u\frac{kp}{N}\right) H[k] + W_{eq}[k] \\ \tilde{H}[k] &= x_u^*[k] x_u[k - p] H[k] + W_{eq}[k] \end{aligned} \quad (6.13)$$

The equation Eq.6.13 represents the channel estimation in frequency for the k^{th} sub-carrier. Now, if we look at the received symbol, on the k^{th} sub-carrier, after the OFDM DFT operation, we have:

$$\tilde{c}_p[k] = x_u[k-p]H[k] + \frac{1}{\sqrt{N}} \sum_{n=0}^{N-1} w[n] \exp\left(-j2\pi\frac{kn}{N}\right) \quad (6.14)$$

In Eq.6.13, the noise term $W_{\text{eq}}[k]$ is expressed as:

$$\begin{aligned} W_{\text{eq}}[k] &= \frac{1}{\sqrt{N}} \sum_{s=0}^{N-1} \frac{1}{\sqrt{N}} \sum_{n=0}^{N-1} w[n] F^{-1}(x_u^*)[n-s] \exp\left(-j2\pi\frac{ks}{N}\right) \\ &= \frac{1}{N} \sum_{n=0}^{N-1} w[n] \sum_{s=0}^{N-1} F(x_u^*)[n-s] \exp\left(-j2\pi\frac{ks}{N}\right) \\ &= \frac{1}{N} \sum_{n=0}^{N-1} w[n] \exp\left(-j2\pi\frac{kn}{N}\right) \sum_{s'=n}^{n-N+1} F(x_u^*)[s'] \exp\left(j2\pi\frac{ks'}{N}\right) \quad \text{with } s' = n - s \\ &= \frac{1}{\sqrt{N}} \sum_{n=0}^{N-1} w[n] \exp\left(-j2\pi\frac{kn}{N}\right) F^{-1}(F(x_u^*))[k] \\ &= x_u^*[k] \frac{1}{\sqrt{N}} \sum_{n=0}^{N-1} w[n] \exp\left(-j2\pi\frac{kn}{N}\right) \end{aligned} \quad (6.15)$$

Consequently, we have the equality:

$$\tilde{H}[k] = x_u^*[k] \tilde{c}_p[k] \quad (6.16)$$

Hence, instead of computing the DFT of the estimated CIR, the same channel estimate in frequency can be obtained by taking the DFT of the received signal and multiply it by $x_u^*[k]$ on the k^{th} sub-carrier. This method decreases greatly the complexity to obtain the channel estimates.

6.3 MRC Equalization with the Channel Estimate

The OFDM frame is composed of Q OFDM symbols, each containing a single CCSK sequence. Considering the OFDM symbol of index $0 \leq m \leq Q - 1$, the corresponding CCSK sequence shift is noted p_m , the channel in frequency H_m , the channel estimated \tilde{H}_m and the noise sequence in frequency W_m .

6.3.1 Equalization of the Same OFDM Symbol

The MRC equalization of the received OFDM symbol of index m with the corresponding channel estimate on the k^{th} sub-carrier is equal to:

$$\begin{aligned} \theta_{m/m}[k] &= \alpha_m \widetilde{c_{p_m}}[k] \widetilde{H_m}^*[k] \\ &= \alpha_m \widetilde{c_{p_m}}[k] x_u[k] \widetilde{c_{p_m}}^*[k] \\ &= \alpha_m x_u[k] |\widetilde{c_{p_m}}[k]|^2 \\ &= \alpha_m x_u[k] (|H_m[k]|^2 + |W_m[k]|^2 + 2\Re(x_u[k-p_m] H_m[k] W_m^*[k])) \end{aligned} \quad (6.17)$$

with $\alpha_m = \frac{1}{\sum_{n=0}^{N-1} |\widetilde{c_{p_m}}[n]|^2}$ the normalization factor of the MRC. From the last expression, computing the cross-correlation of the $\theta_{m/m}$ with the root sequence x_u should lead to a maximum at index 0, independently of the index m . Hence, this equalization removes the shift value p_m , and with it the modulated information.

6.4 Equalization of Adjacent OFDM Symbols

We now consider the OFDM symbol at index as $0 \leq l \leq Q - 1$, and the channel estimate at index $0 \leq m \leq Q - 1$, with $l \neq m$. The MRC equalization becomes:

$$\begin{aligned}\theta_{l/m}[k] &= \alpha_m \widetilde{c_{p_l}}[k] \widetilde{H_m^*}[k] \\ &= \alpha_m (x_u[k - p_l] H_l[k] + W_l[k]) (x_u[k] x_u^*[k - p_m] H_m^*[k] + x_u[k] W_m^*[k]) \\ &= \alpha_m (x_u[k - p_l] x_u[k] x_u^*[k - p_m] H_m^*[k] H_l[k]) + \alpha_m (x_u[k - p_l] x_u[k] H_l[k] W_m^*[k] + \\ &\quad x_u[k] x_u^*[k - p_m] H_m^*[k] W_l[k] + x_u[k] W_m^*[k] W_l[k])\end{aligned}\quad (6.18)$$

The second term of the sum is associated to a noise term and noted $W_{l/m}$. Focusing on the first term, we have:

$$\begin{aligned}\theta_{l/m}[k] &= \alpha_m (x_u[k - p_l] x_u[k] x_u^*[k - p_m] H_m^*[k] H_l[k]) + W_{l/m}[k] \\ &= \alpha_m x_u[k] x_u[p_l] \exp\left(j2\pi u \frac{kp_l}{N}\right) x_u[k] x_u^*[k] x_u^*[p_m] \exp\left(-j2\pi u \frac{kp_m}{N}\right) H_m^*[k] H_l[k] + W_{l/m}[k] \\ &= \alpha_m x_u[k] x_u[p_l] x_u^*[p_m] \exp\left(j2\pi u \frac{k(p_l - p_m)}{N}\right) H_m^*[k] H_l[k] + W_{l/m}[k] \\ &= \alpha_m x_u[k - (p_l - p_m)] x_u^*[p_l - p_m] x_u[p_l] x_u^*[p_m] H_m^*[k] H_l[k] + W_{l/m}[k] \\ &= \alpha_m x_u[k - (p_l - p_m)] x_u^*[p_l] x_u^*[p_m] x_u[p_l] x_u^*[p_m] \exp\left(-j2\pi u \frac{p_l p_m}{N}\right) H_m^*[k] H_l[k] + W_{l/m}[k] \\ &= \alpha_m x_u[k - (p_l - p_m)] \exp\left(j2\pi u \frac{p_m^2 - p_l p_m}{N}\right) H_l[k] H_m^*[k] + W_{l/m}[k]\end{aligned}\quad (6.19)$$

The main term corresponds to a ZC sequence right-shifted by $p_l - p_m$, scaled by a frequency constant complex exponential. Hence, taking the absolute value of the correlation for the CCSK demodulation should lead to a maximum value at index $p_l - p_m$ modulo N. We have obtained a relative information for the shift of the CCSK sequence in OFDM symbol l against the shift in OFDM symbol m . This relative information can be used to demodulate the OFDM frame, as presented in the next section.

6.5 DFTLink and GLAD Algorithms

6.5.1 DFT-Link: Relative Shift Probabilities Matrix

The values of $\theta_{l/m}$ in Eq.6.19 are computed for all couple (l, m) . To evaluate the position of $p_l - p_m$ based on $\theta_{l/m}$, we compute the cross-correlation of $\theta_{l/m}$ with the root sequence x_u :

$$\begin{aligned}R_{l/m}[k] &= \frac{1}{\sqrt{N}} \sum_{n=0}^{N-1} \theta_{l/m}[n] x_u^*[n - k] \\ R_{l/m}[k] &= \alpha_m \frac{1}{\sqrt{N}} \exp\left(j2\pi u \frac{p_m^2 - p_l p_m}{N}\right) \sum_{n=0}^{N-1} x_u[n - (p_l - p_m)] x_u^*[n - k] H_l[n] H_m^*[n] + \\ &\quad \frac{1}{\sqrt{N}} \sum_{n=0}^{N-1} W_{l/m}[n] x_u^*[n - k]\end{aligned}\quad (6.20)$$

Hence, $R_{l/m}$ corresponds to our usual correlation result after the MRC equalization, with the particularity of a constant phase shift $\exp(j2\pi u \frac{p_m^2 - p_l p_m}{N})$ along the sub-carrier. Because of this phase shift, the absolute value of the correlation has to be taken instead of the real part. The maximum of correlation should be at index $k \equiv p_l - p_m \bmod (N)$, providing an estimation of $p_l - p_m \bmod (N)$. We normalize the cross-correlation scores as a probability distribution:

$$P_{l/m}[k] = \frac{|R_{l/m}[k]|}{\sum_{n=0}^{N-1} |R_{l/m}[n]|} \quad (6.21)$$

Thus, each $P_{l/m}$ is a sequence summing to one, where the maximum of “probability” corresponds to the relative shift $p_l - p_m \bmod (N)$. These probabilities are regrouped in a single matrix. To illustrate the result, we consider an OFDM frame of length 3, so that $Q = 2$. The matrix has the following form:

$$\begin{pmatrix} P_{0/0} & P_{1/0} & P_{2/0} \\ P_{0/1} & P_{1/1} & P_{2/1} \\ P_{0/2} & P_{1/2} & P_{2/2} \end{pmatrix} \quad (6.22)$$

The row i corresponds to the equalizations by the channel estimated in OFDM symbol i . The vectors on the diagonal should all have a maximum value at index 0. In the following, we first prove that this matrix has a symmetry and we then propose an algorithm using this matrix to demodulate the CCSK frame.

We describe the process to get this matrix as the DFTLink algorithm.

6.5.2 Symmetric Property

From Eq.6.20 and Eq.6.19, we have:

$$\begin{aligned} R_{l/m}[k] &= \alpha_m \frac{1}{\sqrt{N}} \sum_{n=0}^{N-1} x_u^*[n-k] x_u[n] (x_u[n-p_l] H_l[n] + W_l[n]) (x_u^*[n-p_m] H_m^*[n] + W_m^*[n]) \\ &= \alpha_m \frac{1}{\sqrt{N}} \sum_{n=0}^{N-1} x_u^*[n-k] x_u[n] \tilde{c}_{p_l}[n] \tilde{c}_{p_m}^*[n] \\ &= \alpha_m \frac{1}{\sqrt{N}} \sum_{n=0}^{N-1} x_u^*[n] x_u^*[k] x_u[n] \tilde{c}_{p_l}[n] \tilde{c}_{p_m}^*[n] \exp\left(-j2\pi \frac{nuk}{N}\right) \\ &= \alpha_m x_u^*[k] F(\tilde{c}_{p_l} \tilde{c}_{p_m}^*)[uk] \end{aligned} \quad (6.23)$$

and

$$\begin{aligned} R_{m/l}[k] &= \alpha_l \frac{1}{\sqrt{N}} \sum_{n=0}^{N-1} x_u^*[n-k] x_u[n] (x_u^*[n-p_l] H_l^*[n] + W_l^*[n]) (x_u[n-p_m] H_m[n] + W_m[n]) \\ &= \alpha_l \frac{1}{\sqrt{N}} \sum_{n=0}^{N-1} x_u^*[n-k] x_u[n] \tilde{c}_{p_l}^*[n] \tilde{c}_{p_m}[n] \\ &= \alpha_l \frac{1}{\sqrt{N}} \sum_{n=0}^{N-1} x_u^*[n] x_u^*[k] x_u[n] \tilde{c}_{p_l}^*[n] \tilde{c}_{p_m}[n] \exp\left(-j2\pi \frac{nuk}{N}\right) \\ &= \alpha_l x_u^*[k] F((\tilde{c}_{p_l} \tilde{c}_{p_m}^*)^*)[uk] \\ &= \alpha_l x_u^*[k] F(\tilde{c}_{p_l} \tilde{c}_{p_m}^*)^*[-uk \bmod N] \end{aligned} \quad (6.24)$$

Consequently, we obtain the equality:

$$\frac{|R_{l/m}[k]|}{\alpha_m} = \frac{|R_{m/l}[-k \bmod (N)]|}{\alpha_l} = \frac{|R_{m/l}[N-k]|}{\alpha_l} \quad (6.25)$$

Finally, with the normalization as a probability distribution of the correlation values, we have:

$$\begin{aligned} P_{l/m}[k] &= \frac{|R_{l/m}[k]|}{\sum_{n=0}^{N-1} |R_{l/m}[n]|} \\ &= \frac{|R_{m/l}[N-k]|}{\sum_{n=0}^{N-1} |R_{m/l}[N-n]|} \\ &= \frac{|R_{m/l}[N-k]|}{\sum_{n=0}^{N-1} |R_{m/l}[n]|} \\ &= P_{m/l}[N-k] \end{aligned} \quad (6.26)$$

The equality $P_{l/m}[k] = P_{m/l}[N - k]$ means that symmetric probability vectors share the same values but in a reverse order, always starting at index zero.

6.5.3 Iterative Demodulation

In previous sections of this document, we have described how the DFTLink algorithm calculates the relative shift matrix from the received OFDM frame. In this section, we introduce the GLAD algorithm, which aims to iteratively process the relative shift matrix, in order to aggregate all available information and improve the demodulation process. The algorithm uses an iterative probabilistic graphical model to combine the distributions contained in the relative shift matrix described above. The approach aims to propagate the available information hierarchically to neighbouring variables in the graph using the relative shift relationships linking them.

Description of the Algorithm

The proposed algorithm mostly rely on two steps:

- First, partial versions of all the relative shifts are computed based on all the available relative shift pairs using the following formula:

$$P_{a/b}^{(c)} = P_{a/c} \circledast P_{b/c}$$

where \circledast denotes the cross-correlation operation. Table 6.1 describes one way to obtain the 27 partial relative shifts in the example of a frame with 3 OFDM symbols.

- Then, the different partial versions of a given relative shift are recombined using a product:

$$P_{a/b} = \prod_{c=0}^{N-1} P_{a/b}^{(c)}$$

Table 6.2 describes how the 27 partial relative shifts are recombined to obtain the updated, *a posteriori*, relative shifts. The proposed method being iterative we don't want to influence the updated posterior value of one relative shift by its own value, also referred as *intrinsic* information. Masking procedure is thus put in place to avoid such self-influencing loops in the iterative graph as described by the coloured cells of Table 6.2. Red cells are partial relative shifts that contains the *intrinsic* information - *e.g* the updated value of $P_{0/1}$ should not rely on the partial relative shift $P_{0/1}^{(1)} = P_{0/1} \circledast P_{1/1}$ which contains the *intrinsic* value $P_{0/1}$. Orange cells are partial relative shifts that contain the symmetric relative shift - *e.g* the updated value of $P_{0/1}$ should not rely on the partial relative shift $P_{0/1}^{(0)} = P_{0/0} \circledast P_{1/0}$ which contains the symmetric value $P_{1/0}$. Indeed, the matrix provided by the *DFTLink* algorithm being symmetric, $P_{i/j}[k] = P_{j/i}[N - k]$, as demonstrated in Section 6.5.2 - the symmetric value can be seen has the *intrinsic* value w.r.t. the posterior updates, and thus should not be taken into account.

	0	1	2	3	4	5	6	7	8	9	10	11	12	13	14	15	16	17	18	19	20	21	22	23	24	25	26	
IN \ OUT	$P_{0/0}^{(0)}$	$P_{1/0}^{(0)}$	$P_{2/0}^{(0)}$	$P_{0/0}^{(1)}$	$P_{1/0}^{(1)}$	$P_{2/0}^{(1)}$	$P_{0/0}^{(2)}$	$P_{1/0}^{(2)}$	$P_{2/0}^{(2)}$	$P_{0/1}^{(0)}$	$P_{1/1}^{(0)}$	$P_{2/1}^{(0)}$	$P_{0/1}^{(1)}$	$P_{1/1}^{(1)}$	$P_{2/1}^{(1)}$	$P_{0/1}^{(2)}$	$P_{1/1}^{(2)}$	$P_{2/1}^{(2)}$	$P_{0/2}^{(0)}$	$P_{1/2}^{(0)}$	$P_{2/2}^{(0)}$	$P_{0/2}^{(1)}$	$P_{1/2}^{(1)}$	$P_{2/2}^{(1)}$	$P_{0/2}^{(2)}$	$P_{1/2}^{(2)}$	$P_{2/2}^{(2)}$	
0	$P_{0/0}$	x,y	y	y						x									x									
1	$P_{1/0}$		x			0			0		y	x,y	y			0		0		x			0		0			
2	$P_{2/0}$			x								x							y	y	x,y							
3	$P_{0/1}$				x,y	y	y		0		0		x				0		0		x							
4	$P_{1/1}$		0			x				0			y	x,y	y		0		0		x						0	
5	$P_{2/1}$					x								x						y	y	x,y						
6	$P_{0/2}$						x,y	y	y					x					0		0		x					
7	$P_{1/2}$						0		0		x				0			0		0		x						
8	$P_{2/2}$									x					x					y	y	x,y						

Table 6.1: Partial relative shifts computations using equation: $P_{a/b}^{(c)} = P_{a/c} \circledast P_{b/c} = \mathbf{x} \circledast \mathbf{y}$

IN \ OUT	0	1	2	3	4	5	6	7	8
IN	$P_{0/0}^{(0)}$	$P_{1/0}^{(0)}$	$P_{2/0}^{(0)}$	$P_{0/1}^{(0)}$	$P_{1/1}^{(0)}$	$P_{2/1}^{(0)}$	$P_{0/2}^{(0)}$	$P_{1/2}^{(0)}$	$P_{2/2}^{(0)}$
0	$P_{0/0}^{(0)}$	\mathbf{x}_0							
1	$P_{1/0}^{(0)}$		\mathbf{x}_0						
2	$P_{2/0}^{(0)}$			\mathbf{x}_0					
3	$P_{0/0}^{(1)}$	\mathbf{x}_1							
4	$P_{1/0}^{(1)}$		\mathbf{x}_1						
5	$P_{2/0}^{(1)}$			\mathbf{x}_1					
6	$P_{0/0}^{(2)}$	\mathbf{x}_2							
7	$P_{1/0}^{(2)}$		\mathbf{x}_2						
8	$P_{2/0}^{(2)}$			\mathbf{x}_2					
9	$P_{0/1}^{(0)}$			\mathbf{x}_0					
10	$P_{1/1}^{(0)}$				\mathbf{x}_0				
11	$P_{2/1}^{(0)}$					\mathbf{x}_0			
12	$P_{0/1}^{(1)}$			\mathbf{x}_1					
13	$P_{1/1}^{(1)}$				\mathbf{x}_1				
14	$P_{2/1}^{(1)}$					\mathbf{x}_1			
15	$P_{0/1}^{(2)}$			\mathbf{x}_2					
16	$P_{1/1}^{(2)}$				\mathbf{x}_2				
17	$P_{2/1}^{(2)}$					\mathbf{x}_2			
18	$P_{0/1}^{(0)}$					\mathbf{x}_0			
19	$P_{1/1}^{(0)}$						\mathbf{x}_0		
20	$P_{2/1}^{(0)}$							\mathbf{x}_0	
21	$P_{0/1}^{(1)}$					\mathbf{x}_1			
22	$P_{1/1}^{(1)}$						\mathbf{x}_1		
23	$P_{2/1}^{(1)}$							\mathbf{x}_1	
24	$P_{0/1}^{(2)}$					\mathbf{x}_2			
25	$P_{1/1}^{(2)}$						\mathbf{x}_2		
26	$P_{2/1}^{(2)}$							\mathbf{x}_2	

Table 6.2: Following the partial relative shift computation described in 6.1, this table describes the recombination process of the partial information using equation: $P_{a/b} = \prod_{c=0}^{N-1} P_{a/b}^{(c)} = \prod_{c=0}^{N-1} P_{a/c} \circledast P_{b/c} = \prod_{c=0}^{N-1} \mathbf{x}_c$. Intrinsic, symmetric and extrinsic information are represented in red, orange and green, respectively. One should note that, in this simplified example, only one or two partial shifts remain in each product reduction although more elements participate in these product reductions when considering larger OFDM frames.

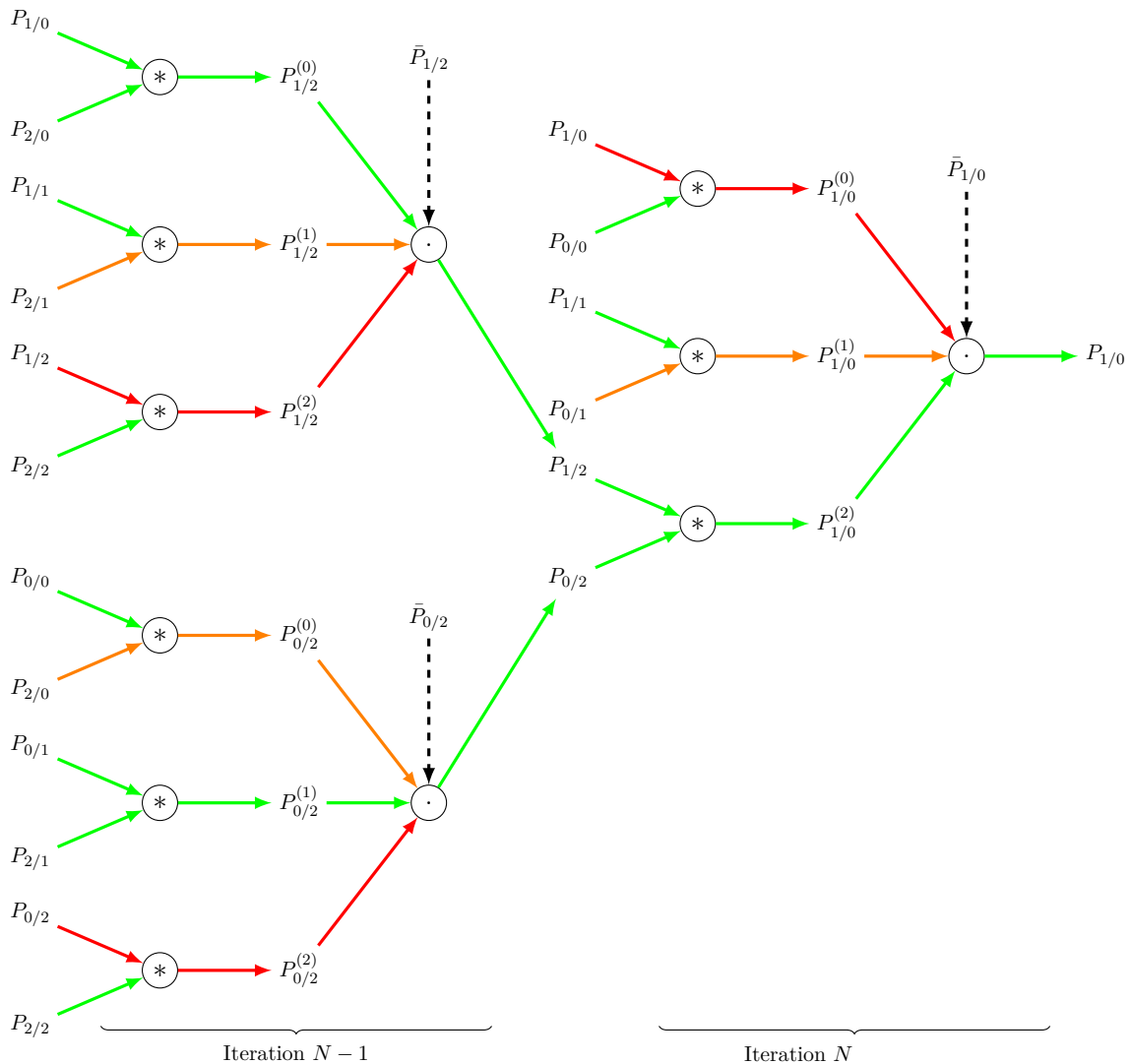


Figure 6.1: Exemple of GLAD computational graph for the $P_{1/0}$ relative shift. $\bar{P}_{i/j}$ denote the *a priori* information that is combined with the *extrinsic* information to update the *a posteriori* distribution at each iteration.

These two algorithmic steps are sequentially and iteratively executed as explicitly described in the example of Figure 6.1, describing the computational graph related to one of the relative shift variable. This figure adopts the same colour code to show the information that should or should not be kept at each iteration, in order not to directly propagate the *intrinsic* information to the next iteration.

Implementation as a Recurrent Cell

In practice, these operations are embedded into a *recurrent* cell to be executed iteratively as shown in Figure 6.2. At each iteration the *a priori* flattened relative shift matrix is provided and combined with the *extrinsic* information from previous iteration, also referred to as the *cell states*. The result is eventually combined with the communication system priors - *e.g.* if pilot symbols are in use, then some of the relative shifts in the matrix are known in advance and thus, certain distributions of the matrix should be multiplied by a Kronecker distribution (a probability of 1 for the pilot value, 0 elsewhere). Then, the *Operator A* extracts the adequate relative shift pairs to compute all the partial relative shifts. Next, *Operator B* extracts the different partial shifts for recombination. Then two computational paths are defined:

- If these results are to be used for next iteration, the extracted partial relative shifts are masked

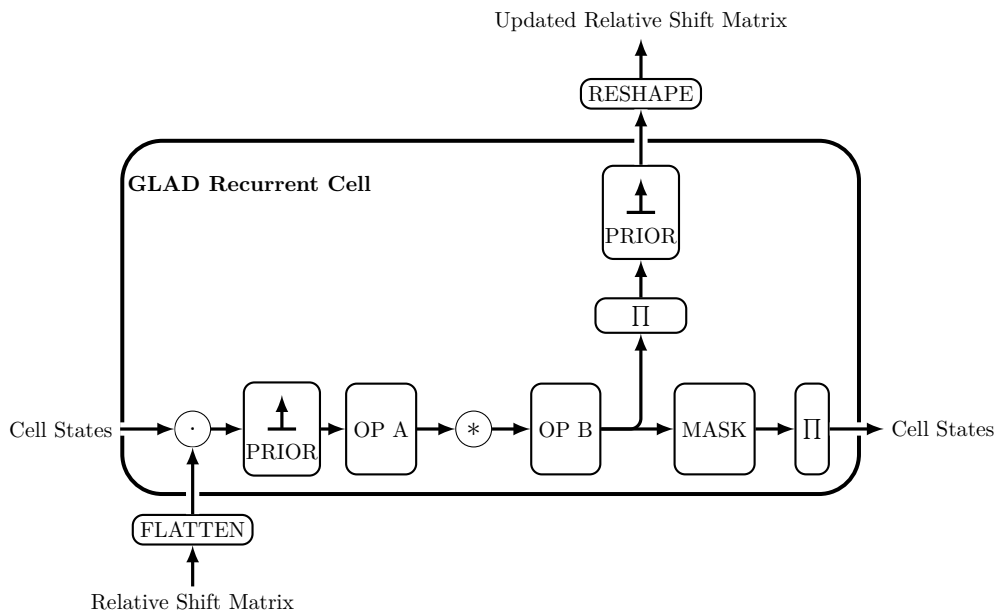


Figure 6.2: Complete computational graph of the proposed iterative demodulation algorithm.

to keep only the extrinsic information, combined using a product and provided to next iteration as the new cell states.

- If these results are to be used as the output of the cell, then the product reduction is directly applied without masking, to keep both, intrinsic and extrinsic information. The obtained result is again multiplied by the communication priors and the then updated relative shift matrix is reshaped in its initial format.

Communication Priors and Pilots Sequences

As shown in Figure 6.2, communication priors¹ can be used in the proposed demodulation algorithm to help the demodulation algorithm in its task. One such example of a communication prior is the use of pilots symbols which provides certainty about the value of certain symbols (and thus relative shifts) upon reception.

We provide here an example of a prior matrix in the case of a 5 OFDM symbols frame where, the symbols 0, 2 and 4 are pilots symbols with a value of the CCSK symbol of 0:

$$\begin{pmatrix} \delta(0) & 1 & \delta(0) & 1 & \delta(0) \\ 1 & \delta(0) & 1 & 1 & 1 \\ \delta(0) & 1 & \delta(0) & 1 & \delta(0) \\ 1 & 1 & 1 & \delta(0) & 1 \\ \delta(0) & 1 & \delta(0) & 1 & \delta(0) \end{pmatrix}$$

The diagonal of the matrix is always known as the relative shift of a symbol to itself and is always a shift of 0. For the pilots symbols which are defined with a value of 0, their relative shifts is also necessarily equal to zero, thus leading to a grid of Kronecker distributions. All the other indices of the relative shift matrix have a uniform prior, meaning that no prior knowledge is known about these relative shifts.

Uniform and Kronecker priors can be seen as the two extreme cases of absolute certainty or uncertainty. Obviously, one can imagine a communication system with other characteristics, and thus

¹These communication priors should not be confused with the *a priori* relative shift matrix. The latter is the *a priori* knowledge we have by looking at the received relative shift matrix (which varies from frame to frame), while the communication priors are the *a priori* knowledge we can have about any communication in this system, even before observing a received frame.

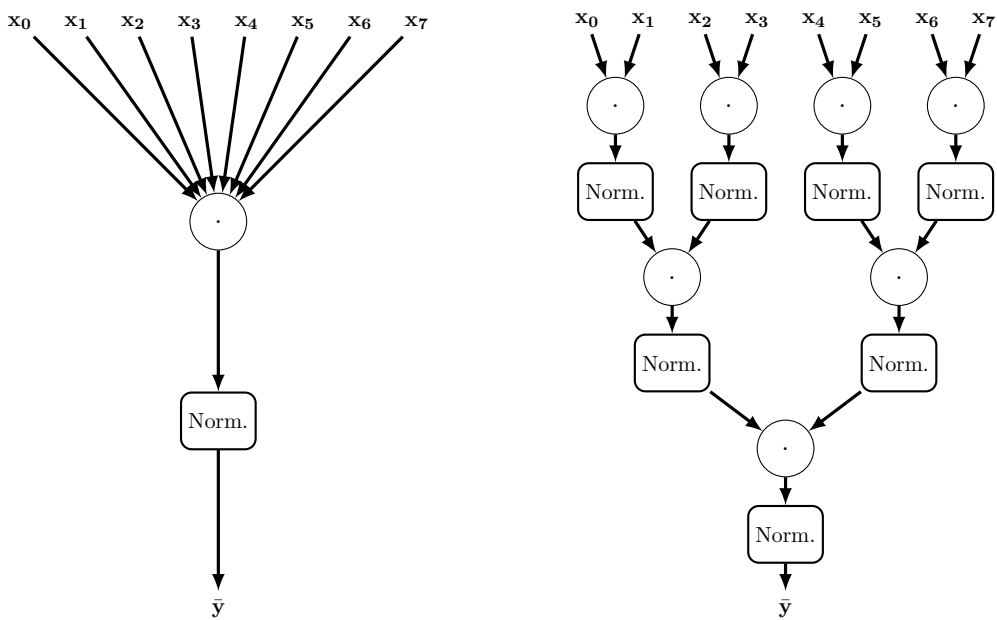


Figure 6.3: (Left) Standard product reduction with normalization - (Right) Partial tree product reduction with intermediate normalizations.

communication priors, to improve the robustness of the transmission, change its rate, or protect more certain parts of the frame than others, *e.g.* by using only a subset of the available values for certain symbols (and the corresponding communication priors upon reception).

Normalization, Product and Numerical Stability

Normalization steps have not been explicitly detailed in the previous description. We assume that the distributions in the relative shift matrix are probability distributions and should thus sum to one. Hence, every product or cross-correlations operations between these distribution occurring in the previously detailed graph is followed by a re-normalization step that ensures that the newly computed distribution sums to one.

One should note that numerical stability issues can occur during the product reduction step when it involves a large number of distribution, *i.e.* when consider a frame with a large number of OFDM symbols. Indeed, the reduction of multiple distributions whose value lies, by definitions between 0 and 1, can rapidly lead to small numbers and arithmetic underflow of the numerical representations used (typically *float32* numbers in the present case). To avoid these numerical issues we propose to use a slightly different product reduction, using a binary tree reduction. The product reduction is applied on pairs of distributions, the results are then normalised, before being again reduced in pairs and normalised, and so on and so forth until having obtained a single distribution (as shown in Figure~6.3).

Shifted Demodulation

We consider a CCSK OFDM frame composed of the shifts $[p_0, \dots, p_{Q-1}]$ with Q the number of CCSK symbols in the frame, and $0 \leq p_i \leq N - 1 \forall i$. The binary frame is integrity protected by a Cyclic Redundancy Check (CRC) or any other mechanism that allows the receiver to confirm that the demodulated bits are correct. Thus, a correct demodulation of the frame should provide the same shifts values as the one transmitted.

Nevertheless, if we consider a constant shift integer in the demodulated CCSK shifts, as $[p_0 + c \bmod (N), \dots, p_{Q-1} + c \bmod (N)]$ for $c \in \mathbb{N}$, the receiver can try each possible value of c and then check the integrity of the binary message. If the data integrity is confirmed for a value of c , the system can

consider this version as the right one. Consequently, in the following, we assume that a demodulated frame shifted by a constant value is correct.

Demodulation from the Relative Shift Matrix

The updated relative shift matrix does not provide the absolute shift of the CCSK sequences. To obtain the absolute shifts and process the final demodulation into binary words, there are two possibilities:

- The system has reference sequences, i.e pilot sequence, with known shift value at the receiver. Based on the known shift value, the receiver can deduct the absolute shift values of the rest of the frame, by taking the matrix line corresponding to the equalization with a reference sequence. If there are several reference sequences with the same shift value, then the different lines can be averaged, to obtain an estimate of the absolute shifts.
- As explained in the previous section 6.5.3, the shifted demodulation can be used to demodulate frame affected by a constant shift offset. Hence, a random sequence can be used as reference, its shift assumed equal to zero, and the corresponding line taken in the relative shift matrix. The obtained shifts are all moved by a constant value equal to the absolute shift of the sequence used as reference. Again this offset is unknown, but the frame can still be demodulated using the principles described in section 6.5.3.

6.6 Results

In this section, we evaluate the performance of the proposed model w.r.t. several parameters and compare it to standard algorithms. Otherwise explicitly stated, we use similar system design assumptions as the ones used throughout Section 5:

- The transmitter and receiver are based on CP-OFDM and CCSK scheme A.
- The dimension of the OFDM symbol is equal to the size of the ZC sequence, and noted $N = 64$. Consequently, each OFDM symbol carries a single ZC sequence, corresponding to a single CCSK symbol, representing binary word of 6 bits.
- The OFDM frame is composed of 20 successive OFDM symbols. The CP length is fixed to 10 symbols.
- The first OFDM symbol is used as a block pilot symbol. Hence the channel is estimated on each sub-carrier in the first OFDM symbol, and then interpolated with the linear interpolator in time over the data symbols. We use the root ZC sequence for the pilot symbol.
- We use the MRC scheme as an equalizer to improve the cross-correlation operation and the performance of the systems.
- Between successive OFDM symbols, the channel on the same sub-carrier is constant, i.e. the maximum Doppler shift is fixed to 0Hz.
- The system assumes a perfect synchronization in time and frequency at symbol rate, in baseband.
- The channel coefficients are not constant in frequency and vary along the sub-carriers. Hence, in time, the channel does not appear as a single path, but as a multi-path channel introducing ISI in time. A RMS delay spread of 400ns is considered.

In the present study, we recall that DFTLink algorithm computes the relative shift matrix which is provided to GLAD algorithm for demodulation.

6.6.1 Comparison with Standard Solutions

The performance of the proposed model is compared with that of standard approaches based on LS, LMMSE (with and without approximations) estimates or perfect channel knowledge, and MRC equalization. Under the general system design assumptions described above, the performance of the proposed algorithm lies between that of LS-MRC approaches and practical implementations of LMMSE-MRC based on approximations.

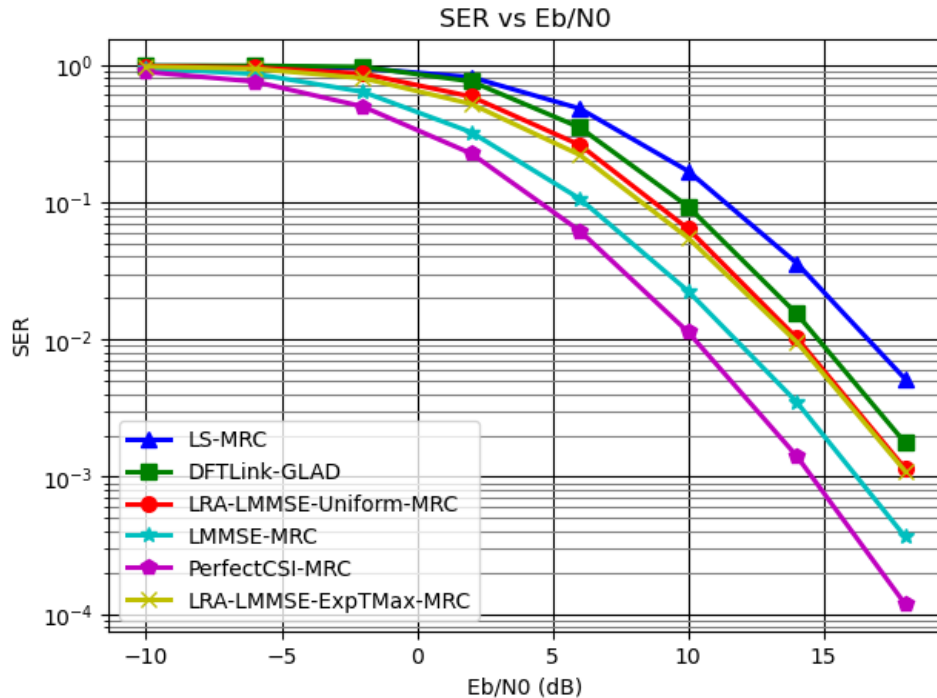


Figure 6.4: Comparison of the performance of the GLAD algorithm with that of different standard approaches.

These results are promising and show that the proposed combination of the DFTLink and GLAD algorithms offers performance close to that of practical implementations of the LMMSE approach. However, the algorithmic complexity of the proposed approach is higher than that of the other models in this comparison. Yet, this extra cost in terms of complexity makes it possible, among other things, to support pilot-less approaches (see section 6.5.3 on shifted demodulation) and could, moreover, be reduced in the future with novel algorithms based on the DFTLink relative shift matrix.

6.6.2 Benefits of the Iterative Approach

In this section, we study the impact of the iterative approach, in order to verify that running several iterations of the proposed algorithm does indeed bring a performance gain. We measure the evolution of the SER of the system after a certain number of iterations for a fixed signal-to-noise ratio ($E_b/N_0 = 18\text{dB}$). As shown in Figure 6.5, the iterative approach effectively improves performance with an observed reduction in the error rate of more than a factor of 3 after 4 iterations (compared with a single iteration). The figure also presents an error floor which shows that it is not necessarily worth applying more than 4 iterations, as the performance gain per additional iteration decreases rapidly.

6.6.3 Channel Diversity

This section address the question of channel diversity, both in time and frequency, and study the impact of the number of pilot and their positions in the frame.

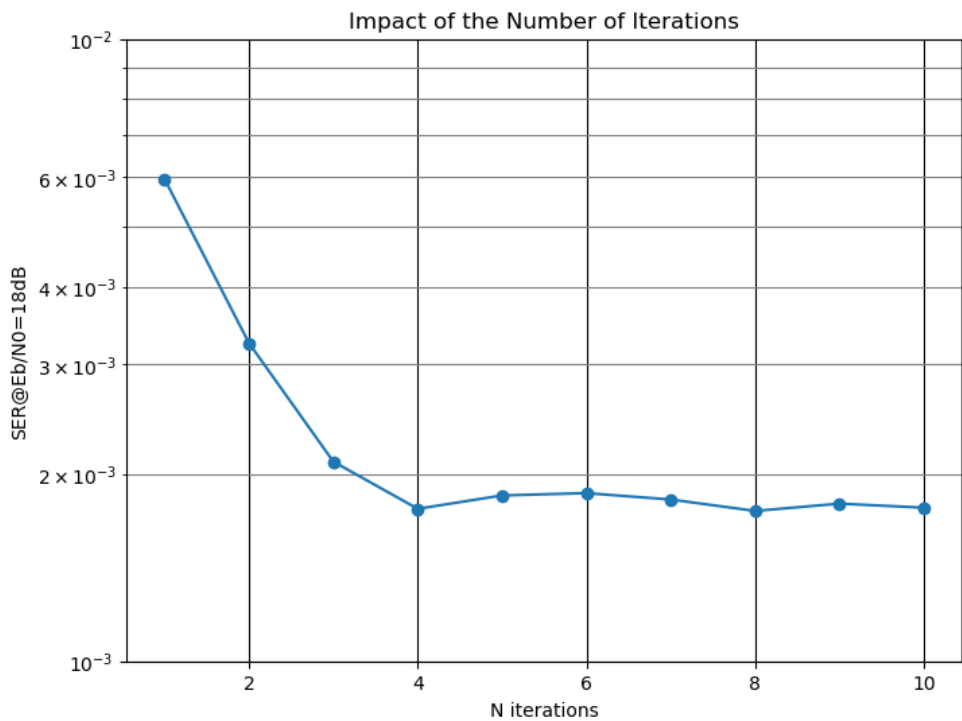


Figure 6.5: Evolution of GLAD algorithm performance as a function of the number of demodulation iterations. While the number of iterations does have an impact on the final performance, it appears to be limited to the first 4 iterations.

Time Diversity - Effects of Doppler Shift and Pilot Positioning

Doppler effect introduces channel evolution in time that can induce severe performance degradation, in particular when the channel varies significantly over the duration of an OFDM frame. We study here the impact of the Doppler with maximum frequencies ranging from 0 Hz (*i.e. no Doppler*) to 10 kHz. The position and number of pilots in the frame is particularly important to accurately estimate and thus counterbalance the evolution of the channel over the duration of the frame. Three pilot configurations are compared:

- A:** A single pilot, at the beginning of the frame (index 0).
- B:** Two pilots, at both beginning and end of the frame (indices 0 and 19).
- C:** Three pilots, at the beginning, middle and end of the frame (indices 0,10,19).

Figure 6.6 describe the performance of the different models at a fixed signal-to-noise ratio ($E_b/N_0 = 14\text{dB}$) for different Doppler frequency. For each model, the three pilot configurations described before are tested and represented using three colors. Several conclusions can be drawn from these results:

- Under no Doppler, it is clear that whereas an increased number of pilot symbols allows for a better channel estimate (and thus better performance) in the case of LS or LMMSE models, it leads, on the contrary, to a reduced efficiency for the GLAD (which use anyway the complete frame for channel estimation) and PerfectCSI models. The more pilots symbols, the less data payload for a same amount of energy used for transmission.
- When the maximum doppler frequency is non zero, whatever the scheme, configurations with more pilots are more robust and thus maintain acceptable performance over a wider doppler range.
- At higher Doppler frequencies ($> 10^3\text{Hz}$), GLAD outperforms the other systems, but error rates remain very high in all cases ($> 20\%$). Whereas the performance of LS and LMMSE all converge

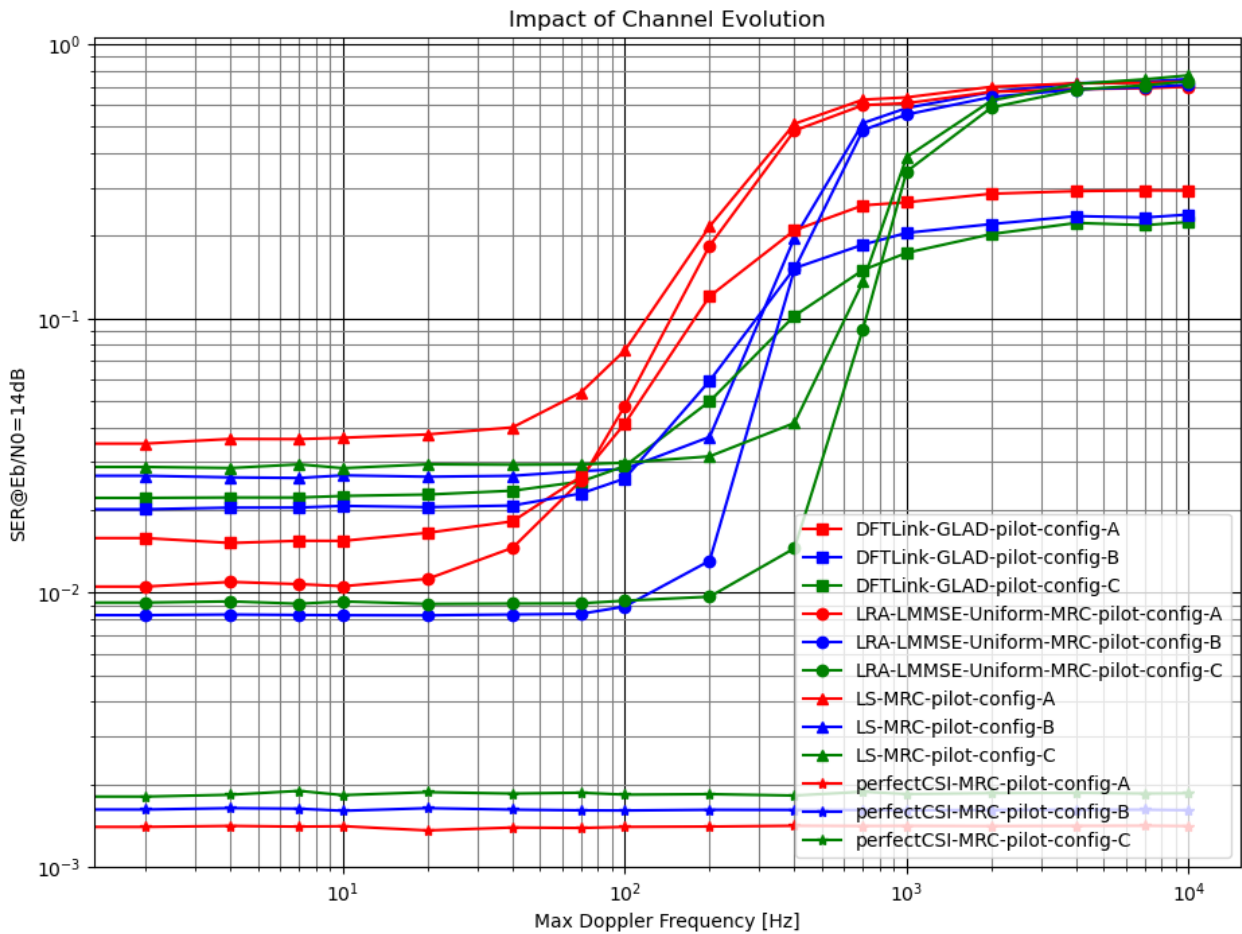


Figure 6.6: Evolution of the performance of GLAD algorithm compared to that of standard methods as a function of the maximum Doppler frequency. Different pilot configurations are tested: (red) A: A single pilot, at the beginning of the frame (index 0) - (blue) B: Two pilots, at both beginning and end of the frame (indices 0 and 19) - (green) C: Three pilots, at the beginning, middle and end of the frame (indices 0,10,19).

towards 70% SER, whatever the number of pilots used, GLAD's performance level increases with the number of pilots (the algorithm is better able to take advantage of the pilots). It should be remembered that, although GLAD estimates the channel using all available symbols, known pilot symbols, considered as communication *priors* described by Kronecker distribution in the relative shifts matrix, still can help improving the estimation of all relative shifts.

In order to better mitigate the effect of channel evolution, we propose an additional treatment in the GLAD algorithm, which consists in filtering out information in the relative shift matrix that is considered unreliable. Indeed, the estimation of the relative shifts between too much spaced symbols in the OFDM frame is likely to be unreliable, and the algorithm should not use them in the presence of significant Doppler, but rather use reliable information, *i.e.* pilot data or the relative shifts between sufficiently close symbols within the frame. This procedure is implemented by applying a windowing mask to the relative shift matrix before the GLAD demodulation procedure. The proposed mask is defined in the form of a unit band matrix, *i.e.* a matrix that has unit elements arranged uniformly

near the diagonal, and zero elsewhere, such as:

$$\text{mask} = \begin{pmatrix} 1 & 1 & 0 & 0 & 0 \\ 1 & 1 & 1 & 0 & 0 \\ 0 & 1 & 1 & 1 & 0 \\ 0 & 0 & 1 & 1 & 1 \\ 0 & 0 & 0 & 1 & 1 \end{pmatrix}$$

In such example, and assuming an OFDM frame of size 5, by using a window of size 3 we consider that only strictly adjacent symbols should be considered in the relative shift updates.

Figure 6.7 displays the results obtained with such procedure with windows of sizes 7 and 15 (over a frame of 20 symbols) and for pilot configurations A, B and C.

In any case, using the windowing procedure in the absence of significant Doppler always degrades performance, which is completely logical since it means discarding reliable estimates of the channel. The proposed method does not seem to provide any performance gain with the pilot configuration A, for any window size. In the case of the pilot configuration B, the window size of 7 seems to be too restrictive and thus do not bring performance gain either.

When the Doppler is too high, the windowing procedure does not help either. On the other hand, in the intermediate tilting zone, with a moderate Doppler (around 10^2 Hz), adequate windowing seems to be able to improve GLAD performance and extend the frequency range beyond which the Doppler degrades the system's performance too much.

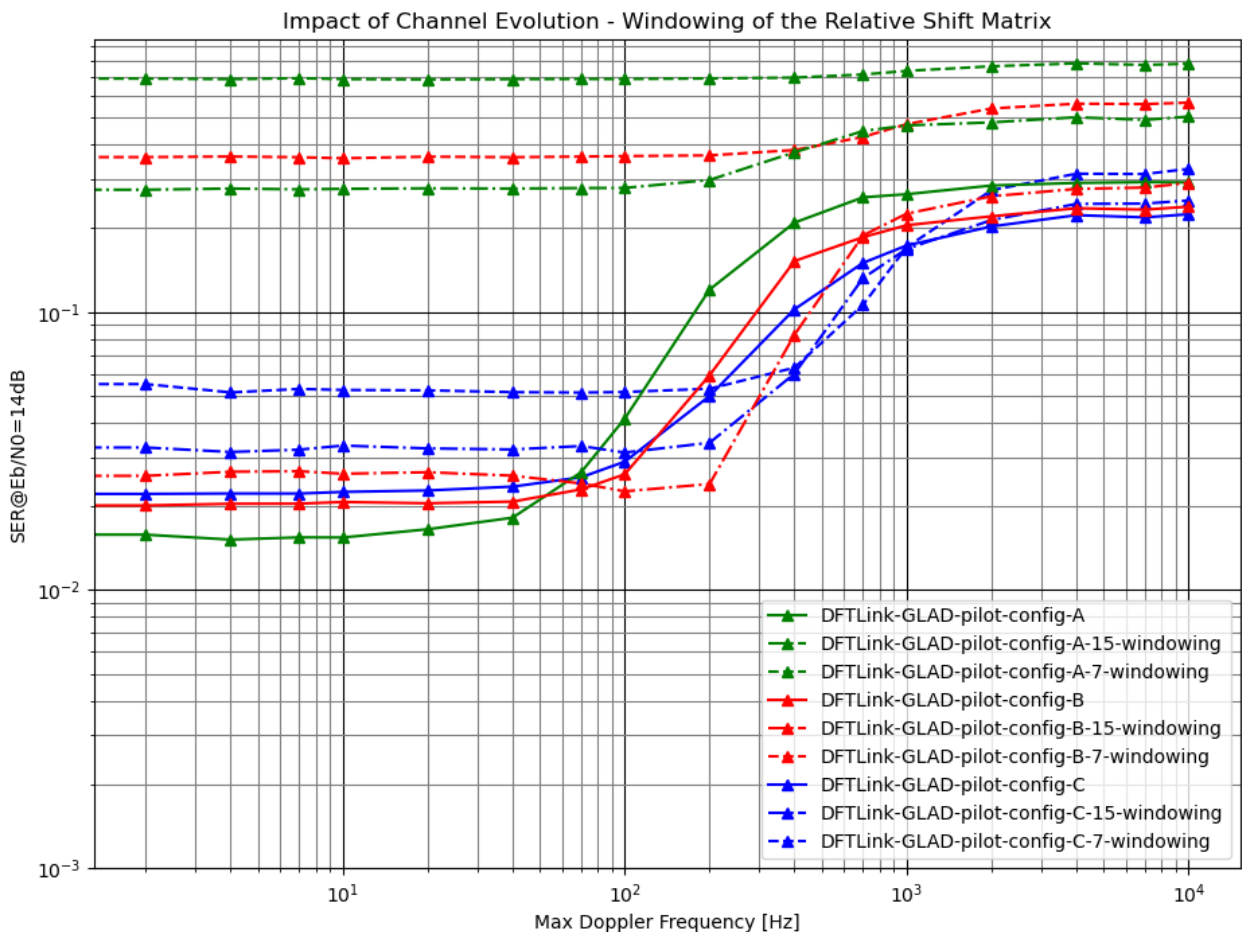


Figure 6.7: Evaluation of the windowing approach applied to GLAD algorithm under different pilot configurations and doppler shift. (solid lines) no windowing - (dashed lines) window of size 7 - (dash-dotted lines) window of size 15. We recall that the total OFDM frame length is 20.

Exploiting Channel Frequency Diversity

Another type of channel diversity can occur in the frequency domain, for example in the presence of multi-path, resulting in a variation in the channel response on different sub-carriers. By modifying the time delay spread of the channel, we study in this section the impact of frequency diversity on the different models.

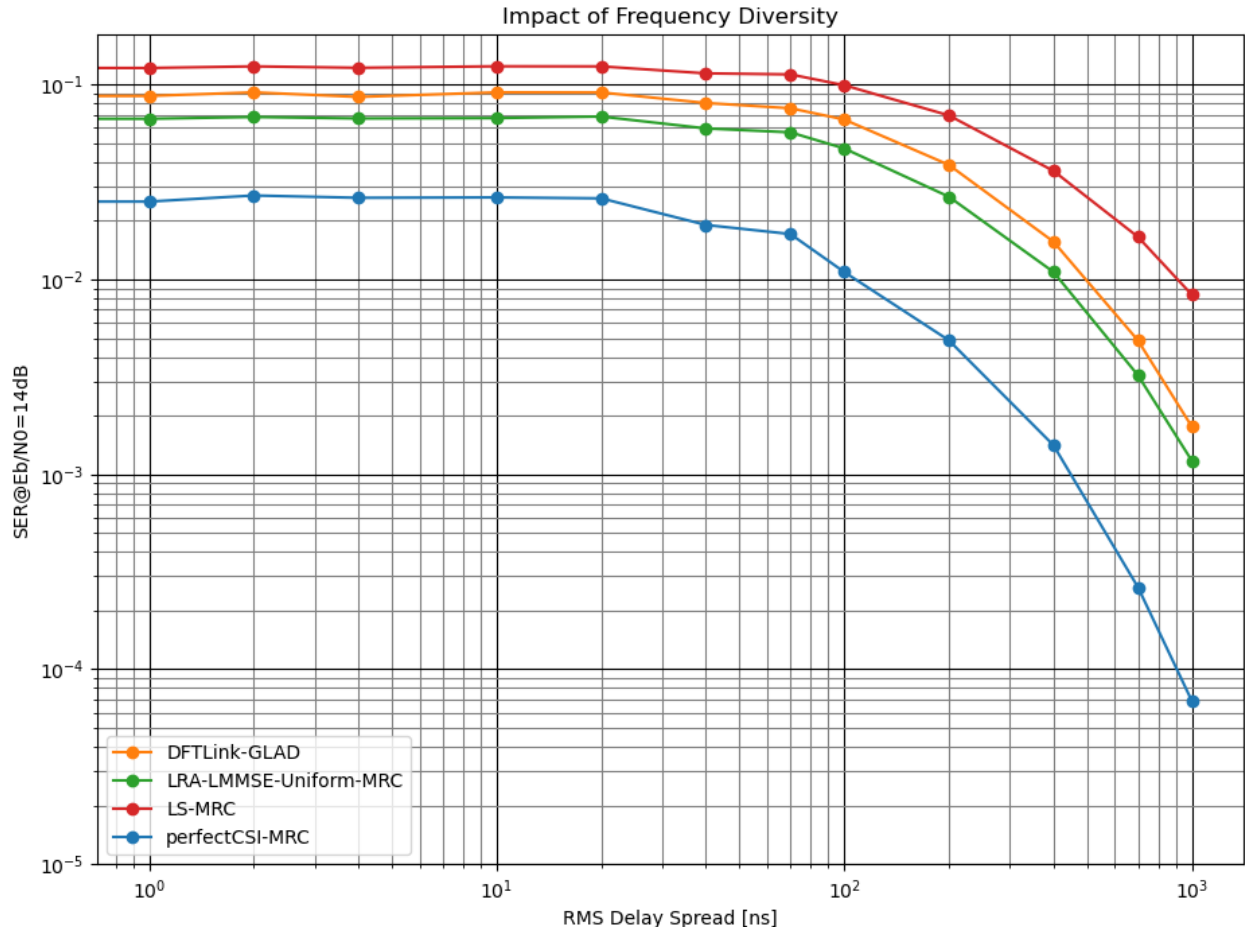


Figure 6.8: Evolution of the performance of the different models under increasing channel delay spread/frequency diversity.

As shown on Figure 6.8, GLAD algorithm benefits of the increased frequency diversity in a similar way to that of LMMSE.

6.6.4 Scaling the OFDM Frame Size

In this section, we investigate the impact of OFDM frame length on system performance. Figure 6.9 displays the SER performance of the different models at a fixed signal-to-noise ratio ($E_b/N_0 = 14\text{dB}$) for different size of OFDM frame (the first symbol of the frame being a pilot). In the case of the LS and LMMSE models, and in the presence of a constant-time channel (no Doppler), the quality of the channel estimation, based on the single pilot symbol at the beginning of the frame, does not improve with frame length. Thus, the observed increase in performance of the LMMSE and LS models is mainly due to the reduction in the relative overhead of the pilot in relation to the frame size (a single pilot inserted in a small frame has a greater negative impact in terms of energy efficiency than in a longer frame). As a result, the relative performance per additional OFDM symbol decreases rapidly before reaching a floor. In contrast, for the GLAD algorithm, the performance gain is also due to the better channel estimates that accompany a larger frame. In fact, the GLAD algorithm uses all the

symbols to estimate the channel and therefore benefits from a longer frame, at least for channels that are constant throughout the frame.

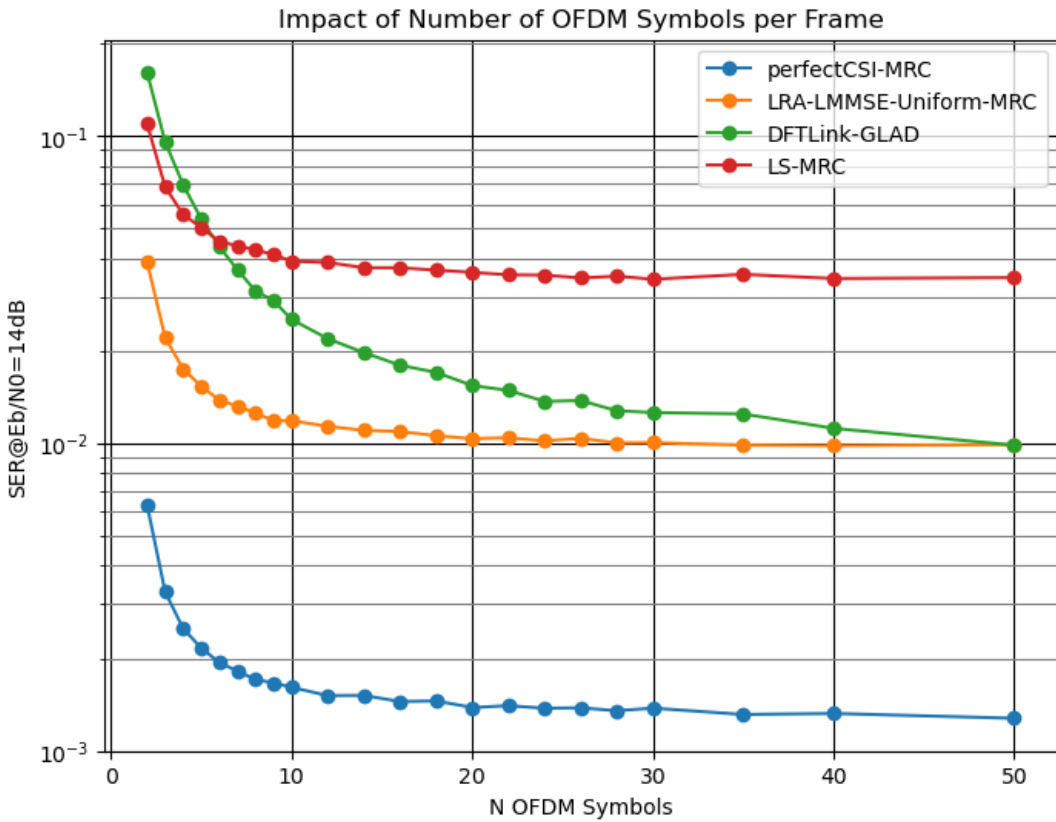


Figure 6.9: Performance of the different models with increasing OFDM frame length. We recall that the frame always start with a single pilot symbol.

For computational reasons, no frames longer than 50 symbols were tested but an interesting question would be that of the asymptotic performance of the GLAD algorithm. Indeed, the latter benefits from a better channel estimate for each added symbol, whereas pilot based approach like LMMSE or LS are obviously limited in their performance by the number of pilots present in the frame. Potentially, under very long frame, DFTLink and GLAD algorithm allow for a perfect channel estimate, and thus similar performance to that of perfectCSI-MRC model.

Another way to study the impact of Doppler shift on the proposed system, is to study its performance when the length of the frame increases (with a single pilot at its beginning), under a certain Doppler frequency. Figure 6.10 shows the performance of the different models under maximum Doppler frequencies of 0,100 and 200 Hz and with frame size ranging from 2 to 50 OFDM symbols.

Once again, we see that GLAD algorithm seems to offer better robustness w.r.t. Doppler shift: its performance start degrading with larger frame than LS or LMMSE, the degradation is slower as the frame size increase, and it finally reach better performance than the other models.

6.6.5 Scaling the CCSK Sequence Length

In this section, we briefly address the issue of CCSK sequence length and its impact on model performance. Figure 6.11 shows the SER performance of the different models at a fixed signal-to-noise ratio ($E_b/N_0 = 14\text{dB}$) for different numbers of bits k per CCSK symbol and hence different sizes 2^k of the CCSK sequence. The performance of the GLAD algorithm falls between that of LS and LMMSE, although the LMMSE algorithm appears to benefit more from increasing the length of the CCSK sequence.

For computational reasons, this study is unfortunately very limited with a number of bits ranging

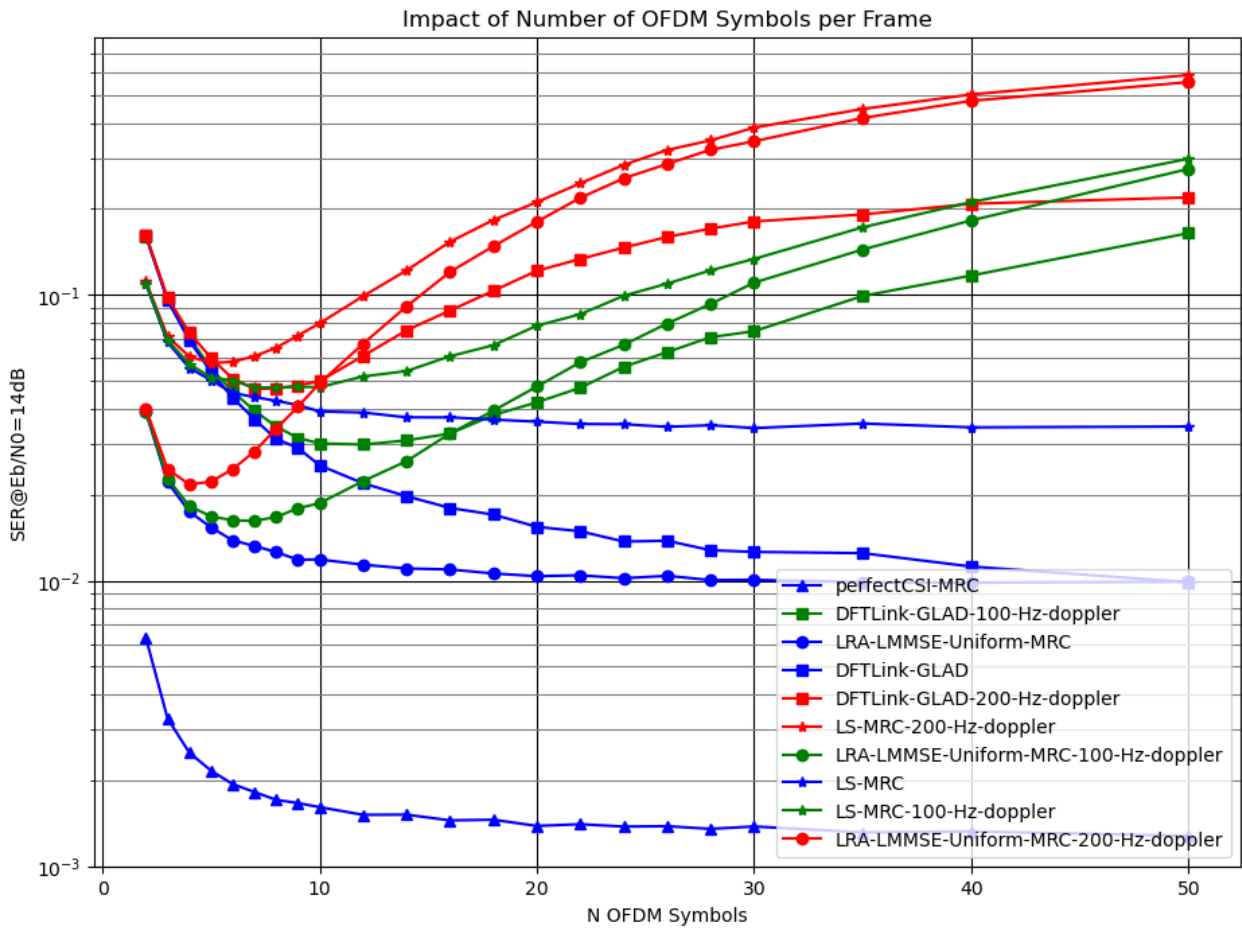


Figure 6.10: Evolution of model performance with increasing frame length in the case of Doppler shift. The longer the frame, the greater the channel is uncorrelated between the beginning and end of the frame. Remember that a single pilot symbol is inserted at the start of the frame.

from 4 to 7 due to the exponential growth in the size of the sequence. No detailed analysis can therefore be carried out in this respect.

6.7 Conclusion on the DFTLink and GLAD Algorithms

The combination of the DFTLink and GLAD algorithms get good performances when compared to more traditional receiver scheme, but at the cost of a high complexity. Further study need to be done to improve the efficiency of the GLAD algorithm, simplifying the graph and using the right approximations. The windowing step is also a promising improvement to increase the robustness against Doppler.

But despite its high complexity and its overall good performances, the DFTLink and GLAD algorithms show specifically great promises in case of constant channel (no Doppler). The capacity to get a channel estimate for each OFDM symbol, and the principle of shifted demodulation enabling the demodulation of the frame without pilot sequence unlock the path for an improved system capacity, especially for short packet.

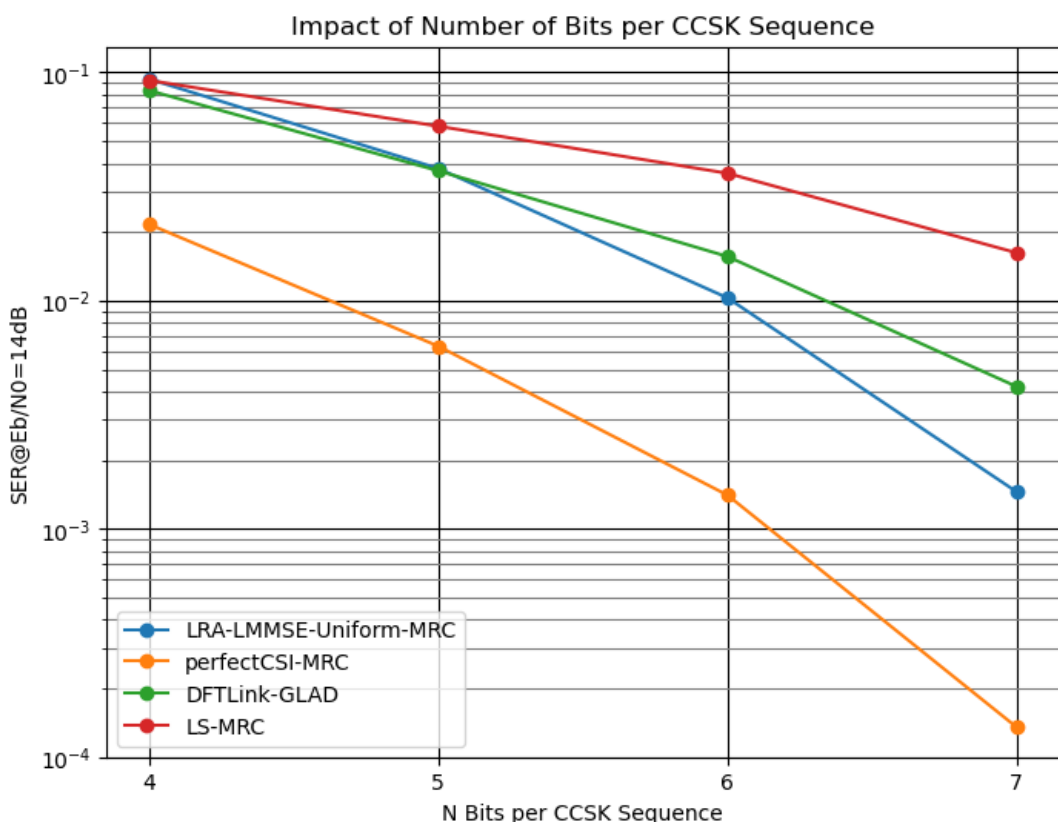


Figure 6.11: Performance of models with different numbers of bits per CCSK symbol, and therefore different CCSK sequence lengths.

7 Time and Frequency Synchronization

In this section, we evaluate the robustness of the CCSK OFDM modulation to imperfect time and frequency synchronization.

7.1 Impact of Synchronization Error in Time

We assume a perfect frequency synchronization and imperfect time synchronization. We also assume, that a coarse time synchronization of the frame is available, i.e. the frame rough position has been detected, and the fine time synchronization is needed. We assume that each OFDM symbol carries a single CCSK sequence. The receiver has to find the start of the frame as the first sample of the first CP. The whole frame spans on $Q * (N + L)$ samples at symbol rate, that the receiver should extract to process the demodulation, with Q the number of OFDM symbols within the frame, N the length of a ZC sequence and L the CP length.

The received samples at symbol rate for an OFDM symbol starts with a CP of length L : $[Y[-L], Y[-L+1], \dots, Y[-1], Y[0], Y[1], \dots, Y[N-1]]$. We assume a synchronization error of $-Z$ samples at symbol rate, with $Z \leq L$, So that the extracted OFDM symbol, after the CP removal is equal to $[Y[-Z], Y[-Z+1], \dots, Y[-Z+N-1]]$. In case of perfect synchronization, $Z = 0$.

Without noise and fading channel, the received CP samples are equal to the end of the OFDM symbol. Noting X the sequence of transmitted symbols, the received samples $[Y[-Z], Y[-Z+1], \dots, Y[N-1-Z]]$ are equal to $[X[N-Z], \dots, X[N-1], X[0], X[1], \dots, X[N-1-Z]]$. The receiver computes the DFT of this sequence:

$$\begin{aligned}
F(X)[k] &= \frac{1}{\sqrt{N}} \sum_{n=0}^{N-1} X[n-Z] \exp\left(-j2\pi \frac{nk}{N}\right) \\
&= \frac{1}{\sqrt{N}} \sum_{n'=-Z}^{N-1-Z} X[n'] \exp\left(-j2\pi \frac{(n'+Z)k}{N}\right) \\
&= \exp\left(-j2\pi \frac{Zk}{N}\right) \frac{1}{\sqrt{N}} \sum_{n'=-Z}^{N-1-Z} X[n'] \exp\left(-j2\pi \frac{n'k}{N}\right) \\
&= \exp\left(-j2\pi \frac{Zk}{N}\right) F(X)[k] \\
&= \exp\left(-j2\pi \frac{Zk}{N}\right) c_p[k]
\end{aligned} \tag{7.1}$$

with c_p the ZC sequence transmitted, modulated with a shift value of p : $c_p[k] = x_u[k-p]$. The synchronization error in time results in a linearly increasing phase shift of the ZC sequence along the sub-carriers. Then, the receiver computes the cross-correlation of the receive sequence with root ZC

sequence to find the maximum of correlation:

$$\begin{aligned}
 R[i] &= \frac{1}{\sqrt{N}} \sum_{k=0}^{N-1} c_p[k] c_0^*[k-i] \exp\left(-j2\pi \frac{Zk}{N}\right) \\
 &= \frac{1}{\sqrt{N}} \sum_{k=0}^{N-1} x_u[k-p] x_u^*[k-i] \exp\left(-j2\pi u u^{-1} \frac{Zk}{N}\right) \\
 &= \frac{1}{\sqrt{N}} \sum_{k=0}^{N-1} x_u[k] x_u[p] \exp\left(j2\pi u \frac{kp}{N}\right) x_u^*[k] x_u^*[i] \exp\left(-j2\pi u \frac{ki}{N}\right) \exp\left(-j2\pi u \frac{u^{-1}Zk}{N}\right) \\
 &= \frac{1}{\sqrt{N}} x_u[p] x_u^*[i] \sum_{k=0}^{N-1} \exp\left(j2\pi u \frac{k(p-i-u^{-1}Z)}{N}\right)
 \end{aligned} \tag{7.2}$$

The sum is not equal to zero if and only if $p - i - u^{-1}Z \equiv 0 \pmod{N}$. For instance, when $i = p - u^{-1}Z \pmod{N}$. This value is unique on $[0, N-1]$. Consequently, we have:

$$R[i] = \begin{cases} \sqrt{N} x_u[p] x_u^*[i], & \text{when } p - i - u^{-1}Z \equiv 0 \pmod{N} \\ 0, & \text{otherwise} \end{cases} \tag{7.3}$$

The last equation means that, to obtain the correlation peak, the absolute value has to be taken, and that the peak is moved by a value of $u^{-1}Z$ from p . The peak is still unique. Moreover, it should be noted that in our system, the values of u^{-1} and Z are constants, at least for the duration of a frame. Hence, our mis-synchronized system is in a typical case of shifted demodulation (see section 6.5.3). After the CCSK demodulation, all the shifts values of the frame should have the same offset of $-u^{-1}Z \pmod{N}$. Considering a shifted demodulation, the resulting frame is correct. This behavior is summarized in Figure 7.1.

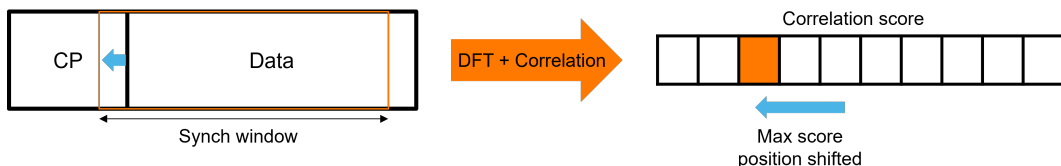


Figure 7.1: Impact of a negative timing error on the final demodulated CCSK shift.

We introduce a new metric named Shifted Block Error Rate (SBLER) to measure the performance of the system in the conditions of a shifted demodulation. The SBLER counts a block error, i.e. an erroneous frame, if the difference between the true shift and the demodulated shift is not constant across the frame. In our case, this difference should be constant and equal to $-u^{-1}Z \pmod{N}$. In Figure 7.2, the SBLER is evaluated for a timing error of respectively minus 4 and minus 8 samples, corresponding to minus 1 and minus 2 symbols, our system using an oversampling factor of 4. The performance confirms that the SBLER is not impacted by the negative timing error, when the synchronized window includes the CP.

Of course, in case of multipath fading, the CP is also affected by interference from the previous OFDM symbol. These interference mitigate the correlation scores and the performances. Yet, the principles outlined above remain valid and a shifted demodulation can be processed. One could increase the CP length to take both effect into account: multipath fading and synchronization errors.

If the synchronization error is now positive, so that it includes the CP of the following OFDM symbol, the equations stay the same, replacing the $-Z$ by a $+Z$. Because of the interference of the next CP, the performance will decrease compare to the better case of a negative synchronization error. The Figure 7.3 highlights the impact on the SBLER performances when the timing error is positive.

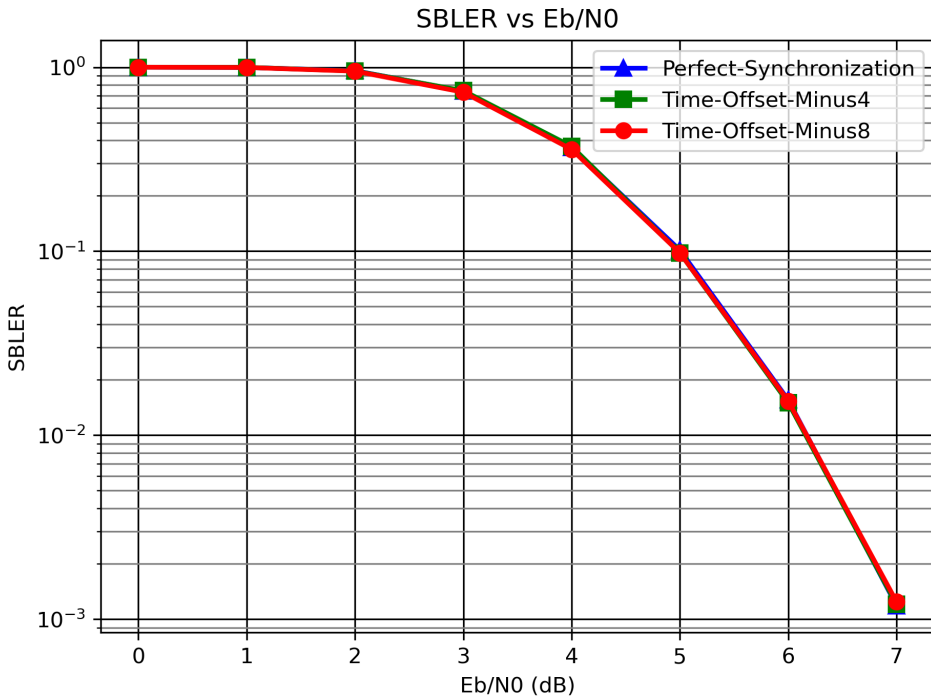


Figure 7.2: SBLER vs Eb/N0 for negative timing error at symbol rate.

7.2 Impact of Synchronization Error in Frequency

We assume that the system is perfectly synchronized in time, but not in frequency, so that a frequency offset remains in baseband. A coarse frequency synchronization is available and the remaining offset range from a fraction of sub-carrier spacing to a few sub-carrier spacing. Again we assume that each OFDM symbol carries a single CCSK sequence. Moreover, we suppose that the frequency offset stays constant throughout the frame.

Considering an OFDM system, it is common to decompose the frequency offset as an integer part and a fractional part of the sub-carrier spacing:

$$f_0 = (f_i + f_r)\Delta_f \quad (7.4)$$

with f_0 the frequency offset in baseband, $f_i \in \mathbb{Z}$ the integer part, $f_r \in [-0.5, 0.5]$ the fractional part and Δ_f the sub-carrier spacing.

If f_r is not equal to zero, the orthogonality of the OFDM modulation is broken, and all subcarriers interfere with each other.

If f_i is not equal to zero all the subcarriers will be shifted by f_i positions, and under the right conditions of filtering, aliasing in frequency will occur. This phenomena of aliasing is represented in Figure 7.4, where a frequency offset of $f_0 = \Delta_f$ is represented. If the low-pass filter is not too sharp, all the shifted sub-carriers are included in the spectrum and the downsampling creates an aliasing, moving the last sub-carrier at the first position. As represented in Figure 7.4, this exactly corresponds to a shifting of the CCSK sequences by one position. Hence, an integer frequency offset creates an additional shift in the CCSK sequences, assuming compatible filtering conditions. Moreover, if the frequency offset is constant throughout the frame, all the CCSK symbols are shifted by the same value f_i , allowing a shifted demodulation to occur. The SBLER performance for plus or minus one sub-carrier frequency shift is provided in Figure 7.5, showing no difference with the perfect synchronization case.

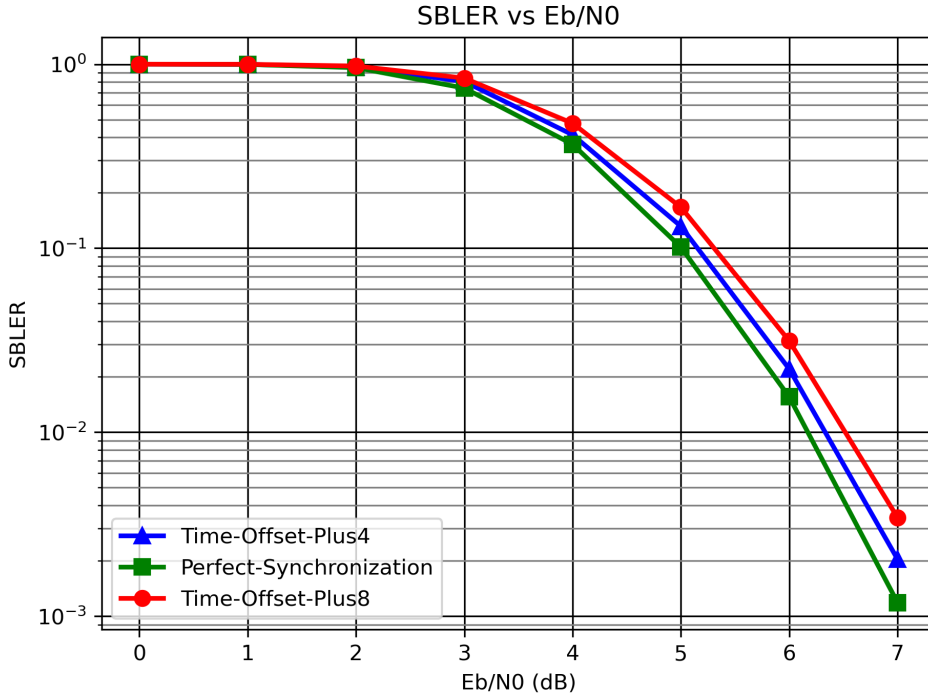


Figure 7.3: SBLER vs Eb/N0 for positive timing error at symbol rate.

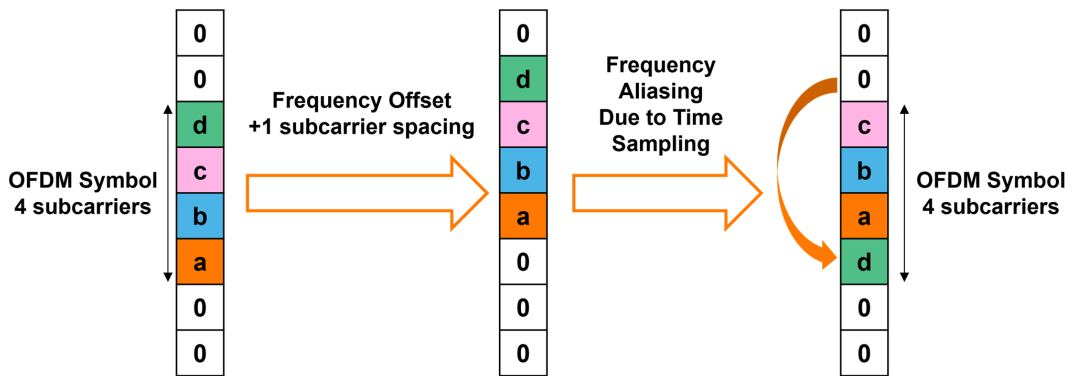


Figure 7.4: Impact of an integer frequency error on the final demodulated CCSK shift.

7.3 Including Iterative Mapping

The iterative mapping, i.e. transmitting several CCSK sequences within each OFDM symbol (see section 4.4.1), also benefits from the shifted demodulation in case of time synchronization error and integer frequency offset.

In case of time offset, the linearly increasing phase shift $\exp(-j2\pi \frac{Zk}{N})$ is the same in frequency. Looking at a specific sequence at the position m within the OFDM symbol, the observed phase shift for this sequence increases at a rate q , equal to the number of CCSK sequences multiplexed: $\exp(-j2\pi \frac{Z(qk+m)}{N})$. The rest of the computation in Eq.7.2 is the same, with a maximum of correlation reached when $p - i - u^{-1}qZ \equiv 0 \pmod{N}$ equal to $\sqrt{N}x_u[p]x_u^*[i] \exp(-j2\pi \frac{Zm}{N})$.

In case of integer frequency offset, the impact is more complex. To illustrate the phenomenon, consider two OFDM symbols carrying each three CCSK sequences with an iterative mapping, as illustrated in Figure 7.6. We identify three groups of sub-carriers, depending on their index in the OFDM symbols. The Figure 7.7 describes the impact of an integer frequency offset of one position.

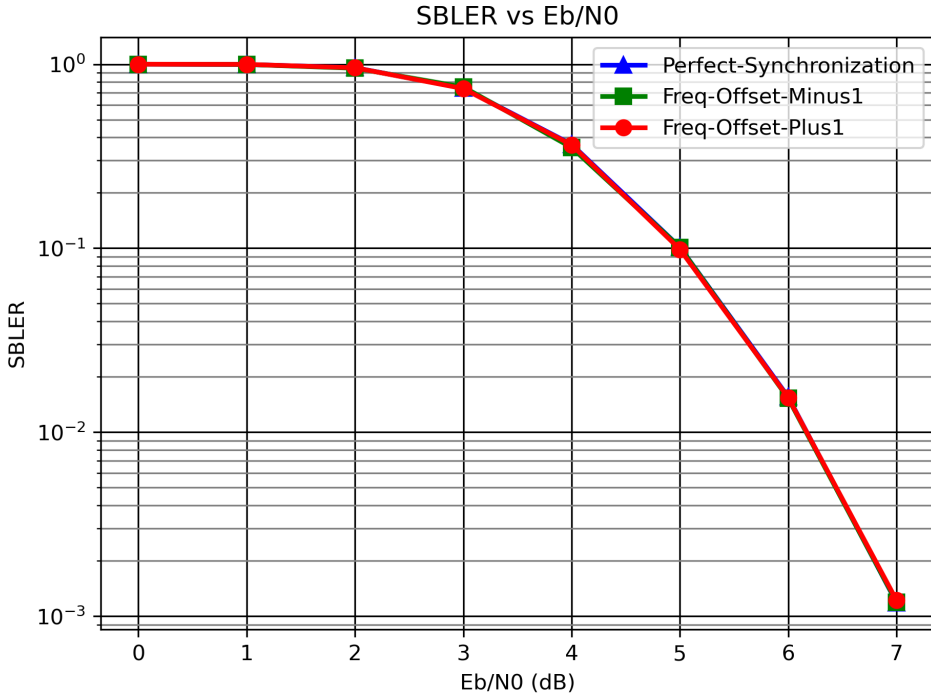


Figure 7.5: SBLER vs Eb/N0 for integer frequency offset.

All the six sequences are shifted by one position upward and cyclically returned to the bottom by the aliasing effect. The groups positions do not change, leading to a switch of group for all sequences. The ones in Orange group moves to the Green group; the ones in the Green group moves to the Blue group; and the Blue group to the Orange group. Now, we can notice that the sequences that have migrated from the Orange group to the Green group, i.e. the aliased ones, have also both circularly shifted by one position. Hence, for each additional sub-carrier frequency offset, the sequences continues to move from group to group, and the aliased ones also circularly shift from one position. The Figure 7.8 presents the sequences state after a shift of two sub-carriers.

Consequently, at the receiver, the sequences in each group had the same position in the OFDM spectrum at the transmission and are subject to the same number of circularly shifts. Hence, the shifted demodulation can be independently applied to each group. Nevertheless, the system needs to include a mechanism to determine the original positions of the sequences as this may impact the following binary word processing.

7.4 Detection and Synchronization System

7.4.1 System Model

To evaluate the impact of imperfect time and frequency synchronizations on a CCSK OFDM communications scheme, we assume the following basic system:

- Each OFDM symbol carries a single CCSK sequence, represented by a ZC sequence of length $N = 64$. The CCSK scheme A is used as a basis for the CCSK OFDM transmission. A CP of length 10 is added to each OFDM symbol.
- The frame is 20 symbols long, with $Q = 20$. The frame is composed of $(N + 10) * Q = 1480$ samples at symbol rate.

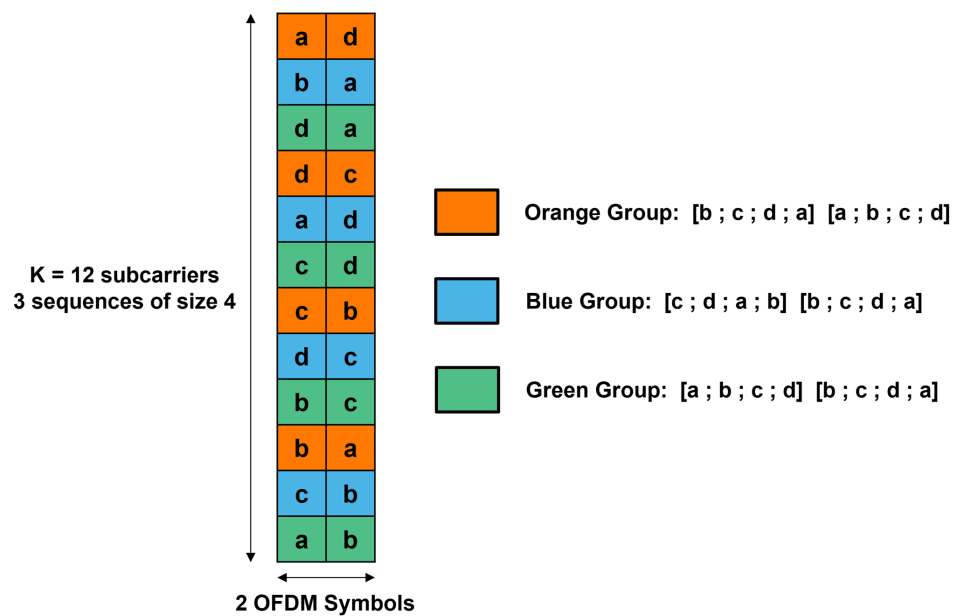


Figure 7.6: Group mapping for CCSK sequences.

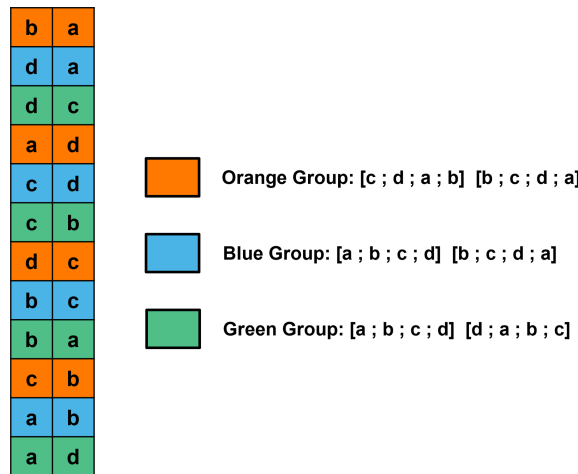


Figure 7.7: Impact of a frequency offset of one sub-carrier.

- The channel is a complex AWGN. No fading channel is considered to avoid side effects as ISI and focus the performance analysis on the features previously presented.
- The simulation uses an oversampling of 4, and the oversampled frame length is 5920 samples.
- The frame needs to be first detected. The data frame of Q OFDM symbols is placed between two blocks of zeros (noise), each also of length 5920 samples.

The Figure 7.9 provides a global overview of the simulated frame. Once the receiver has selected a sample as the frame start, it selects the following 5920 samples and downsamples them at symbol rate to obtain the final 1480 samples. Removing the CP leads to a total of 1280 samples. Then, the receiver individually applies a DFT to each OFDM symbol and use the CCSK cross-correlation for the demodulation operation. Since the channel is an AWGN, no MRC equalization is used, but the absolute value of the correlation score should be taken as a mis-synchronization in time or a in (fractional) frequency can lead to a shifted complex result.

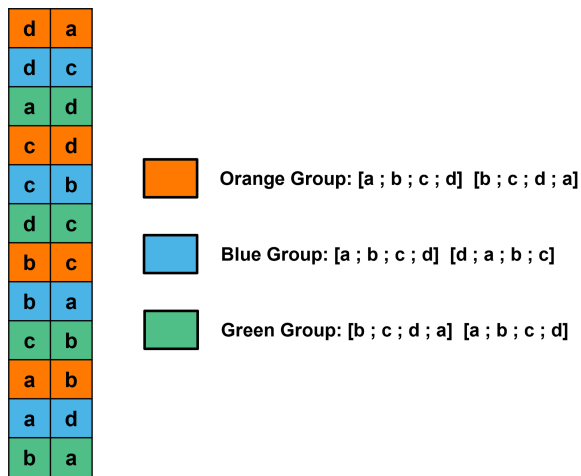


Figure 7.8: Impact of a frequency offset of two sub-carriers.

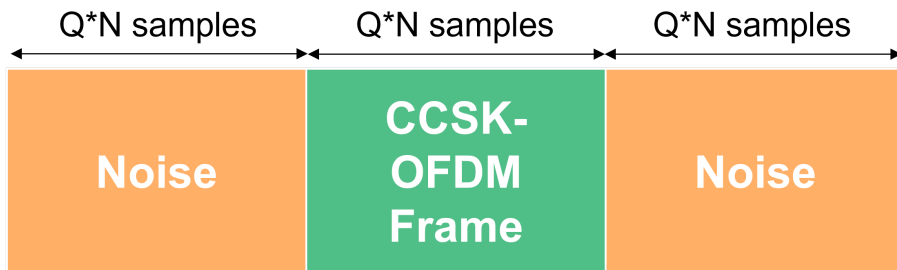


Figure 7.9: System model for frame detection and synchronization.

7.4.2 Shifted Demodulation with a CRC

The shifted demodulation relies on the ability of the system to detect the right shift offset, between the transmitted frame and the demodulated frame. As explained in section 6.5.3, this can be done with a CRC, checking the integrity of the frame for each possible shift offset.

To test this method, we consider the previously described system, with a perfect time synchronization and a perfect fractional frequency offset synchronization. Considering a frequency offset $f_0 \in [-2.5\Delta_f, 2.5\Delta_f]$, the resulting spectrum can be shifted by ± 2 , ± 1 or 0 sub-carriers, leading to a possible common shift offset for the frame.

We add a CRC of size 24 bits at the end of the frame. Hence, the last 4 CCSK sequences out of 20 are dedicated to the CRC. The Figure 7.10 compares the SBLER and the BLER performances of the system. We check the CRC for all possible shift of the frame. When a possibly correct frame is identified, it is compared to the transmitted one. As false positive can happen, the BLER is always higher than the SBLER. But as described here, the two curves are close, proving the possibility to use a CRC for that matter.

Several remarks can be made. First, the size of the CRC has a direct impact on the false positive rate. If the CRC is too small, a high number of false positives can be detected, greatly decreasing the advantage of the shifted demodulation. More studies need to be done on the right CRC choice for this type of system, as the CRC was not designed for this kind of usage. Lastly, it could be interesting to look for an innovative way to check for the frame integrity. As the shifted demodulation is not usually considered in communications systems, there is a need for a dedicated design, which could improve the efficiency of the integrity check.

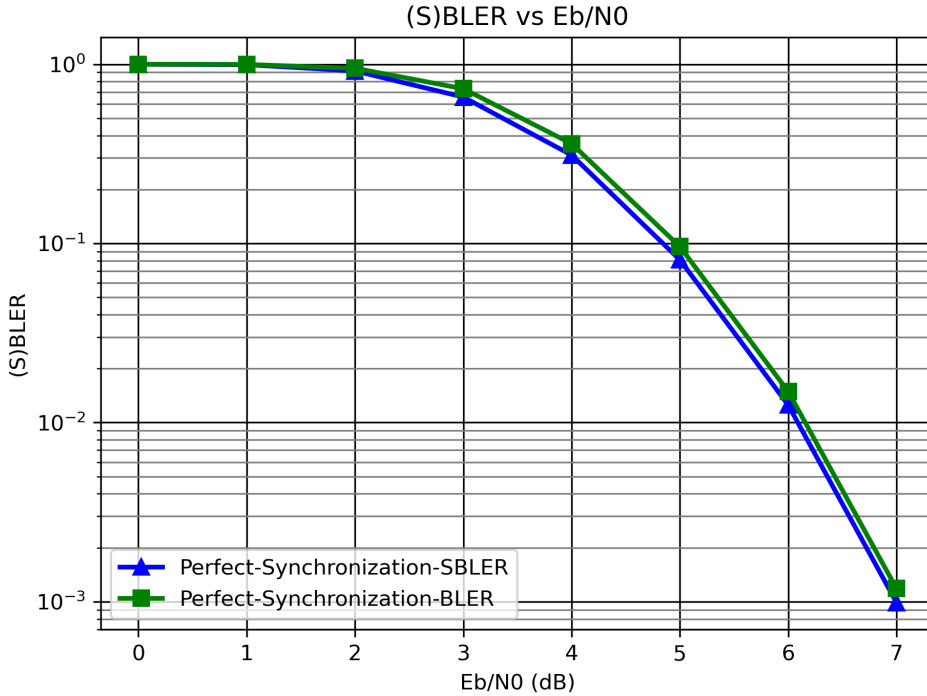


Figure 7.10: Comparison of SBLER and actual BLER with a CRC of size 24 bits.

7.4.3 CP-Based Algorithm

The state of the art provides an algorithm based on the CP to get a coarse time-synchronization of the frame and of the fractional frequency offset [31] [32]. The idea is to use the natural repetition of the CP in each OFDM symbol. Noting $r[k]$ the k^{th} processed sample and o the oversampling rate, we define the quantities:

$$\begin{aligned}\gamma[n] &= \sum_{k=n}^{(n+N-1)o} r[k]r^*[k+oN] \\ \phi[n] &= \frac{1}{2} \sum_{k=n}^{(n+N-1)o} |r[k]|^2 + |r[k+oN]|^2 \\ \rho &= \frac{|\mathbb{E}\{r[k]r^*[k+oN]\}|}{\sqrt{\mathbb{E}\{|r[k]|^2\}\mathbb{E}\{|r[k+oN]|^2\}}}\end{aligned}\quad (7.5)$$

The joint maximum likelihood estimation of the frame starting sample and the fractional frequency offset are expressed as:

$$\begin{aligned}n_{\text{ML}} &= \underset{n}{\operatorname{argmax}}(|\gamma[n]| - \rho\phi[n]) \\ f_{\text{ML}} &= -\frac{1}{2\pi} \angle \gamma[n_{\text{ML}}]\end{aligned}\quad (7.6)$$

with \angle the angle operator. To adapt the algorithm to the case of sporadic OFDM frame surrounded by noise, and using the multiple CP in the frame, we modify the previous equations leading to:

$$\begin{aligned}n_{\text{ML}} &= \underset{n}{\operatorname{argmax}} \left| \frac{1}{Q} \sum_{k=0}^{Q-1} \gamma[n+kQ] \right| \\ f_{\text{ML}} &= -\frac{1}{2\pi} \angle \left(\frac{1}{Q} \sum_{k=0}^{Q-1} \gamma[n_{\text{ML}}+kQ] \right)\end{aligned}\quad (7.7)$$

Figures 7.11, 7.12 and 7.13 respectively describe the performances of the CP-based algorithm in terms of SBLER, mean time synchronization error and mean fractional frequency estimation error. From the results we can conclude that, in our system, the CP-based algorithm quickly provides an accurate time synchronization, but the remaining fractional frequency offset has a major impact on the SBLER performances. In Figure 7.13, at around 4 dB of Eb/N0, the fractional frequency offset error starts to mainly decrease because of the noise, the algorithm providing an accurate starting point of the frame.

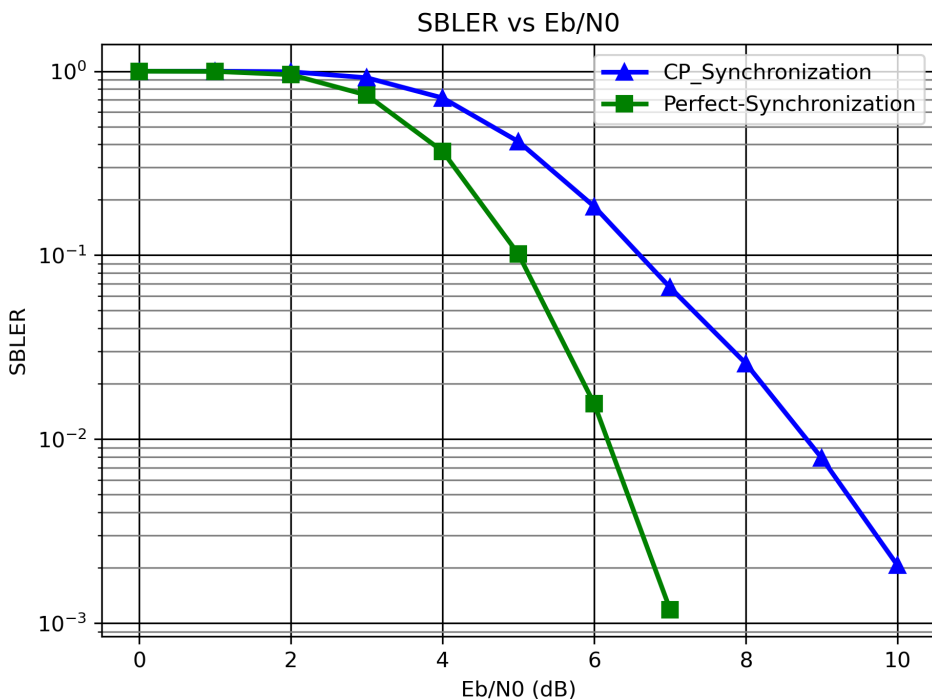


Figure 7.11: SBLER vs Eb/N0.

7.5 Conclusion on Time and Frequency Synchronizations

In this section, we have studied the impact of time and frequency synchronization on a typical CCSK OFDM system. We have showed the importance of the shifted demodulation in these cases, as this transmission scheme can relax the accuracy of time synchronization and integer frequency synchronization, even with the iterative mapping. The CP-based algorithm represents a good start, providing a coarse time synchronization and a coarse estimate of the fractional frequency offset, but the inherent CCSK sequences have a high potential for detection and synchronization purpose. Further study should be done to describe an algorithm using these sequences. The Deliverables 2.2 and 2.3 should give good leads.

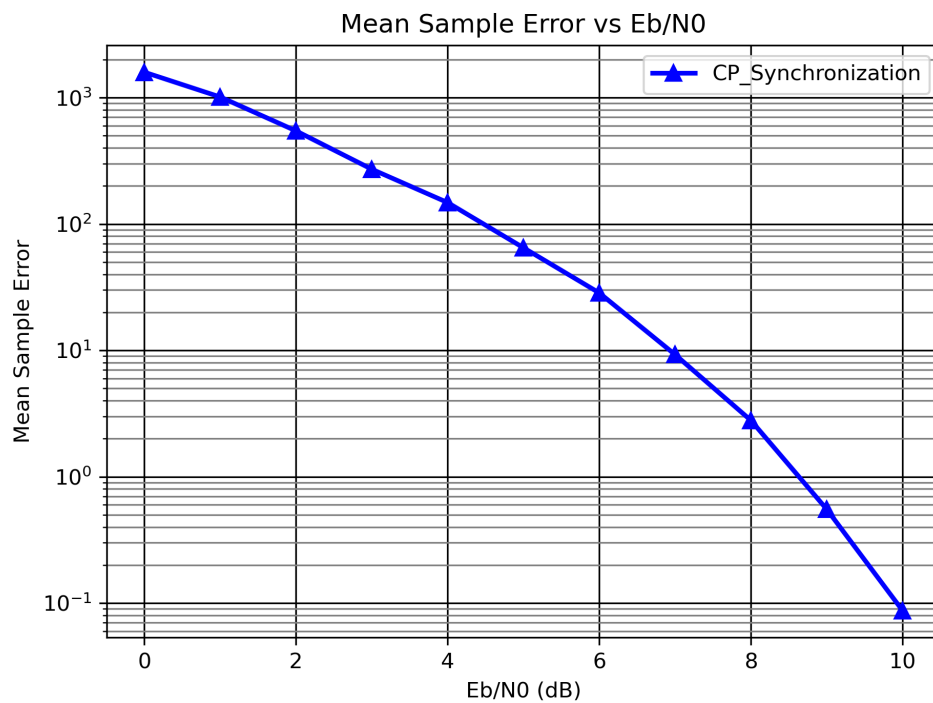


Figure 7.12: Mean time synchronization error in samples.

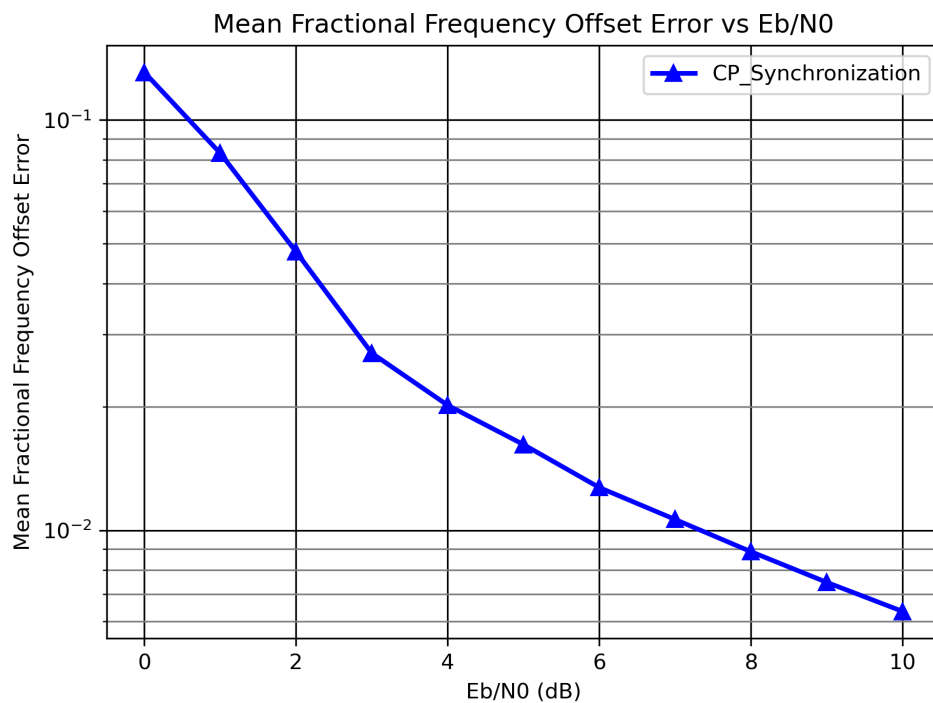


Figure 7.13: Mean fractional frequency estimation error.

8 General Conclusion

The QCSP project proposes the CCSK modulation as a solution to a common difficulty with small data packet: the overhead of the pilots needed for detection, time and frequency synchronization, and channel estimation. This document looks at this solution in the scope of a 3GPP framework, and study the association of the CCSK and the (CP-)OFDM modulation. To maintain the objective of a lower pilot overhead, this work has proposed innovative solutions to enable all the aforementioned tasks without the need of pilot sequences.

The study realized in this document mainly keeps an experimental approach, and further analytical studies are needed to complete the simulation results presented here. Moreover, interesting proposals where made, especially the DFTLink and GLAD algorithms, that need to be more investigated to really evaluate the potential of these technical solutions.

Finally, by showing the usage of the shifted demodulation in case of time and frequency synchronizations errors, and demonstrating its feasibility by testing this principle with a CRC check, the CCSK CP-OFDM represents a promising end to end small packets communications scheme.

Appendix

A.1 Mathematical tools and demonstrations

This appendix contains useful mathematical tools and demonstrations that are used to derive some equations in this paper.

A.1.1 Convolution Property of Fourier Transform

We consider two N-periodic sequences g_N and h_N . Their circular or cyclic convolution is defined as:

$$(g_N \circledast h_N)[t] = \sum_{\tau=0}^{N-1} g_N[\tau]h_N[t-\tau] \quad (\text{A.1})$$

With \circledast is the circular convolution operator. The circular convolution is a N-periodic function. If the original sequences g and h are actually finite N length sequence, their circular convolution uses a periodic extension of the sequences.

The DFT of the circular convolution of these sequences is equal to:

$$\begin{aligned} F(g_N \circledast h_N)[k] &= \frac{1}{\sqrt{N}} \sum_{n=0}^{N-1} (g_N \circledast h_N)[n] \exp\left(-j2\pi \frac{nk}{N}\right) \\ &= \frac{1}{\sqrt{N}} \sum_{n=0}^{N-1} \sum_{\tau=0}^{N-1} g_N[\tau]h_N[n-\tau] \exp\left(-j2\pi \frac{nk}{N}\right) \\ &= \frac{1}{\sqrt{N}} \sum_{\tau=0}^{N-1} g_N[\tau] \exp\left(-j2\pi \frac{\tau k}{N}\right) \sum_{n=0}^{N-1} h_N[n-\tau] \exp\left(-j2\pi \frac{(n-\tau)k}{N}\right) \\ &= \sqrt{N} F(g_N)[k] F(h_N)[k] \end{aligned} \quad (\text{A.2})$$

The last equality comes from the fact that h_N is a N-periodic sequence, as well as the complex exponential. So the DFT of a circular convolution is equal to the Hadamard product of the DFT of the sequences. Hence, the Hadamard product of two DFT is equal to the DFT of the circular convolution of the sequences. The normalization factor has to be taken into account when doing actual computations, as it may influence the final result.

A.1.2 Fourier Transform of Gate Function

The gate function $G(t)$ is defined as:

$$G(t) = \begin{cases} 1 & , 0 \leq t < \tau \\ 0 & , \text{ elsewhere} \end{cases} \quad (\text{A.3})$$

The Fourier transform of the Gate function is computed as:

$$\begin{aligned} F(G)(f) &= \int_{-\infty}^{\infty} G(t) \exp(j2\pi ft) dt \\ &= \int_0^{\tau} \exp(j2\pi ft) dt \\ &= \exp(j\pi f\tau) \frac{\exp(j\pi f\tau) - \exp(-j\pi f\tau)}{j2\pi f} \\ &= \tau \exp(j\pi f\tau) \operatorname{sinc}(\pi f\tau) \end{aligned} \quad (\text{A.4})$$

This function is null whenever $f = \frac{k}{\tau}$, $k \in \mathbb{Z}^*$, hence at the multiple of the frequency $\frac{1}{\tau}$.

A.1.3 Multi-Carrier Modulation and OFDM

We use a MCM that splits the overall bandwidth B into N sub-carriers. The sub-carrier spacing is equal to $\Delta f = \frac{B}{N}$. The duration of the MCM symbol corresponds to the time needed to transmit one sub-carrier symbol $T_u = \frac{1}{\Delta f}$. During T_u , the N sub-carriers symbols are transmitted in parallel in frequency.

On each sub-carrier is mapped a symbol from a standard constellation (e.g. M-QAM). The sub-carrier n carries the symbol a_n for $0 \leq n \leq N - 1$. The transmitted symbol $s(t)$ is defined as the sum of the sub-carrier signals:

$$s(t) = \Re \left[\frac{1}{\sqrt{N}} \sum_{n=0}^{N-1} a_n G_{T_u}(t) \exp(j2\pi(f_0 + n\Delta f)t) \right] \quad (\text{A.5})$$

with $G_\tau(t)$ the gate function on the interval $[0; \tau]$ and f_0 the frequency of the first sub-carrier. The gating over the period T_u means that the signal spectrum is a sum of sinc having their zeros at $\frac{k}{\Delta f}$. Hence the sub-carriers signals do not interfere with the of each other. We can use the central frequency $f_c = f_0 + \frac{N}{2}\Delta f$. The sub-carriers are centered around f_c , so that in baseband, the system spectrum is centered around the Direct Component (DC).

$$s(t) = \Re \left[\frac{1}{\sqrt{N}} \exp(j2\pi f_c t) \sum_{n=0}^{N-1} a_n G_{T_u}(t) \exp\left(j2\pi\left(n - \frac{N}{2}\right)\Delta f t\right) \right] \quad (\text{A.6})$$

Based on the spectrum occupied by $s(t)$ in baseband $[-\frac{B}{2}, \frac{B}{2}]$, it can be sampled and recovered at a frequency of $B = N\Delta f$. The sampling instant of $s(t)$ are expressed as $\frac{k}{N\Delta f}$ for $0 \leq k < \frac{1}{\Delta f} = T_u$:

$$\begin{aligned} s\left(\frac{k}{N\Delta f}\right) &= \Re \left[\frac{1}{\sqrt{N}} \exp\left(j2\pi f_c \frac{k}{N\Delta f}\right) \sum_{n=0}^{N-1} a_n \exp\left(j2\pi\left(n - \frac{N}{2}\right) \frac{k}{N}\right) \right] \\ &= \Re \left[\exp\left(j2\pi f_c \frac{k}{N\Delta f}\right) \exp(-j\pi k) \frac{1}{\sqrt{N}} \sum_{n=0}^{N-1} a_n \exp\left(j2\pi \frac{nk}{N}\right) \right] \end{aligned} \quad (\text{A.7})$$

The last equation describes the samples of the transmitted signal, as the real part of its complex envelop. The first term describes the central frequency modulation. The normalized sum corresponds to the IDFT of the a_n sequence. The exponential $\exp(-j\pi k) = (-1)^k$ enables the spectrum to be centered around DC in baseband. Without the last simplification, one can see the sum as an IDFT with sub-carriers mapping shifted by $-\frac{N}{2}$:

$$\begin{aligned} \sum_{n=0}^{N-1} a_n \exp\left(j2\pi\left(n - \frac{N}{2}\right) \frac{k}{N}\right) &= \sum_{u=-\frac{N}{2}}^{\frac{N}{2}-1} a_{u+\frac{N}{2}} \exp\left(j2\pi \frac{uk}{N}\right) \\ &= \sum_{u=0}^{N-1} a_{u+\frac{N}{2}} \exp\left(j2\pi \frac{uk}{N}\right) \end{aligned} \quad (\text{A.8})$$

The last equality stands because we extended the sequence a_n as N -periodic. Consequently, sub-carrier index 0 is mapped to $a_{\frac{N}{2}}$, sub-carrier index $\frac{N}{2} - 1$ to a_{N-1} , sub-carrier index $\frac{N}{2}$ to a_0 and sub-carrier index $N - 1$ to $a_{\frac{N}{2}-1}$. The sub-carrier index from $\frac{N}{2}$ corresponds to negative frequencies. Using the IDFT and DFT operations for MCM corresponds to the OFDM modulation.

Bibliography

- [1] D. Chu, "Polyphase codes with good periodic correlation properties (corresp.)," *IEEE Trans. Inf. Theor.*, vol. 18, no. 4, p. 531–532, Sep. 2006. [Online]. Available: <https://doi.org/10.1109/TIT.1972.1054840>
- [2] Z. Zhang, J. Liu, and K. Long, "Low-complexity cell search with fast pss identification in lte," *IEEE Transactions on Vehicular Technology*, vol. 61, no. 4, pp. 1719–1729, 2012.
- [3] J. W. Kang, Y. Whang, B. H. Ko, and K. S. Kim, "Generalized cross-correlation properties of chu sequences," *IEEE Transactions on Information Theory*, vol. 58, no. 1, pp. 438–444, 2012.
- [4] T. E. Hull and A. R. Dobell, "Random number generators," *SIAM Review*, vol. 4, no. 3, pp. 230–254, 1962. [Online]. Available: <https://doi.org/10.1137/1004061>
- [5] M. A. Richards, "The discrete-time fourier transform and discrete fourier transform of windowed stationary white noise," Tech. Rep., 2013.
- [6] B. Popovic, "Efficient dft of zadoff-chu sequences," *Electronics Letters*, vol. 46, pp. 502–503(1), April 2010. [Online]. Available: <https://digital-library.theiet.org/content/journals/10.1049/el.2010.3510>
- [7] M. Ram Murty and S. Pathak, "Evaluation of the quadratic gauss sum," Department of Mathematics and Statistics, Queen's University, Kingston, CANADA, Tech. Rep., 2010.
- [8] R. Chang, "Synthesis of band-limited orthogonal signals for multichannel data transmission," *Bell System Technical Journal*, vol. 45, pp. 1775–1796, 1966.
- [9] A. Y. Wong and V. C. M. Leung, "Code-phase-shift keying: a power and bandwidth efficient spread spectrum signaling technique for wireless local area network applications," in *CCECE '97. Canadian Conference on Electrical and Computer Engineering. Engineering Innovation: Voyage of Discovery. Conference Proceedings*, vol. 2, 1997, pp. 478–481 vol.2.
- [10] G. M. Dillard, M. Reuter, J. Zeiddler, and B. Zeidler, "Cyclic code shift keying: a low probability of intercept communication technique," *IEEE Transactions on Aerospace and Electronic Systems*, vol. 39, no. 3, pp. 786–798, 2003.
- [11] O. Abassi, L. Conde-Canencia, M. Mansour, and E. Boutillon, "Non-binary low-density parity-check coded cyclic code-shift keying," in *2013 IEEE Wireless Communications and Networking Conference (WCNC)*, 2013, pp. 3890–3894.
- [12] ——, "Non-binary coded ccsk and frequency-domain equalization with simplified llr generation," in *2013 IEEE 24th Annual International Symposium on Personal, Indoor, and Mobile Radio Communications (PIMRC)*, 2013, pp. 1478–1483.
- [13] L. Jing and J. Huang, "Cyclic shift keying spread spectrum ofdm method over underwater acoustic channel," in *2012 IEEE International Conference on Signal Processing, Communication and Computing (ICSPCC 2012)*, 2012, pp. 798–801.
- [14] Y. Liu, Z. Tan, H. Hu, L. J. Cimini, and G. Y. Li, "Channel estimation for ofdm," *IEEE Communications Surveys and Tutorials*, vol. 16, no. 4, pp. 1891–1908, 2014.
- [15] V. Savaux and Y. Louët, "LMMSE channel estimation in OFDM context: a review," *IET Signal Processing*, vol. 11, no. 2, pp. 123–134, 2017. [Online]. Available: <https://hal.archives-ouvertes.fr/hal-01431313>

- [16] M.-H. Hsieh and C.-H. Wei, "Channel estimation for ofdm systems based on comb-type pilot arrangement in frequency selective fading channels," *IEEE Transactions on Consumer Electronics*, vol. 44, no. 1, pp. 217–225, 1998.
- [17] P. Hoeher, S. Kaiser, and P. Robertson, "Two-dimensional pilot-symbol-aided channel estimation by wiener filtering," in *1997 IEEE International Conference on Acoustics, Speech, and Signal Processing*, vol. 3, 1997, pp. 1845–1848 vol.3.
- [18] M. Sandell and O. Edfors, "A comparative study of pilot-based channel estimators for wireless ofdm," 1996.
- [19] J. Cavers, "An analysis of pilot symbol assisted modulation for rayleigh fading channels (mobile radio)," *IEEE Transactions on Vehicular Technology*, vol. 40, no. 4, pp. 686–693, 1991.
- [20] P. Hoeher, "Tcm on frequency-selective land-mobile fading channels," in *In Proc. 5th Tirrenia International Workshop on Digital Communications*, 1991, pp. 317–328.
- [21] J.-J. van de Beek, O. Edfors, M. Sandell, S. Wilson, and P. Borjesson, "On channel estimation in ofdm systems," in *1995 IEEE 45th Vehicular Technology Conference. Countdown to the Wireless Twenty-First Century*, vol. 2, 1995, pp. 815–819 vol.2.
- [22] O. Edfors, M. Sandell, J.-J. van de Beek, S. Wilson, and P. Ola Borjesson, "Ofdm channel estimation by singular value decomposition," in *Proceedings of Vehicular Technology Conference - VTC*, vol. 2, 1996, pp. 923–927 vol.2.
- [23] S. Yushi and M. Ed, "Channel estimation in ofdm systems," Freescale Semiconductor, Tech. Rep., 2006.
- [24] S. Coleri, M. Ergen, A. Puri, and A. Bahai, "Channel estimation techniques based on pilot arrangement in ofdm systems," *IEEE Transactions on Broadcasting*, vol. 48, no. 3, pp. 223–229, 2002.
- [25] S. McKinley and M. Levine, "Cubic spline interpolation," Available at <https://www.rajgunesh.com/resources/downloads/numerical/cubicsplineinterpol.pdf> (2022/09/15).
- [26] J. Barry, "Equalization," School of Electrical and Computer Engineering, Georgia Institute of Technology, Atlanta, Tech. Rep., 2015.
- [27] D. Brennan, "Linear diversity combining techniques," *Proceedings of the IEEE*, vol. 91, no. 2, pp. 331–356, 2003.
- [28] T. Eng, N. Kong, and L. Milstein, "Comparison of diversity combining techniques for rayleigh-fading channels," *IEEE Transactions on Communications*, vol. 44, no. 9, pp. 1117–1129, 1996.
- [29] R. H. Clarke, "A statistical theory of mobile-radio reception," *The Bell System Technical Journal*, vol. 47, no. 6, pp. 957–1000, 1968.
- [30] M. Pätzold, *Mobile Fading Channels*. Wiley, 2002. [Online]. Available: <https://books.google.fr/books?id=CxJTAAAAMAAJ>
- [31] J. van de Beek, M. Sandell, and P. Borjesson, "MI estimation of time and frequency offset in ofdm systems," *IEEE Transactions on Signal Processing*, vol. 45, no. 7, pp. 1800–1805, 1997.
- [32] K. Manolakis, D. M. Gutierrez Estevez, V. Jungnickel, W. Xu, and C. Drewes, "A closed concept for synchronization and cell search in 3gpp lte systems," in *2009 IEEE Wireless Communications and Networking Conference*, 2009, pp. 1–6.